CLOUD POINT EXTRACTION, PRECONCENTRATION AND SPECTROPHOTOMETRIC DETERMINATION OF MAGNESIUM(II) BY USING 2,4-DIMETHYLPENTAN-3-ONE

Shawket K. Jawada[a] and Faris H. Hayder[b]*

Keywords: Magnesium; cloud point extraction, solvent extraction, solvation, pre-concentration.

The cloud point extraction (CPE) method has been applied to the extraction and pre-concentration of Mg^{2+} ions. The extracted solvated species showed a maximum absorbance at λ_{max} = 249 nm. The optimum conditions for extraction of solvated species to CPL are the presence of 0.5 M KNO_3 for 50 µg Mg^{2+} ion in 10 ml aqueous solution with 1×10^{-4} M of extractant, 2,4-dimethyl-pentan-3-one (2,4-DMP) and heating up to 90 °C for 15 minutes and addition of 0.5 mL of 1 % Triton X–100 as surfactant. The study showed that different extractant have different extraction efficiency, acetophenone showing higher extraction efficiency but ethyl methyl ketone has a lower efficiency. The effect of different salts and variable concentration of nitrate salts on the extraction efficienct has been studied. Determination of Mg^{2+} in different samples has been studied with a *RSD* = 0.0074, *DL* = 1.84×10^{-5} and Sandel's sensitivity = 3.58×10^{-9} µg cm^{-2}.

* Corresponding Authors
Tel: 07803827996
E-Mail: farissiraf3@gmail.com
[a] Chemistry department, College of Education for Girls, Kufa University, Al-Najaf - Republic of Iraq.
[b] Chemistry department, College of Education for Girls, Kufa University, Al-Najaf - Republic of Iraq.

Introduction

The extraction and estimation of Mg(II) by CPE methodology has not been attempted so far though the methodology has been used for extraction of several other elements with high efficiency. One sensitive application is the CPE for extraction Ni(II) by crown ether DB18C6.[1] Separation and micro determination of Pb(II) and Cd(II) by CPE methodology, using 2-[1-benzothiazolylazo]-4-benzylphenol for Pb(II) and 2-[(3-bromophenyl)azo]-4,5-diphenyl-imidazole for Cd(II) have also been reported.[2] Zn(II) was removed from aqueous solution as ion-pair complex by CPE technique with 3-[2-pyridylazo]-1-nitroso-2-naphthol (PANN).[3] Dual detection of drug norfloxacin (NOR) and iron (III) ion have been performed in biological and pharmaceutical samples.[4] CPE methodology and cetyltrimethylammonium bromide (CTAB) surfactant was used for extraction and determination Al^{3+}.[5] Similarly, Triton X-100 and dithizone have been used to determine selenium in kanykony (*ipomoea reptans p.*).[6] CPE methodology coupled with flame atomic absorption spectrometry has been developed for separation, pre-concentration and determination of trace amount of iron in different samples.[7,8] SDS has ben used as surfactant for pre-concentration and spectrophotometric determination of Pb(II) and Cu(II) by N^1,N^2-diphenylhydrazine-1,2-dicarbothioamide (PHCT).[9] CPE methodology was also used to determine Hg(II) with a new complexing agent[10] and Ni(II) with DMG by UV-Vis spectrophotometry.[11]

Experimental

Biochrom model (80-7000-11) Libra s60 Cambridge CB40FJ spectrophotometer with 1 cm quartz cell was used for recording the absorbance spectra and absorbance. Electrostatic water bath (WNB7-45) (England) was used to maintain the temperature.

All chemicals used in experiments are of analytical grade and were used without further purification. Stock solution of Mg(II) (1 mg mL^{-1}) was prepared in a volumetric flask by dissolving 0.6101 g of $Mg(NO_3)_2$ in 100 mL distilled water containing 0.5 mL of concentrated HNO_3. Other solutions were prepared by dilution of the stock solution with distilled water. Buffer solution, pH = 9.6, was prepared by dissolving 60 gm of NH_4Cl in distilled water with 120 mL of concentrated ammonia solution and diluted to 1 L by distilled water. A 0.02 % solution of Eriochrome black-T was also prepared.

Principal method

A mixture of aqueous solution of 10 mL containing 50 µg Mg^{2+} and 0.5 mL of 1 % Triton X–100 with suitable concentration of KNO_3 and 1×10^{-4} M of 2,4-DMP as the extractant was prepared. The mixture was heated at a fixed temperature with lime to form cloud point layer (CPL) which was separated. It was dissolved in 5 mL of ethanol and its absorbance at λ_{max} was measured at against a blank prepared in the same manner without Mg^{2+} ion but treated with Eriochrome black-T.[12] The distribution ratio (DR) was calculated.

In the stripping method, ethanolic CPL solution was shaken with 2 x 5 mL of diluted HNO_3. The results showed that the both the type of analysis gave the identical results.

Result and discussion

The UV-VIS spectrum (Figure 1) of the extracted solvated species, obtained by CPE method showed maximum absorbance at wavelength λ_{max}= 249 nm.

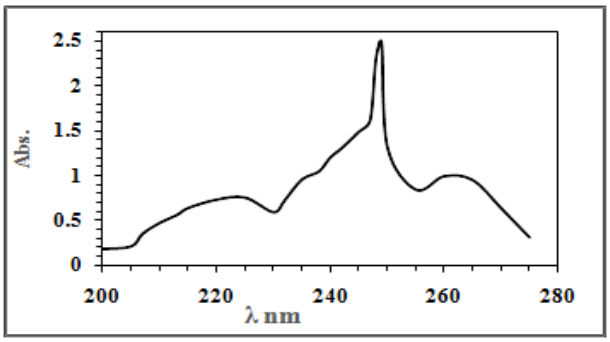

Figure 1. UV-VIS spectrum of the ion-pair complex extracted to cloud point.

Variation of KNO_3 concentration

An aqueous solution (10 mL) was prepared which contained 50 µg Mg(II), 0.5 mL of 1 % Triton X–100, 1×10^{-4} M 2,4-DMP and varying concentration of KNO_3. It was heated at 90 C° for 15 min for the formation of CPL. The CPL was separated from aqueous solution and dissolved in 5 ml of ethanol and its absorbance at 294 nm was measured against a blank, prepared in the similar manner but without Mg(II).[12] By the use of calibration curve (Figure 2), the remaining quantity of Mg(II) ion in aqueous solution after extraction was determined. The transferred amount of Mg(II) was also determined and the DR was calculated according to procedure described above in the section of principal method. The results are presented in Figures 3 and 4.

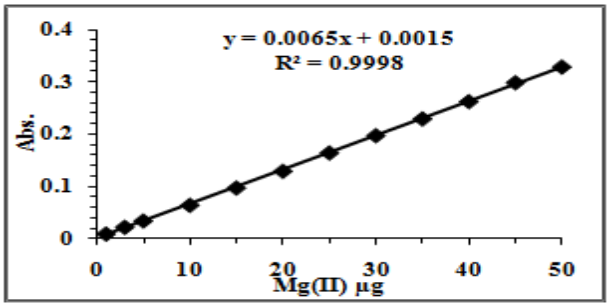

Figure 2. Calibration curve

The results indicate that increase in KNO_3 concentration increases the extraction of the of the solvated species to CPL. The absorbance and DR reach a maximum with 0.5 M KNO_3. The degree of solvation depends on thermodynamic equilibrium of species formed, and in the present case, 0.5 M KNO_3 gives favourable thermodynamic equilibrium for formation, and extraction, but at KNO_3 concentration less than the optimum, the thermodynamic equilibrium of the formation of solvated species is not reached. A high concentration of KNO_3 may hinder the formation of CPL by increasing micelles diffusion to aqueous solution.

Variation of Mg(II) concentration

Aqueous solutions (10 mL each) containing different amounts of Mg(II), 0.5 M KNO_3, 0.5ml of 1 %Triton X–100, and 1×10^{-4} M 2,4-DMP was subjected to the standard procedure to form CPL and their absorbance (Figure 3) were measured and DR were calculated.

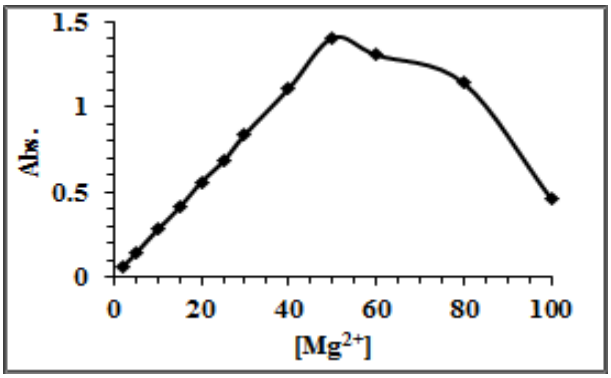

Figure 3. Dependence of absorbance on Mg(II) concentration.

The results show that the optimum value of Mg(II) concentration is 50 µg. At this concentration an optimum value for the following equilibrium is reached.

$$Mg^{2+} + 2NO_3 + 2,4\text{-DMP} \rightleftharpoons 2,4\text{-DMP-}Mg(NO_3)_2 \qquad (1)$$

Metal ion concentration less than the optimum value is not enough to establish the equilibrium fully and results in a decrease in the extraction efficiency. Similarly, any metal ion concentration more than the optimum value is also not suitable for extraction because it tends to decline the extraction efficiency.

Variation of 2,4-DMP concentration

50 µg of Mg(II) ion from10 ml aqueous solution in presence 0.5 M KNO_3, 0.5 ml of 1%Triton X–100, and different concentrations of 2,4-DMP was extracted according to procedure detailed in principal method.

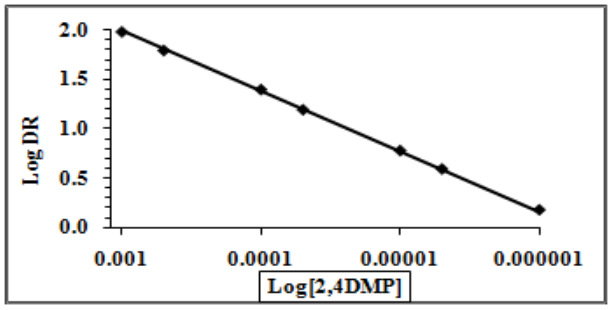

Figure 4. Dependence of distribution ratio on the concentration of 2,4-DMP.

The results show there is linear relation between extraction efficiency and 2,4-DMP concentration, i.e. extraction of the solvated species to CPL increase with an increase in the concentration of 2,4-DMP. Similarly, the DR varies linearly with the concentration of 2,4-DMP (Figure 4).

The slope of straight line in Figure 4 is 0.603, which indicate that one molecule of 2,4-DMP is coordinating with Mg(II) in $Mg(NO_3)_2$ forming 2,4-DMP-$Mg(NO_3)_2$.

Effect of different salts

50 µg of Mg(II) ion from10 ml aqueous solution, under optimum reaction conditions was extracted according to procedure detailed in principal method, in the presence 0.5 M of different salts. The results show extraction efficiency change with nature of salt added, and the best extraction and DR is achieved in the presence of $Al(NO_3)_3$ (Figure 5).

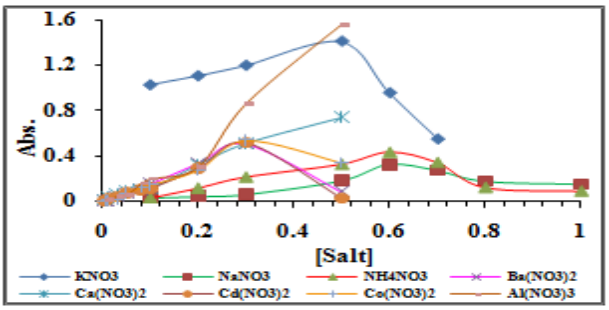

Figure 5. Effect of different salts on the extraction process.

Effect of concentration of different salts

Extracted 50 µg Mg^{2+} ion from10 ml aqueous solution containing varying concentration of different salts was carried out according to procedure detailed in principal method. The results show that for most of the salts, the extraction efficiency and DR increases up to a concentration between 0.5 M to 0.6 M and thereafter either declines or remain constant.

Temperature variation

Extraction of Mg(II), under optimum conditions, was carried out different temperatures between 70 and 95 °C. The results show that CPE is an endothermic process. The absorbance of complex and DR value increase with an increase in temperature up to the optimum temperature of 90 °C but decreases thereafter. The most suitable temperature for attaining the equilibrium of the extraction process and the formation CPL is 90 °C. At lower temperatures, the equilibrium is not fully attained and the extraction efficiency does not reach the optimum value. It seems that at temperature higher than 90 °C, micelles are dehydrated, the density of CPL is reduced and extraction efficiency is also reduced. The extraction constant K_{ex} at each temperature was calculated according to Eqn. (2).

$$K_{ex} = \frac{D}{\left[Mg^{2+}\right]\left[2,4\text{-DMP}\right]} \qquad (2)$$

It was found that a plot of log K_{ex} against reciprocal of temperature is linear with a negative slope. From the slope of the plot, values of thermodynamic parameters for the equilibrium were calculated. The values are ΔH = 0.23 kJ mol^{-1}, ΔS_x = 173.3 J mol^{-1} K^{-1} and ΔG = - 63.1 kJ mol^{-1}. The small value of ΔH indicate a strong binding of 2,4-DMP with $Mg(NO_3)_2$ to form stable solvated species extracted to CPL. The high value of ΔS reflects entropic nature of the extraction process.

Variation of heating time

Extraction of Mg(II), as per the standard, process was carried out while varying the heating period. The results show optimum heating time is 15 min. Heating for 15 min gives favourable aggregation of micelles and complete dehydration to give CPL with smaller volume and higher density to enable extraction of maximum concentration of solvated species to result in higher absorbance and DR values. It seems that heating for 15 min. is required to produce good CPL, less than 15 min. is not sufficient to produce good CPL. More heating time also declines extraction efficiency as it decreases dehydration and increase diffusion of micelles.

Variation of surfactant concentration

Effect of variation in the volume of 1 % solution of Triton X–100 was studied by keeping other reaction condition at the optimum level. The results (Figure 6) showed that the optimum volume of Triton X–100 is 0.5 mL up to which both the absorbance and DR value increase. Less than 0.5 mL of surfactant solution is not sufficient enough to produce good CPL for extraction. Higher concentration of the surfactant than optimum value tend to increase diffusion and decrease dehydration and extraction efficiency.

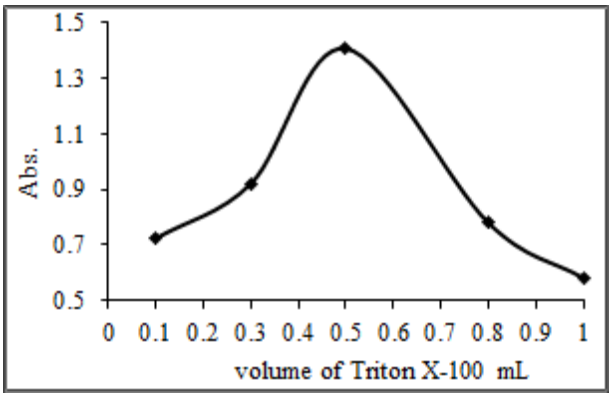

Figure 6. Effect of surfactant concentration on extraction efficiency.

Extractant variation

The extraction process was carried in 2,4-DMP, ethyl methyl ketone, methyl isobutyl ketone (MIBK), tributyl phosphate (TBP) and acetophenone, keeping other optimum reaction conditions constant. The results showed that the best extractant for the present process is acetophenone. The efficiency of the extractants exhibited the following order.

Acetophenone>MIBK>2,4-DMP>TBP>Ethyl methyl ketone

This effect of extractant may be explained on the basis of strength of coordinate bonding between extractant and neutral molecule of magnesium nitrate as well as the stability of the binding between the species extracted into CPL. And extractant.

Spectrophotometric determination

For determination, Mg(II) ion spectrophotometrically, a calibration curve (Figure 7) was prepared by carrying the extraction process as detailed under principal method with varying concentration of the metal ion and recording the absorption at 249 nm. Calculations based on this calibration curve, yielded the values of molar attenuation coefficient, ε = 6710.1 L mol^{-1} cm^{-1}, *RSD* = 0.0074, *D.L*=1.84×10^{-5} and Sandel's sensitivity=3.58 ×10-9 µg cm^{-2}.

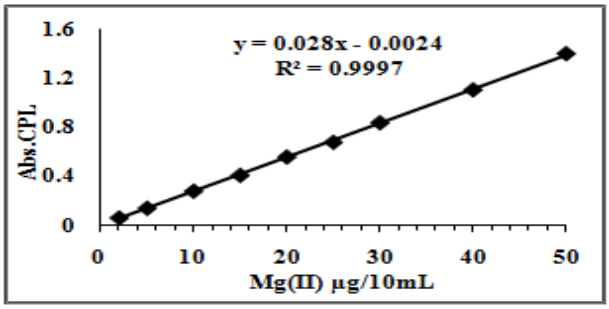

Figure 7. Calibration curve for spectrophotometric determination of Mg(II).

This calibration curve was used for the determination Mg(II) ions in different naturally occurring samples and the results are given in Table 1.

Table 1. Determination of Mg(II) in various samples.

S. No.	Sample	Mg(II)
1	Agriculture soil of Al.mishkab	8.2
2	Unagriculture soil of Al-Mishkab	2.2
3	Chickens meat	9.2
4	Chickens liver	8.4
5	Native beef	8.2
6	Lakes fish	8.6
7	Fish of waste of farms	10
8	Lepidium sativum	4.4
9	Aplum gravealens	5

References

[1]Jawad, S. K., Azooz, E. A., *Int. J. Sci. Technol.*, **2014**, *9(1)*, 17–23.

[2]Jawad, S. K., Muslim J. R., *Irq. Nat. J. Chem..*, **2012**, 47,401- 412.

[3]Jawad, S. K., Azooz, E. A., *Int. J. Sci. Technol.*, **2014**, *9(1)*, 17–23.

[4]Khammas, Z. A., Mubdir, N. S., *Chem. Sci. Trans.*, **2015**, *4(2)*, 483-497.

[5]Hejri, O., Bzorgzadeh, E., Soleimani, M., Mazaheri, R., *World Appl. Sci. J.*, **2011**, *15*, 218-222.

[6]Oktariza, Y., Putra, O. D., Insanu, M., Miftah, A. M., *Int. J. Pharm. Pharm. Sci..*, **2013**, *5(4)*, 498-501.

[7]Duran, C., Ozdes, D., Kaya, E. Ç., Kantekin, H., Bulut, V. N., Tufekci, M., *Turk. J. Chem.*, **2012**, *36(3)*, 445-456.

[8]Ghaedi, M., Niknam, K., Soylak, M. (2011). *Pak. J. Anal. Environ. Chem.*, **2011**, *12(1 & 2)*, 42-48.

[9]Bahram, M., Shahmoradi, S., Mozaffari, S., Niko, A., Dilmaghani, K. A., *Jordan J. Chem..*, **2013**, 8(1), 45-55.

[10]Khammas, Z. A.. Ghali, A. A., Kadhim, K. H., *Irq. Nat. J. Chem..*, **2013**, *49*, 25-37.

[11]Bahram, M., Khezri, S., *Curr. Chem. Lett..*, **2013**, *2(1)*, 49-56.

[12]Marczenko, Z., "*Separation and spectrophotometric determination of elements*", Allis Horwood Ltd., **1986**.

Received: 20.05.2015.
Accepted: 14.08.2015.

AN EFFICIENT AND REGIOSELECTIVE BROMINATION OF AROMATIC AMINES AND PHENOLS USING LANTHANUM(III) NITRATE HEXAHYDRATE AS A CATALYST

Sudam S. Pandule[a]*, Suresh U. Shisodia[a], Mahadeo R. Patil[b] and Vasant V. Chabukswar[a]

Keywords: regioselectivity, bromination, amines, phenols, catalysis.

A simple, highly efficient and economic method for the mono-bromination of number of aromatic amines and phenols using $La(NO_3)_3 \cdot 6H_2O$ as a catalyst is explained. The protocol is regioselective, high-yielding and applied at room temperature to a number of aromatic amines and phenols having electron donating or withdrawing substituents.

* Corresponding Author
Fax: +91-20-26164117
E-Mail: sudampandule2015@gmail.com
[a] Department of Chemistry, Nowrosjee Wadia College, 19, Bund Garden Road, V. K. Joag Path, Pune 411001, India.
[b] Centre for Nano and Material Sciences, Jain University, Jain Global Campus, Bangalore 562112, Karnataka, India.

Introduction

The brominated aromatic compounds have been widely utilized as starting materials and intermediates in the production of pharmaceuticals, agrochemicals and speciality chemicals.[1,2] Moreover it is also known that they can form C-C bond via trans-metalation/cross-coupling reactions such as Stille,[3] Suzuki,[4-8] Heck,[9-12] Sonogashira,[13,14] Ullmann[15] and Wurtz reaction. A well-known method for preparation of brominated aromatic compounds is the reaction with elemental bromine in the presence of transition metal based catalyst.[16-17] Several methods have been reported in the past for the bromination of aromatic compounds which uses reagents such as Br_2-Lewis acids,[18] NBS-H_2SO_4-CF_3CO_2H,[19] NBS-NaOH,[20] NBS-SiO_2,[21] Br_2-Al_2O_3,[22] NBS-Amberlyst,[23] NBS-H-form zeolite-5 (HZSM-5),[24] tert-BuOOH or H_2O_2-HBr,[25] NBS-sulfonic-acid-functionalized silica,[26] NBS/BF_3-H_2O,[27] NBS-NH_4OAc,[28] NBS-tetraethyl ammonium bromide,[29] NBS-$Pd(OAc)_2$,[30] NBS-PTSA,[31] hexamethylenetetramine-Br_2,[32] Br_2/SO_2Cl_2/Zeolite[33] tribromoisocyanuric acid,[34] bromodichloroisocyanuric acid,[35] NH_4VO_3-H_2O_2-HBr,[36] NaBr-$PhI(OAc)_2$[37] and $CuBr_2$.[38] However some of these methods suffer from poor selectivity, use of expensive reagents and formation of polysubstituted products.

The major concern with aniline or phenol derivatives is that these active systems tend to undergo mono to poly bromination, when treated with elemental bromine under usual bromination conditions.[16,17,39] Therefore, it's challenging to perform selective mono-bromination of these compounds. In order to overcome the problem only few improved protocols have been reported in literature, for example, the combination of aqueous TBHP or H_2O_2 together with hydrohalic acid,[40] use of n-BuLi and R_3SnCl,[41] etc. but still these methods have certain limitations like use of harsh reaction conditions, low yields of the products, etc. Therefore there is a pressing need of protocol which can offer selectivity as well as better yields using simple reaction conditions. The chemistry of $La(NO_3)_3 \cdot 6H_2O$ as a catalyst for various types of reactions on number of substrates is well-exploited by Y. Venkateswarlu.[42] This catalyst is a mild, inexpensive, comparatively non-toxic, readily available, easy to handle and insensitive to air. This encouraged us to use this mild Lewis acid catalyst for the bromination of amines and phenols.

Herein we describe an economic, efficient and regioselective mono-bromination method for activated aromatic amines and phenols using cheaper and safe Lanthanum (III) nitrate hexahydrate [$La(NO_3)_3 \cdot 6H_2O$]. The reaction proceeds at ambient conditions while offering excellent yields of the products. The reaction parameters study show that it requires short time and most of the anilines and phenols were converted immediately.

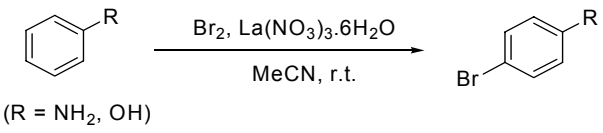

Scheme 1. Bromination of aromatic amines and phenols using $La(NO_3)_3 \cdot 6H_2O$.

Experimental

All chemicals and reagents were purchased from commercial suppliers and used without purification. Aromatic amines and phenols were purchased from Across organics, Lanthanum (III) nitrate hexahydrate ($La(NO_3)_3.6H_2O$), liquid bromine and silica gel for column chromatography (230-400 mesh) from Aldrich, acetonitrile (CH_3CN) from Merck and ethyl acetate, sodium sulphate (Na_2SO_4), and NaCl were purchased from Fisher Scientific.

The melting points of the products are uncorrected. The ^{1}H and ^{13}C NMR spectra were recorded on a Bruker Avance spectrometer operating at 300 MHz for ^{1}H and 100 MHz for ^{13}C nuclei, respectively at 295 K in $CDCl_3$. The chemical shifts were assigned in comparison with the residual proton and carbon resonance of the solvent $CDCl_3$ (δ H = 7.25 ppm, δ_C = 77.0 ppm) and tetramethylsilane (TMS) as the internal reference. MS analysis was done on an APEX 2 spectrometer from Bruker Daltonic with electrospray ionization (ESI) method. FTIR spectra were recorded on Bruker Vertex-70 spectrometer in the range of 400-4000 cm^{-1} and peak positions are given as transmittance (%) against wave numbers (cm^{-1}).

General procedure for bromination of aromatic amines and phenols

In a single-neck round bottom flask, a solution of aniline or phenol (1.47 mmol) in CH_3CN was taken and to this $La(NO_3)_3{\cdot}6H_2O$ (1.47 mmol) was added in one portion. To this mixture, liquid Br_2 (1.47 mmol) diluted in 2 mL CH_3CN was added drop wise at room temperature. The progress of the reaction was monitored by thin layer chromatography (TLC). After completion of the reaction, solvent was evaporated under reduced pressure and water was added to the residue and the mixture was extracted with ethyl acetate (3×10 mL). The combined ethyl acetate layers were washed with saturated solution of $NaHCO_3$ and NaCl, dried over Na_2SO_4, concentrated under vacuum and subjected to column chromatography for purification using ~10% ethyl acetate-hexane solvent system to obtain pure brominated aniline or phenol.

Spectral data of selected compounds

4-Bromoaniline (Table 1, entry 1): IR: 3472, 3379, 1615, 1489, 1282 cm^{-1}. ^{1}H NMR (300 MHz, $CDCl_3$): δ 3.60 (br s, 2H), 6.61 (d, *J*=6.5 Hz, 2H), 7.32 (d, *J*=6.9, 2H). MS (m/z): 173.

2-Bromo-4-methylaniline (Table 1, entry 4): IR: 3464, 3372, 3012, 2912, 1614 cm^{-1}. ^{1}H NMR (300 MHz, $CDCl_3$): δ 2.21 (s, 3H), 3.94 (br s, 2H), 6.62 (d, *J*=0.8 Hz, 1H), 6.91 (d, *J*=2.4 Hz, 1H), 7.20 (s, 1H). MS (m/z): 187.

4-Bromo-2-chloroaniline (Table 1, entry 5): IR: 3423, 3328, 3220, 2924, 1622, 1484 cm^{-1}. ^{1}H NMR (300 MHz, $CDCl_3$): δ 5.51 (br s, 2H), 7.09 (m, 3H).

4-Acetyl-2-bromoaniline (Table 1 entry 7): ^{1}H NMR (300 MHz, $CDCl_3$): δ 7.99 (d, *J*=2.0 Hz, 1H), 7.66 (dd, *J*=8.0, 2.0 Hz, 1H), 6.70 (d, *J*=8.0 Hz, 1H), 4.82 (br s, 2H), 2.46 (s, 3H). MS (m/z): 215, 213.

2-Amino-5-bromopyridine (Table 1, entry 9): IR: 3402, 3186, 1650, 1569, 1485 cm^{-1}. ^{1}H NMR (300 MHz, DMSO): δ 6.82 (br s, *J*=1 Hz, 2H), 8.24 (s, 2H); ^{13}C NMR (100 MHz, DMSO): 104.2, 155.2, 159.0, 161.7. MS (m/z): 175.

2-Amino-5-bromo-3-methylpyridine (Table 1 entry 10): ^{1}H NMR (300 MHz, $CDCl_3$): δ 2.01 (s, 3H), 5.02 (br s, 2H), 7.32 (d, *J*=2.0 Hz, 1H), 7.85 (d, *J*=2.0 Hz, 1H). MS (m/z): 188, 186.

2-Amino-1-bromonaphthalene (Table 1, entry 12): ^{1}H NMR (300 MHz, $CDCl_3$): δ 5.75 (br s, 1H), 7.41-7.62 (m, 4 H), 7.81-7.93 (m, 2H). MS (m/z): 224.

4-Bromo-2-methylphenol (Table 2 entry 2): ^{1}H NMR (300 MHz, $CDCl_3$): δ 2.18 (s, 3H,), 4.86 (br s, 1H), 6.56 (d, *J*=8.0 Hz, 1H), 7.10 (dd, *J*=8.0, 2.0 Hz, 1H), 7.18 (d, *J*=2.0 Hz, 1H). MS (m/z): 188, 186.

4-Bromo-3-methylphenol (Table 2, entry 3): ^{1}H NMR (300 MHz, $CDCl_3$): δ 2.31 (s, 3H), 5.28 (br s, 1H), 6.54 (dd, *J*=8.55, 2.81Hz, 1H), 6.72 (d, *J*=2.81 Hz, 1H), 7.32 (d, *J*=8.55, 1H).

3-Bromo-4-hydoxy-5-methoxybenzaldehyde (Table 2 entry 8): ^{1}H NMR (300 MHz, $CDCl_3$): δ 3.96 (s, 3H), 7.28 (s, 1H), 7.59 (s, 1H), 9.72 (s, 1H), 10.01 (br s, 1H). MS (m/z): 232, 230.

1-Bromo-2-napthol (Table 2, entry 10): ^{1}H NMR (300 MHz, $CDCl_3$): δ 5.73 (br s, 1H), 7.42-7.61 (m, 4H), 7.82-7.92 (m, 2H). MS (m/z): 224.

1-Bromo-3-methoxy-2-napthol (Table 2, entry 11): ^{1}H NMR (300 MHz, $CDCl_3$): δ 3.43 (s, 3H), 5.61-5.74 (br s, 1H), 7.31-7.54 (m, 4H), 7.63 (s, 1H); ^{13}C NMR (100 MHz, $CDCl_3$): 105.3, 119.0, 122.5, 126.1, 127.0, 133.4, 145.0. MS (m/z): 254.

Results and Discussion

Firstly, aniline was chosen as a model substrate to find out optimal reaction conditions. We varied several reaction parameters to optimize the reaction conditions, including the amount of the catalyst $La(NO_3)_3{\cdot}6H_2O$, brominating agent, reaction temperature and use of different solvents. The optimum reaction conditions are when aniline (1.47 mmol), $La(NO_3)_3{\cdot}6H_2O$ (1.47 mmol) and Br_2 (1.47 mmol) were reacted for just 3 minutes at room temperature, 84% of the 4-bromoaniline was obtained. The reaction was carried out in various protic and aprotic solvents and acetonitrile (CH_3CN) was found to be the most suitable one. Also it is well known that bromination and chlorination reactions are more challenging compare to iodination because of lower nucleophilicity of the bromide and chloride than iodide. Considering this acetonitrile, apolar aprotic solvent is effective for bromination of anilines and phenols.

The effectiveness of the catalyst $La(NO_3)_3{\cdot}6H_2O$ was studied by performing the reaction of aniline with elemental bromine in the presence and absence of catalyst. In the presence of catalyst the reaction was complete in just 3 min whereas without the catalyst the reaction was not completed even after 24 h. The use of the catalyst significantly reduced the reaction time along with the enhancement in the yield. The bromination was carried out with different aniline derivatives having electron donating or withdrawing substituents. It was generally observed that when aniline has electron donating substituents (Table 1, entry 1-4), the yield of the mono-brominated product was more compared to one having electron withdrawing groups (Table 1, entry 5-8). Similar trend was also observed in the cases of phenols (Table 2).

Table 1. Bromination of aromatic anilines using $La(NO_3)_3{\cdot}6H_2O$ at room temperature.

S. No.	Substrate	Time (min)	Product	Yield (%)	Mp. (°C)
1	Aniline	3	4-Bromoaniline	84	61-63
2	N-Methylaniline	4	4-Bromo-N-methylaniline	80	54-56
3	N,N-Dimethylaniline	10	4-Bromo-N,N-dimethylaniline	83	53-56
4	4-Methylaniline	7	2-Bromo-4-methylaniline	81	27-29
5	2-Chloroaniline	4	4-Bromo-2-chloroaniline	78	68-72
6	4-Chloroaniline	5	2-Bromo-4-chloroaniline	75	64-66
7	4-Acetylaniline	3	4-Acetyl-2-bromoaniline	73	155-158
8	4-Aminobenzoic acid	13	4-Amino-3-bromobenzoic acid	72	211-215
9	2-Amino-pyridine	8	2-Amino-5-bromopyridine	84	135-138
10	2-Amino-3-methylpyridine	10	2-Amino-5-bromo-3-methyl-pyridine	80	90-94
11	2-Bromoaniline	15	2,4-Dibromoaniline	75	78-80
12	2-Aminonaphthalene	5	2-Amino-1-bromonaphthalene	81	-

Table 2. Bromination of aromatic phenols using $La(NO_3)_3{\cdot}6H_2O$ at room temperature.

S. No	Substrate	Time (min)	Product	Yield (%)	Mp. (°C)
1	Phenol	5	4-Bromophenol	88	64-66
2	2-Methylphenol	10	4-Bromo-2-methylphenol	80	62-64
3	3-Methylphenol	28	4-Bromo-3-methylphenol	81	61-63
4	4-Methylphenol	13	2-Bromo-4-methylphenol	77	55-57
5	2-Hydroxy-benzaldehyde	42	4-bromo-2-hydroxybenzal-dehyde	74	-
6	2,6-Dimethyl-phenol	34	4-Bromo-2,6-dimethylphenol	80	76-79
7	4-Methoxy-phenol	22	2-Bromo-4-methoxyphenol	88	-
8	4-Hydroxy-3-methoxy-benzaldehyde	55	3-Bromo-4-hydroxy-5-methoxy-benzaldehyde	84	162-166
9	4-Nitrophenol	18	2-Bromo-4-nitrophenol	75	113-115
10	2-Naphthol	24	1-Bromo-2-naphthol	83	83-85
11	3-Methoxy-2-naphthol	17	1-Bromo-3-methoxy-2-naphthol	82	98-101

The method used cheaper catalyst $La(NO_3)_3{\cdot}6H_2O$ compared to other expensive transition metal catalyst and found to be effective against number of aniline and phenol derivatives with very good yields. The structure of brominated anilines and phenols were confirmed with NMR and mass spectroscopy and spectral data of some selected compounds is presented. The melting points of the products determined by capillary method are found in accordance with the literature ones.

Conclusion

In conclusion, we have presented a simple, efficient and economic methodology for mono-bromination of anilines and phenols using $La(NO_3)_3{\cdot}6H_2O$ as catalyst. The method is regioselective, offering potential in various synthetic applications giving up to 85% yield of the products. The protocol was successfully applied to number of aniline and phenol derivatives.

Acknowledgment

The authors are thankful to Nowrosjee Wadia College Pune for providing the laboratory facilities for this research work.

References

[1]Taylor, R., *Electrophilic Aromatic Substitution*, Wiley, New York, **1990.**

[2]Butler, A., Walker, J. V., *Chem. Rev*., **1993**, *93*, 1937.

[3]Stille, J. K., *Pure Appl. Chem*., **1985**, *57*, 1771.

[4]Miyaura, N., Suzuki, A., Chem. Rev., **1995**, 95, 2457.

[5]Herrmann, W. A., Reisinger, C. P., Haerter, P., In *Aqueous-Phase Organometallic Catalysis*; B. Cornils, Herrmann, W. A., Wiley-VCH: Weinheim, Germany, **2004**.

[6]Zhao, D. B., Fei, Z. F., Geldbach, T. J., Scopelliti, R., Dyson, P. J., *J. Am. Chem. Soc*., **2004**, *126*, 15876.

[7]Bedford, R. B., Hazlewood, S. L., Limmert, M. E., Albisson, D. A., Draper, S. M., Scully, P. N., Coles, S. J., *Chem. Eur. J.*, **2003**, *9*, 3216.

[8]Choudary, B. M., Madhi, S., Chowdari, N. S., Kantam, M. L., Sreedhar, B., *J. Am. Chem. Soc*., **2002**, *124*, 14127.

[9]Beletskaya, I. P., Cheprakov, A. V., *Chem. Rev*., **2000**, *100*, 3009.

[10]Eberhard, M. R., *Org. Lett.*, **2004**, *6*, 2125.

[11]Oestreich, M., Sempere-Culler, F., Machotta, A. B., *Angew. Chem. Int. Ed.*, **2005**, *44*, 149.

[12]Kressierer, C. J., Muller, T. J. J., *Angew. Chem. Int. Ed*., **2004**, *43*, 5997.

[13]Sonogashira, K., *Comprehensive Organic Synthesis;* B. M. Trost, I. Fleming (Eds.); Pergamon Press: New York, **1991**.

[14]Garcia, D., Cuadro, A. M., Alvarez-Builla, J., Vaquero, J. J., *Org. Lett*., **2004**, *6*, 4175.

[15]Wolf, C., Liu, S., Mei, X., August, A. T., Casimir, M. D., *J. Org. Chem*., **2006**, *71*, 3270.

[16]De La Mare, P. B. D., *Electrophilic Halogenation: Reaction Pathways Involving Attack by Electrophilic Halogens on Unsaturated Compounds*; Cambridge University Press: London **1976**.

[17]Bedekar, A. V., Gadde, R., Ghosh, P. K., U.S. Patent *US 6838582*, **2004**.

[18]Schmid, H., *Helv. Chim. Acta*, **1946**, *29*, 1144.

[19]Duan, J. X., Zhang, L. H., Dolbier, W. R., *Synlett*, **1999**, 1245.

[20]Auerbach, J., Weissman, S. A., Blacklock, T. J., Angeles, M. R., Hoogsteen, K. N., *Tetrahedron Lett.*, **1993**, *34*, 931.

[21]Konishi, H., Aritomi, K., Okano, T., Kiji, J., *Bull. Chem. Soc. Jpn*., **1989**, *62,* 591.

[22]Ramu, B. C., Sarkar, D. C., Chakraborty, R., *Synth. Commun.,* **1992**, *22,* 1095.

[23]Goldberg, Y., Alper, H., *J. Mol. Catal.*, **1994**, *8*8, 377.

[24]Paul, V., Sudalai, A., Daniel, T., Srinivasan, K. V., *Tetrahedron Lett*., **1994**, *35*, 7055.

[25]Barhate, N. B., Gajare, A. S., Wakharkar, R. D., Bedekar, A. V., *Tetrahedron Lett*., **1998**, *39*, 6349.

[26]Das, B., Venkateswarlu, K., Krishnaiah, M., Holla, H., *Tetrahedron Lett.*, **2006**, *47*, 8693.

[27]Prakash, G. K. S., Mathew, T., Hoole, D., Esteves, P. M., Wang, Q., Rasul, G., Olah, G. A., *J. Am. Chem. Soc.*, **2004**, *126*, 15770.

[28]Das, B., Venkateswarlu, K., Majhi, A., Siddaiah, V., Reddy, K. R., *J. Mol. Catal. A: Chem*., **2007**, *267,* 30.

[29]Ganguly, N. C., De, P., Dutta, S., *Synthesis,* **2005**, 1103.

[30]Kalyani, D., Dick, A. R., Anani, W. Q., Sanford, M. S., *Org. Lett.,* **2006**, *8*, 2523.

[31]Pravst, I., Zupan, M., Stavber, S., *Tetrahedron*, **2008**, *64*, 5191.

[32]Heravi, M. M., Abdolhosseini, N., Oskooie, H. A., *Tetrahedron Lett.*, **2005**, *46*, 8959.

[33]Gnaim, J. M., Sheldon, R. A., *Tetrahedron Lett.*, **2005**, *46*, 4465.

[34]De Almeida, L. S., Esteves, P. M., De Mattos, M. C. S., *Synthesis,* **2006**, 221.

[35]De Almeida, L. S., Esteves, P. M., De Mattos, M. C. S., *Synlett,* **2007**, 1687.

[36]Moriuchi, T., Yamaguchi, M., Kikushima, K., Hirao, T., *Tetrahedron Lett*., **2007**, *48*, 2667.

[37]Karade, N. N., Tiwari, G. B., Huple, D. B., Siddiqui, T. A. J., *J. Chem. Res. Synop.*, **2006**, 366.

[38]Bhatt, S., Nayak, S. K., *Synth. Commun*., **2007**, *37*, 1381.

[39]Choudary, B. M., Someshwar, T., Reddy, C. V., Kantam, M. L., Ratnam, J. K., *Appl. Catal. A: General*, **2003,** *251*, 397.

[40]Podgorsek, A., Stavber, S., Zupan, M., Iskra, J., *Tetrahedron*, **2009**, *65*, 4429.

[41]Smith, M. B., Guo, L., Okeyo, S., Stenzel, J., Yanella, J., LaChapelle, E., *Org. Lett.*, **2002**, *4*, 2321.

[42]Prabhakar, P., Suryakiran, N., Narasimhulu, M., Venkateswarlu, Y., *J. Mol. Catal. A:Chem.*, **2007**, *274*, 72.

Received: 23.06.2015.
Accepted: 14.08.2015.

X-RAY STUDIES OF 2-AMINO-4-ISOPROPYL-5-OXO-4,5-DIHYDROPYRANO[3,2-*c*]CHROMENE-3-CARBONITRILE

Suresh Sharma[a], Goutam Brahmachari[b], Bubun Banerjee[b], Rajni Kant[a] and Vivek K. Gupta[a] *

Keywords: 2-amino-4-isopropyl-5-oxo-4,5-dihydropyrano[3,2-*C*]chromene-3-carbonitrile, X-ray structure, space group, direct methods, π-π interactions.

The title compound, 2-amino-4-isopropyl-5-oxo-4,5-dihydropyrano[3,2-c]chromene-3-carbonitrile ($C_{16}H_{14}N_2O_3$) is synthesized *via* one-pot multi-component reaction (MCR) at room temperature using commercially available urea as inexpensive and environmentally benign organo catalyst and crystallizes in the triclinic space group P -1 with the unit-cell parameters: a = 7.8231(4), b = 8.0622(4), c = 12.3038(5) Å, α = 99.443(4)°, β = 102.419(4)°, γ = 109.907(4)° and Z = 2. The crystal structure was solved by direct methods using single-crystal X-ray diffraction data collected at room temperature and refined by full-matrix least-squares procedures to a final R-value of 0.0405 for 2118 observed reflections. The packing of molecules within the unit cell is stabilized by N-H…O and N-H…N type of intermolecular hydrogen interactions. In addition C-H…π and π-π interactions are also observed in the crystal structure.

*Corresponding Authors
Tel: +91 9419102467
E-Mail: vivek_gupta2k2@hotmail.com
[a] X-ray Crystallography Laboratory, Post-Graduate Department of Physics & Electronics, University of Jammu, Jammu Tawi - 180 006, India
[b] Laboratory of Natural Products & Organic Synthesis, Department of Chemistry, Visva-Bharati (a Central University), Santiniketan – 731235, West Bengal, India.

Introduction

4*H*-Pyran-annulated heterocyclic scaffolds represent a "*privileged*" structural motif well distributed in naturally occurring compounds[1] with a broad spectrum of significant biological activities.[2] Synthetic 2-amino-3-cyano-4*H*-pyrans have been evaluated to possess potent anticancer,[3] antibacterial,[4] antifungal,[5] and anti-rheumatic[6] properties. In this communication, we wish to report the crystal structure of a 4*H*-pyran-annulated heterocyclic compound, namely 2-amino-4-isopropyl-5-oxo-4,5-dihydropyrano[3,2-*c*] chromene-3-carbonitrile which is synthesized *via* one-pot multi-component reaction (MCR) at room temperature using commercially available urea as inexpensive and environmentally benign organocatalyst. The structure of the title compound was elucidated by spectral methods and XRD studies.

Experimental

An oven-dried screw cap test tube was charged with a magnetic stir bar, isobutyraldehyde (0.072 g, 1 mmol), malononitrile (0.066 g, 1.1 mmol), urea (0.007 g, 10 mol % as organo-catalyst), and EtOH:H_2O (1:1 v/v; 4 ml) in a sequential manner; the reaction mixture was then stirred vigorously at room temperature for about 30 min. After that, 4-hydroxycoumarin (0.162 g, 1 mmol) was added to the stirred reaction mixture, and the stirring was continued for 10 h.[7] The progress of the reaction was monitored by TLC. On completion of the reaction, a solid mass precipitated out that was filtered off followed by washing with aqueous ethanol to obtain crude product which was then purified just by recrystallization from ethanol without using column chromatography. White solid. (0.240 gm, yield 85 %). m.p. 524-526 K. IR (KBr) ν_{max}/cm^{-1}: 3379, 3308, 3198, 2962, 2189, 1707, 1666, 1605, 1383, 1317, 1261, 1178, 1061, 960, 754. ^{1}H NMR (400 MHz, DMSO-*d*6) δ/ppm: 7.81 (1H, d, J = 7.6 Hz, , aromatic H), 7.69 (1H, t, J = 7.2 Hz, aromatic H), 7.46 (2H, d, J = 8.0 Hz, , aromatic H), 7.38 (2H, s, NH_2), 3.31 (1H, d, J = 2.8 Hz, C*H*), 2.00 (1H, m, C*H*), 1.01 (3H, d, J = 6.8 Hz, CH_3), 0.69 (3H, d, J = 6.4 Hz, CH_3). ^{13}C NMR (100 MHz, DMSO-*d*6) δ/ppm: 161.21, 160.48, 154.95, 152.46, 133.12, 125.00, 122.53, 121.08, 116.94, 113.38, 105.25, 51.88, 37.53, 33.18, 20.57, 16.89. TOF-MS: 305.0887 $[M+Na]^+$. Elemental analysis: Calcd. (%) for $C_{16}H_{14}N_2O_3$: C, 68.07; H, 5.00; N, 9.92; found: C, 68.03; H, 4.98; N, 9.94.

The structure of 2-amino-4-isopropyl-5-oxo-4,5-dihydropyrano[3,2-*c*]chromene-3-carbonitrile was confirmed by analytical as well as spectral studies including FT-IR, ^{1}H NMR, ^{13}C NMR, and TOF-MS. Single crystals were obtained from DMSO as a solvent. For crystallization 50 mg of compound dissolved in 5 ml DMSO and left for several days at ambient temperature which yielded white block shaped crystals. The chemical structure of title compound is shown in Figure 1.

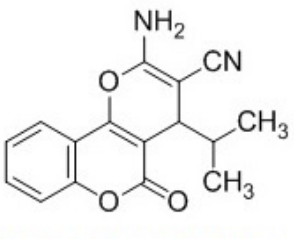

Figure 1. Chemical structure of 2-amino-4-isopropyl-5-oxo-4,5-dihydropyrano[3,2-c]chromene-3-carbonitrile

X-Ray Structure determination

X-ray intensity data of 11113 reflections (of which 2695 unique) were collected on *X'calibur* CCD area-detector diffractometer equipped with graphite monochromated MoKα radiation (λ = 0.71073 Å). The crystal used for data collection was of dimensions 0.30 x 0.20 x 0.20 mm. The cell dimensions were determined by least-squares fit of angular settings of 5360 reflections in the θ range 3.50° to 28.97°**.** The intensities were measured by ω scan mode for θ ranges 3.51° to 25.99°. 2118 reflections were treated as observed (I > 2σ(I)). Data were corrected for Lorentz, polarization and absorption factors. The structure was solved by direct methods using SHELXS97.[8] All non-hydrogen atoms of the molecule were located in the best E-map. Full-matrix least-squares refinement was carried out using SHELXL97.[8] The final refinement cycles converged to an R = 0.0405 and wR (F^2) = 0.1007 for the observed data. Residual electron densities ranged from -0.161 < Δρ < 0.179 eÅ^{-3}. Atomic scattering factors were taken from International Tables for X-ray Crystallography (1992, Vol. C, Tables 4.2.6.8 and 6.1.1.4). The crystallographic data are summarized in Table 1.

Table 1. Crystal data and other experimental details

CCDC Number	**1409950**
Crystal description	Block
Crystal size	0.30 x 0.20 x 0.20 mm
Empirical formula	$C_{16}H_{14}N_2O_3$
Formula weight	282.29
Radiation, Wavelength	MoK_α, 0.71073 Å
Unit cell dimensions	a= 7.8231(4) Å
	b= 8.0622(4) Å
	c= 12.3038(5) Å
	α= 99.443(4)°
	β = 102.419(4)°
	γ= 109.907(4)°
Crystal system, Space group	triclinic , *P-1*
Unit cell volume	688.37(6) Å^3
No. of molecules per unit cell, Z	2
Absorption coefficient	0.096 mm^{-1}
F(000)	296
θ range for entire data collection	3.50 <θ< 28.97
Reflections collected / unique	11113/ 2695
Reflections observed I > 2σ(I))	2118
Range of indices	h= -9 to 9
	k= -9 to 9
	l= -15 to 15
No. of parameters refined	192
Final R-factor	0.0405
$wR(F2)$	0.1007
R_{int}	0.0287
R_σ	0.0236
Goodness-of-fit	1.038
Final residual electron density	-0.161 < Δρ < 0.179 eÅ^{-3}

Result and discussions

An ORTEP [9] view of the compound with atomic labeling is shown in Figure 2. The geometry of the molecule was calculated using the WinGX, [10] PARST[11] and PLATON[12] software.

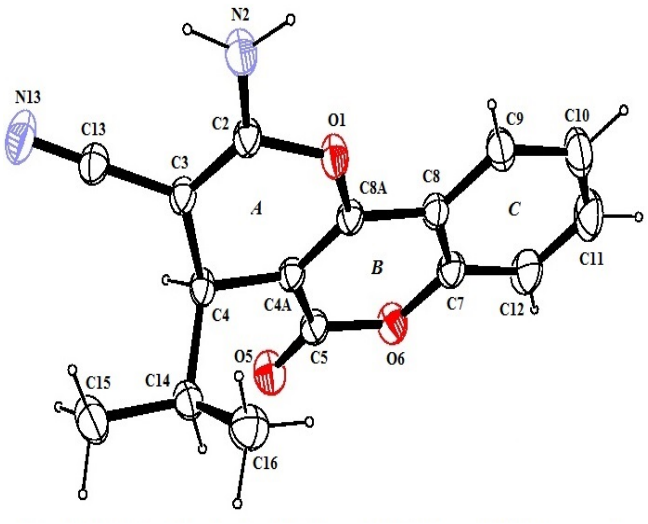

Figure 2. ORTEP view of the molecule with displacement ellipsoids drawn at 40%. H atoms are shown as small spheres of arbitrary radii.

The title compound comprises of three rings in which two are pyran rings (*A* and *B*) and third is phenyl ring (*C*). The pyran ring *A* deviates significantly from planarity and adopts boat conformation with best mirror plane passing through atoms O1 and C4 with asymmetry parameter ΔC_S(O1) = 1.297 and bisecting the bonds C2-C3 and C4A-C8A with asymmetry parameter ΔC_S(C2-C3) = 6.915. The pyran ring *B* and phenyl ring *C* are nearly planar with maximum deviation from planarity is observed for atom C5 by -0.0263 Å in pyran ring *B* and atom C7 by -0.0080 Å in phenyl ring *C* respectively. The pyran ring *B* makes the dihedral angle of 6.00(4)° and 2.13(5)° with the pyran ring *A* and phenyl ring *C* respectively, reflect that all these three rings are nearly coplanar. The mean plane of isopropyl group makes the dihedral angle of 56.75(9)° with pyran ring *A* which reflects that mean plane of isopropyl group deviate significantly from the mean plane of pyran ring *A*. The bond distances O1-C2, O1-C8A, O6-C5 and O6-C7 are 1.3749(16), 1.3648(16), 1.3754(17) and 1.3767(18) Å respectively which are close to each other and agree well with the corresponding values in the related structure. [13] The bond distances C5-O5 and C13-N13 are 1.2072(17) Å and 1.1420(18) Å confirm their respective double and triple bond character and are close to literature values.[14] The bond angles C16-C14-C4, C15-C14-C4 and C16-C14-C15 about the C14 atom of isopropyl group are 112.39(12)°, 111.24(13)° and 110.76(14)° respectively and deviate slightly above the ideal value of 109.5°. The bond angle N13-C13-C3 has the value 179.36(19)°, confirm the linear character of carbonitrile group. Some important bond distances and bond angles are listed in the Table 2. The dihedral angle N2-C2-C3-C13 with value 5.7(3)° reflects that the amino and carbonitrile groups are nearly coplanar. The torsion angle C13-C3-C4-C14 with value -78.28(17)° implies that the carbonitrile and isopropyl group deviate significantly from each other. All other values of torsion angles are reasonable and some important torsion angles are listed in the Table 2.

Analysis of the crystal packing of title compound shows the presence of intermolecular N-H…N and N-H…O hydrogen bonds in the structure [Table 3].

Table 2. Selected bond lengths (Å), bond angles (º) and torsion angles(º) for non hydrogen atoms (e.s.d.'s are given in parentheses)

Bond distances(Å)		**Bond angles(°)**		**Torsion angles(°)**	
O1-C2	1.3749(16)	C16-C14-C15	110.76(14)	N2-C2-C3-C13	5.7(3)
O1-C8A	1.3648(16)	C16-C14-C4	112.39(12)	C13-C3-C4-C14	-78.28(17)
C5-O6	1.3754(17)	C15-C14-C4	111.24(13)	C8A-C4A-C5-O5	-176.69(15)
O6-C7	1.3767(18)	O5-C5-O6	116.55(13)	C4A-C4-C14-C16	59.26(16)
C5-O5	1.2072(17)	O5-C5-C4A	125.42(13)	C3-C4-C14-C15	62.64(16)
C13-N13	1.1420(18)	N13-C13-C3	179.36(19)	C4-C4A-C8A-O1	-4.1(2)
C4-C14	1.549(2)	C8A-O1-C2	118.11(11)	C5-C4A-C8A-C8	-1.9(2)
C2-N2	1.3334(18)	C5-O6-C7	122.01(11)	O6-C7-C8-C8A	3.2(2)

Table 3. Geometry of intermolecular hydrogen bonds

D-H…A	**D-H (Å)**	**H…A (Å)**	**D…A (Å)**	**θ[D-H…A (º)]**
N1-H2A..N13^{i}	0.86	2.22	3.064(2)	166
N2-H2B-O5^{ii}	0.86	2.18	3.018(2)	165
C4-H4-*Cg3*^{iii}	0.98	3.12	3.760(2)	124.32

where *Cg*3 represent the centre of gravity of phenyl ring *C, s*ymmetry codes: i. -x+1,-y+1,-z+1; ii. x+1, y, z; iii. -x, -y+1/2,-z

Table 4. Geometry of π-π interaction

CgI-CgJ	***CgI...CgJ (Å)***	***CgI...P (Å)***	**α(º)**	**β(º)**	**Δ(Å)**
Cg2-Cg2^{i}	3.5077(8)	3.483	0.00	6.75	0.416

where *Cg2* represent the centre of gravity of pyran ring *B; s*ymmetry codes: i. -x, -y+1,-z

Both the hydrogen atoms of amino group are involved in hydrogen bonds with N-H…O interactions link the molecules to form chain like structure and these parallel chains are linked together with N-H…N hydrogen interactions. Further the N-H….N interactions are responsible for the formation of dimmers as shown in Figure 3.

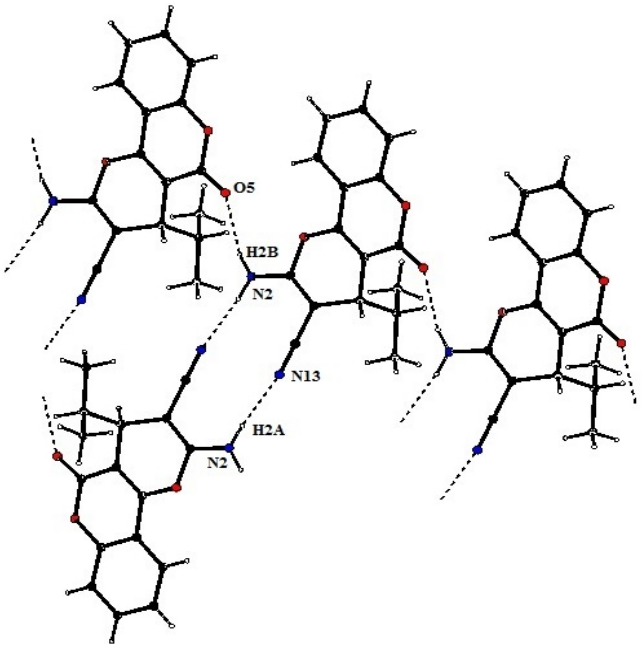

Figure 3. Partial view of intermolecular hydrogen interactions between the molecules.

In addition C-H…π interactions are also observed in the crystal structure. The geometry of these intermolecular hydrogen interactions is given in Table 3. Crystal structure is further stabilized by aromatic π-π stacking interactions and their geometry is given in Table 4.

Acknowledgments

GB is thankful to the CSIR, New Delhi for financial support [Grant No. 02(0110)/12/EMR-II]. BB is grateful to the UGC, New Delhi for awarding him a Senior Research Fellowship.

References

[1]Brahmachari, G., *Handbook of Pharmaceutical Natural Products.* Vol. 1 & 2, Wiley-VCH Verlag GmbH & Co. KGaA: Weinheim, Germany, **2010**.

[2]Raj, T., Bhatia, R. K., Kapur, A., Sharma, M., Saxena, A. K. and Ishar, M. P. S., *Eur. J. Med. Chem.*, **2010**, *45*, 790.

[3]Kemnitzer, W., Drewe, J., Jiang, S., Zhang, H., Zhao, J., Crogan-Grundy, C., Xu, L., Lamothe, S., Gourdeau, H., Denis, R., Tseng, B., Kasibhatla, S. and Cai, S. X., *J. Med. Chem.*, **2007**, *50*, 2858.

[4]Paliwal, P. K., Jetti, S. R. and Jain, S., *Med. Chem. Res.*, **2013**, *22*, 2984.

[5]Kumar, D., Reddy, V. B., Sharad, S., Dube, U. and Kapur, S., *Eur. J. Med. Chem.*, **2009**, *44*, 3805.

[6]Smith, C. W., Bailey, J. M., Billingham, M. E. J., Chandrasekhar, S., Dell, C. P., Harvey, A. K., Hicks, C. A., Kingston, A. E. and Wishart, G. N., *Bioorg. Med. Chem.*, **1995**, *5*, 2783.

[7]Brahmachari, G. and Banerjee, B., *ACS Sustainable Chem. Eng.,* **2014,** *2*, 411.

[8]Sheldrick, G.M., *Acta Cryst.,* **2008,** *A64*, 112.

[9]Farrugia, L.J. *J Appl Cryst.,* **1997,** *30*, 565.

[10]Farrugia, L.J., *J Appl Cryst.,***1999,** *32*, 837.

[11]Nardelli, M., *J Appl Cryst*., **1995,** *28*, 659.

[12]Spek, A.L., *Acta Cryst*., **2009,** *D65,* 148.

[13]Sharma, S., Brahmachari, G., Banerjee, B., Rajni Kant and Gupta, V.K., *Eur. Chem. Bull.,* **2014**, *3(7),* 654.

[14]Allen, F. H., Kennard,O., Watson,D.G., Brammer,L., Orpen,A.G., and Taylor,R. *J. Chem.Soc., Perkin Trans-II.*, **1987**, S1.

Received: 02.07.2015.
Accepted: 14.08.2015.

SPECTROPHOTOMETRIC DETERMINATION OF OXYMETAZOLINE HYDROCHLORIDE VIA CHARGE TRANSFER REACTION USING 2,3-DICHLORO-5,6-DICYANO-1,4-BENZOQUINONE (DDQ) REAGENT

Theia'a N. Al-Sabha[a]*, Nidhal M. S. Mohammed[b] and Payman A. Abdul-Jabar[b]

Keywords: oxymetazoline, 2,3-dichloro-5,6-dicyano-1,4-benzoquinone (DDQ), spectrophotometry, charge transfer complex.

Simple, sensitive and reproducible spectrophotometric method was developed for estimation of oxymetazoline hydrochloride via charge transfer complex formation reaction. The method is based on the reaction of oxymetazoline as n-donor with DDQ reagent as π-acceptor in basic aqueous medium of pH 9.79. The maximum absorption is 421 nm. Beer's law was obeyed in the range 0.4-4.0 μg mL^{-1} with molar absorptivity 2.5 x 10^4 L mol^{-1} cm^{-1}. The limit of detection (LOD) and limit of quantitation (LOQ) were 0.0093 and 0.028 μg mL^{-1} respectively. The stability constant has been determined and the mechanism of the reactions was proposed. The proposed method was applied to determine the oxymetazoline hydrochloride in dosage form as drop, and the results were statistically compared with official BP method.

Corresponding Author
E-Mail: dr_theiaa@yahoo.co.uk
[a] Department of Chemistry , College of Education , University of Mosul, Iraq
[b] Department of Chemistry, Faculty of Science, University of Zakho, Iraq

Introduction

Oxymetazoline hydrochloride[1] (OMZH), 3-[(4,5.dihydro-1*H*-imidazol-2-yl)methyl]-6-(1,1-dimethylethyl)-2,4-dimethylphenol hydrochloride (Figure 1), belongs to non-selective adrenergic drugs and has been m used as eye and nose drops and acting on adrenergic receptors causing a strong vasospasm leading to an increase of a blood pressure.[2] Oxymetazoline is used to treat epitasis and eye redness due to minor irritation.[3,4]

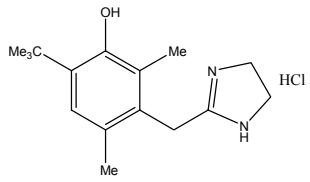

Figure 1. Oxymetazoline hydrochloride.

Various analytical techniques, including high performance liquid chromatography,[2,5-8] liquid chromatographic-mass spectrometry,[9] chemiluminescence[10] and potentiometry[1,11] have been used for the determination of OMZH. These techniques require sophisticated instruments and expensive reagents, and involve several manipulation steps and derivatization reactions. However, spectrophotometric techniques continue to be the most preferred method for routine analytical work due to their simplicity and reasonable sensitivity, along with significant economical advantages. Literature survey revealed that three spectrophotometric methods have been used for determination of OMZH. These methods are based on the reduction of ferric to ferrous ions by OMZH in acidic medium and followed by complexation with 1,10-phenanthroline,[12] potassium ferricyanide[13] and 2,4,6-tris(2-pyridyl)-5-triazine reagent.[14] Other methods used 2,6–dichloroquinone–chlorimide in the presence of an oxidant,[15] 4-aminoantipyrine reagent in the presence of potassium periodate as oxidizing agent[16] and sodium cobaltinitrite in acetic acid medium.[17] Some of these methods are time-consuming, involve extraction procedures or heating and require strictly controlled reaction conditions. Others are less sensitive. The aim of the present work was to provide a simple, sensitive, and rapid spectrophotometric method for determining of OMZH in pure form as well as in pharmaceutical drop formulations via charge transfer reaction using 2,3-dichloro-5,6-dicyano-1,4-benzoquinone (DDQ) reagent.

Experimental

Apparatus

All spectrophotometric measurements are made on a Perkin- Elmer, Lambda 25 U.V- visible double beam spectrophotometer with 1 cm matched silica cells.

Reagents

All chemicals used are of the highest purity available. The following solutions were prepared.

DDQ solution ($1x10^{-3}$M) was prepared freshly by dissolving 0.0227g of DDQ in absolute methanol and diluted to the mark in 50 mL volumetric flask with the same solvent. This solution was prepared daily and used immediately.Standard solution of OMZH (100 μg mL^{-1}) was prepared by dissolving 0.01 g of oxymetazoline.HCl in 5 mL methanol and diluted to the mark with distilled water in 100 mL volumetric flask. This solution was further diluted with water as needed.

Sodium hydroxide solution (1×10^{-2} M) was prepared by dissolving 0.04 g of NaOH in 100 mL of distilled water. Surfactant solutions (0.1 %) were prepared by dissolving of 0.1g of different surfactants (positive, neutral and negative) in 100 mL absolute ethanol.

Recommended procedure

Aliquots of the working solution of OMZH (100 μg mL^{-1}) were transferred into a series of 25 mL calibrated flasks. Then, 1.4 mL of 1×10^{-3} DDQ and 0. 5 mL of 0.01 M NaOH were added and the solutions were diluted to the mark with distilled water. The absorbance was measured at 421.79 nm at room temperature against reagent blank.

Procedure for OMZH assay in Iliadin drops

Five Iliadin drop containers were mixed well and an accurately measured volume solution, equivalent to 5 mg of OMZH was transferred into a 100 mL calibrated flask and diluted to the mark with distilled water. The drug solution was analysed as described in the recommended procedure.

Results and discussion

Spectral characteristics

The proposed method involves the reaction of OXZH as n-donor with DDQ reagent as π-acceptor in the presence of NaOH to form a red colored charge transfer complex having maximum absorption at 421.79 nm. This wavelength was used for all subsequent measurements. The absorption spectra of the reaction product are shown in Figure 2. The corresponding reagent blank has low absorbance at this wavelength.

Optimum reaction conditions

In order to optimize the proposed spectrophotometric method, the effect of some experimental variables was studied. The effects of reagents were studied by measuring the absorbance of solutions containing 3 μg mL^{-1} of OMZH and varied amounts of the reagent separately.

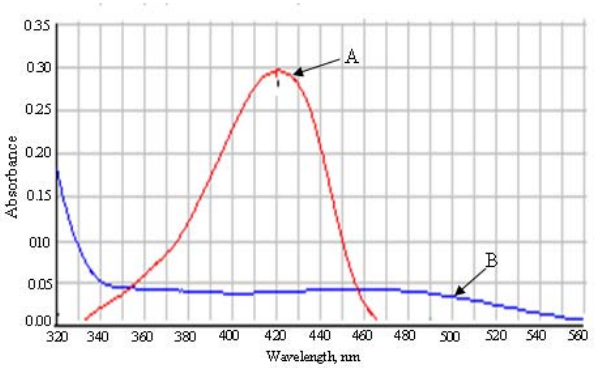

Figure 2. Absorption spectra of (A) OXZH (3 μg mL-1) complex with DDQ reagent(1×10-3M) in the presence of 0.01 M NaOH against reagent blank and (B) reagent blank against distilled water, under optimum conditions.

Effect of solvent

Different solvents such as methanol, ethanol, acetonitrile, acetone and water as medium for the reaction, between OMZH and DDQ, in the presence of NaOH, have been tried in order to achieve maximum sensitivity and complex stability. The absorbance of solutions was measured against corresponding blank after 5 min at room temperature. As shown in Table 1, it was found that on using water as solvent for OMZH and methanol as solvent for DDQ and dilution with water were gave maximum color intensity at 421.79 nm.

Table 1. Effect of solvent on colour intensity of OMZH – DDQ complex.

OMZH solvent	DDQ solvent	Diluent	λ_{max} (nm)	Absor-bance
Water	Methanol	Water	421.79	0.216
Water	Methanol	Methanol	408.99	0.114
Methanol	Methanol	Water	421.83	0.174
Methanol	Methanol	Methanol	413.08	0.071
Water	Ethanol	Water	418.19	0.216
Water	Ethanol	Ethanol	421.95	0.103
Ethanol	Ethanol	Water	422.06	0.132
Ethanol	Ethanol	Ethanol	432.24	0.168

Effect of pH and buffer solution

The effect of pH on the absorption of the complex was studied in basic medium in the range of 8.64-11.31, by using different volumes of 1×10^{-2} M NaOH. It was observed that the complex was formed with low sensitivity at pH 8.64, in the absence of NaOH, but this sensitivity was increased by addition of NaOH and reached its maximum absorption at pH range 9.79-10.86 in the presence of 0.5-1.5 mL NaOH, (Figure 3). Different bases such as sodium hydroxide, potassium hydroxide, sodium carbonate and ammonium hydroxide with fixed volume (0.5 mL) and a concentration of 0.01M were examined. It was found that sodium hydroxide gave maximum color intensity (Figure 4). However; different buffers of pH 9.79, such as borate ($Na_2B_4O_7$+HCl), carbonate (Na_2CO_3+NaOH), bicarbonate ($NaHCO_3$+NaOH) and phosphate (Na_2HPO_4+NaOH) were prepared to examine the sensitivity. A negative effect was observed on the color intensity in comparison with NaOH, (Figure 5).

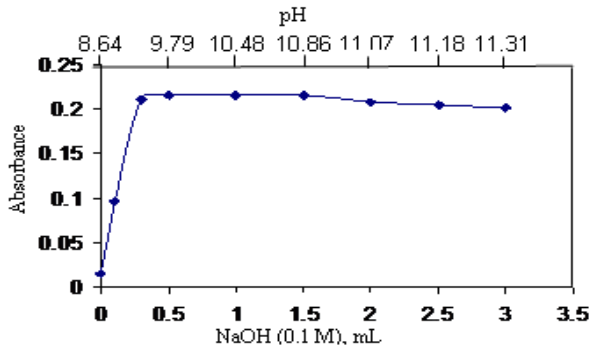

Figure 3. Effect of pH and NaOH on the absorption of 3 μg mL^{-1} OMZH complex with DDQ

Effect of reagent concentration

The effect of changing the DDQ concentration (0-3 mL of 1×10^{-3}M) on the absorbance of a solution containing a fixed amount of OMZH (3 μg mL^{-1}) in the presence of NaOH was studied. It was observed that the absorbance increases with increasing DDQ concentration and reached maximum on using 1.4 mL of 1×10^{-3} M solution (Figure 6). Therefore, this much volume of the solution was used in the subsequent work.

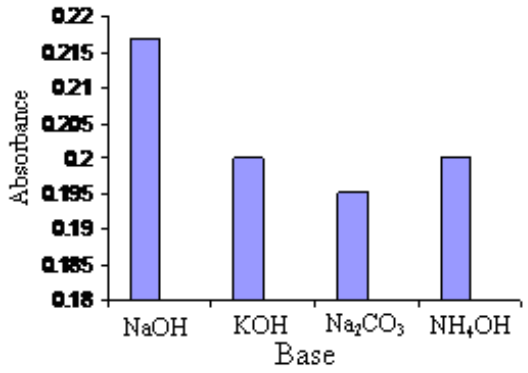

Figure 4. Effect of bases on the absorption of 3 μg mL^{-1} OMZH complex with DDQ.

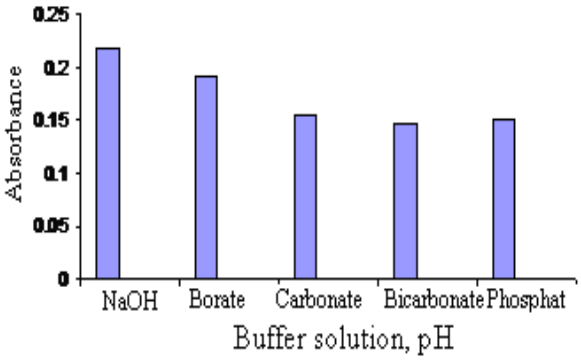

Figure 5. Effect of different buffer solutions on the absorption of 3 μg mL^{-1} OMZH complex with DDQ.

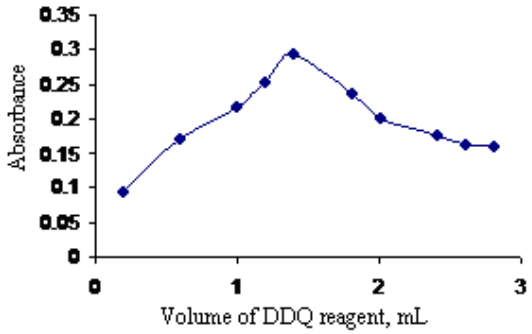

Figure 6. Effect of amount of DDQ reagent on the absorption of 3 μg mL^{-1} OMZH

Effect of the order of addition

In order to obtain the high color intensity, the order of the addition of reagents should be followed as given in the recommended procedure, otherwise a loss in color intensity was observed.

Effect of temperature and reaction time

The reaction time was determined by following the color development at room temperature and in a thermostatically controlled water-bath at different temperatures up to 50°C. The absorbance was measured at 5 min intervals against reagent blank treated similarly. It was observed that the complex was formed after addition of DDQ reagent immediately at room temperature and remained constant for about 15 min after which the absorbance faded (Figure 7).

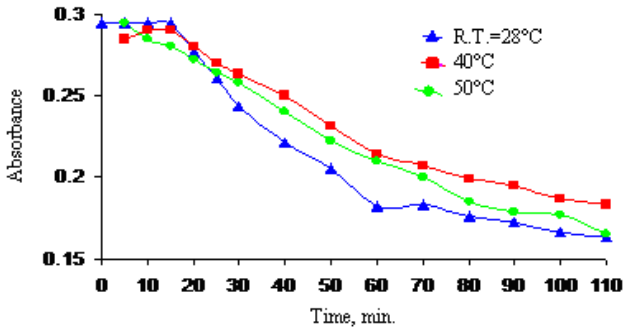

Figure 7. Effect of the time and temperature on the absorbance of 3 μg mL^{-1} OMZH.

Quantification

In order to investigate the range in which the colored complex adhere to Beer's law, the absorbance of the complex was measured at 421.79 nm after developing the colour by following the suggested procedure for a series of solutions containing increasing amounts of OMZH drug. The Beer's law limits, molar absorptivity and Sandell's sensitivity values were evaluated and are given in Table 2, which indicated that the method is sensitive. The linearity was represented by the regression equation and the corresponding correlation coefficient for the OMZH determined by the proposed method represents excellent linearity. The relative standard deviation (RSD) and accuracy (average recovery %) for the analysis of five replicates of each three different concentrations of OMZH indicated that the method is precise and accurate. Limit of detection (LOD) and limit of quantitation (LOQ) were calculated according to the following eqns. (1) and (2).

$$LOD = 3.3\sigma/b \quad (1)$$

$$LOQ = 10\sigma/b \quad (2)$$

where σ is the standard deviation of five reagent blank determinations and b is the slope of the calibration curve. The results obtained are in the accepted range below the lower limit of Beer's law range, (Table 2).

Table 2. Summary of optical characteristics and statistical data for the recommended method.

Parameter	Value
Beer's law limits	0.5-3.2 μg mL^{-1}
Molar absorptivity	2.5×10^4 L mol^{-1} cm^{-1}
LOD	0.0093 μg mL^{-1}
LOQ	0.028 μg mL^{-11}
Average recovery (%)**	99.488
Correlation coefficient	0.9825
Slope, *a*	0.0935
Intercept, *b*	0.0406
*RSD***	≤ 1.47

* $Y = a X + b$, where X is the concentration of OMZH in μg mL^{-1}.
** Average of five determinations

Interference

The extent of interferences by some excipients which are often present in pharmaceutical preparations were studied by measuring the absorbance of solutions containing 3 μg mL^{-1} of OMZH and various amounts of diverse species in a final volume of 25 ml. It was found that the studied excipients do not interfere in the determination of OMZH in its dosage forms. An error of 5.0 % in the absorbance readings was considered tolerable. Typical results are given in Table 3.

Table 3. Effect of excipients on the assay of OMZH.

Exciepient	Recovery (%) of OMZH (3 μg mL^{-1}) in the presence of exciepients (μg mL^{-1})			
	50	100	150	200
NaCl	95	96	98	105
Lactose	95	94	104	98
Glucose	105	108	103	99
Starch	103	95	96	95
Acacia	95	104	103	101

Analytical application

The proposed method was successfully applied to determine OMZH in its pharmaceutical preparation as nasal drops. The obtained results were compared statistically by a Student's *t*-test for accuracy with the official method[1] (depending on potentiometric titration for pure drug using 0.1 M perchloric acid) at the 95 % confidence level with three degrees of freedom. The results showed that the experimental *t*-test and *F*-test with three degrees of freedom are 1.37 and 4.31 respectively, which are less than the theoretical value ($t = 4.303$, $F = 9.28$), indicating that there was no significant difference between the proposed method and official method, (Table 4).

Stoichiometry, stability constant and reaction mechanism

The molar ratio of the complex formed between OMZH and DDQ reagent was investigated by applying the mole ratio and continuous variation (Job's) methods.[18] The results indicated that complex was formed in the ratio of 1:2 OMZH : DDQ (Figure 8). This finding supports that the n-π* CT complex is formed through an interaction of hydroxyl and amino groups.[19,20].

According to the results described above, the apparent stability constant was estimated by comparing the absorbance of a solution containing stoichiometric amounts of each OMZH and DDQ (A_s) to one containing an excess of DDQ reagent (A_m). The average conditional stability constant of the complex was calculated by applying the following equations.

$$K_{st}=1-\alpha/ 4\alpha^3C^2 \quad (3)$$

$$\alpha = A_m-A_s/A_m \quad (4)$$

where K_{st} is the stability constant, α the dissociation degree and C is the concentration of the complex which is equal to the concentration of OMZH.

Table 4. Assay of *OMZH* in pharmaceutical nasal drops using the proposed method, standard addition procedure

Procedure applied	Name	Amount present (μg mL^{-1})	Recovery (%)	Average recovery (%)*	Drug found (mg)	Stated value (mg)
Proposed method	Iliadin drops	1 2 3	101.6 97.7 99.1	99.48	2.32	2.5
Standard Addition method	Iliadin drop	1 2	102.0 99.0	100.5	2.51	2.5
British Pharmacopiea method		200 mg	100.9 103.1 102.0	102.0	204	200

The results shown in Table 5 indicate that the complex is stable.

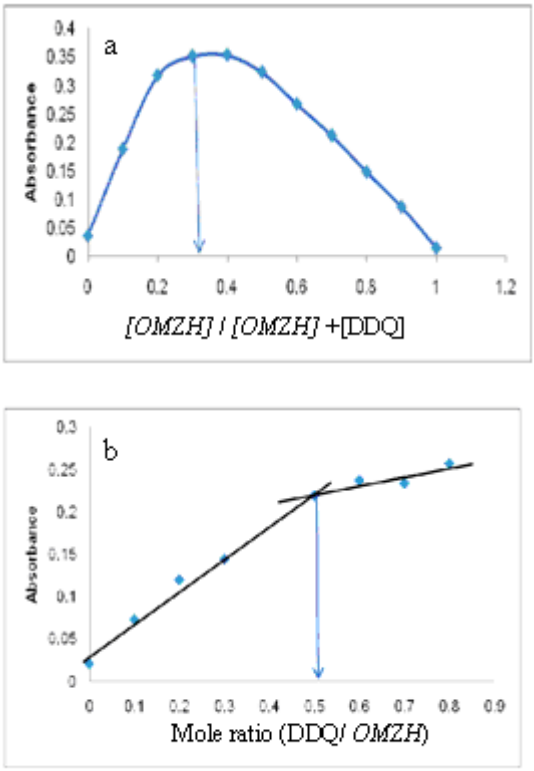

Figure 8. Continuous variation (a) and mole ratio (b) plots for OMZH-DDQ complex under the optimum conditions.

Table 5. Stability constant of *OMZH* -DDQ complex.

Volume, mL	Conc. mM	Absorbance		α	Average K_{st}, L mol^{-1}
		A_s	A_m		
0.4	0.032	0.175	0.280	0.375	9.01×10^9
0.8	0.064	0.310	0.388	0.201	
1.2	0.096	0.355	0.399	0.110	

The interaction of OMZH, as n-donor with DDQ, as π-acceptor is a charge-transfer complexation, followed by the formation of a radical ions. Complete electron transfer from the donor to the acceptor moiety took place with the formation of intensely colored radical ions with high molar absorptivity values. However, the probable reaction mechanism is given in Scheme 1.

Comparison with the reported methods

Table 6 shows the comparison between some of analytical variables obtained from present method with that of the recent spectrophotometric methods. From the table, the proposed method is more sensitive than some other methods, simple, carry on at room temperature and take short time for color development.

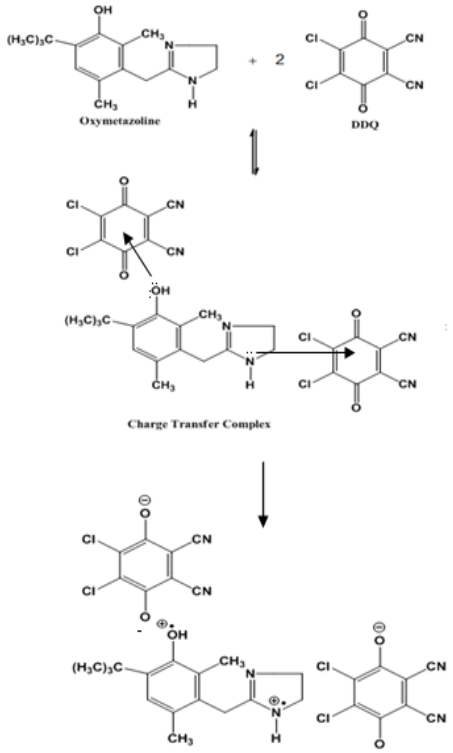

Scheme 1. Proposed reaction mechanism for assay of OMZH

Table 6. Comparison of the present method with reported spectrophotometric methods.

Parameters	Methods		
	DDQ	Ferroin[12]	4-Amino-antipyrine[16]
λ_{max}, nm	420	510	480
pH	9.79	---	13.15
Solvent	water	water	water
Temp.°C	R.T.	70	70
Development time, min	5	40	25
Stability period, min	15	60	60
Beer's law range, µg.ml^{-1}	0.5-3.0	0.1-7.0	1.0-20.0
Molar absorptivity, L mol^{-1} cm^{-1}	2.5×10^4	5.74×10^4	5.34×10^3
Recovery (%)	99.48	100.53	~ 99
RSD (%)	≤ 1.47	≤ 1.6	0.36-1.58
Type of reaction	Charge transfer	Oxidation-reduction	Oxidative coupling
Applications	Iliadin Drop 0.025%	Nazordin 0.05% Oxymet 0.025%	Nazordin 0.05% Oxymet 0.025%

Conclusion

The proposed method is simple and more sensitive than most of the previously reported spectrophotometric methods. The statistical parameters and the recovery test data indicate the high reproducibility and accuracy of the proposed method. Analysis of authentic samples containing *OMZH* showed no interference from common additives and auxiliary substances. Hence, this method can be considered for the determination of *OMZH* in both pure form and in pharmaceutical preparations**.**

References

[1]*British Pharmacopoeia* (2005), version 4, CD-ROM, Her Majesty's Stationery Office, pp. 1185.

[2]Stanszis, B., Nowinski, W., *Acta Polon. Pharm -Drug Res.*, **2000**, *57*, 399.

[3]Katz, R.I., Hovagim, A.R., Finkelstein, H.S., Grinberg Y., Boccio, R.V., Poppers, P.J., *J. Clin. Anesth*., **1990**, *2*,16-20

[4]Krempl G.A., Noorily, A.D., *Ann Otol. Rhinol. Laryngol.*, **1995**, *104*, 704.

[5]Hoffmann T. J., Thompson R. D., Seifert J. R., *Drug Dev. Ind. Pharm.*, **1989**, *15*, 743.

[6] Sane R.T., Joshi L.S., Ladage K.D., Kothurkar R.M., Bhate, V.R., *Indian J. Pharm. Sci.*, **1990,** *52*, 38.

[7]Starsz, B., Nowinski, W., *Acta Polon. Pharm*., 2001, 57, 344.

[8]Sirimas, S., Leonard, K., David, A. W., *J. Pharm. Biomed. Anal*., **2006**, *40*, 1273.

[9]Hayes, F. J., Baker, T. R., Dobson, R. L. M., Tsueda, M. S., *J. Chromatogr A*, **1995**, *692*, 73.

[10]García-Campaña, A. M., Sendra, J. M. B., Vargas, M. P. B., Baeyens, W. R. G., Zhang X., *Anal. Chim. Acta*, **2004**, *516*, 245.

[11]Issa, Y.M., Zayed, S.I., *Anal. Sci.*, **2004** ,*20*, 297.

[12]Al-Sabha, T. N., Rasheed, B. A., *Jordan J. Chem.*, **2011**, *6*, 403.

[13]Othman, N. S., Fathe, S. A., *Raf. J. Sci.*, **2013**, *24*, 84.

[14]Sankar, D. G., Sastry, C. S. P., Ready, M. N., Akuna, M., *Indian J. Pharm . Sci.,***1988**, *50*, 178.

[15]Snakar D.G., Sastry C.S.P., Ready M.N. and Prasad S. Ind. R., *Ind. J. Pharm .Sci.*, **1987,** *49*,69.

[16]Zakaria, S. A., *Raf. J. Sci.*, **2011**, *22*, 97.

[17]Shingbal, D. M., Naik, S. D., *East Pharm.*, **1983**, *26*, 201.

[18]Hargis, L.G., "*Analytical Chemistry, Principles and Techniques*", Prentice- Hall Inc., New Jersey, **1988,** pp. 424- 427.

[19]Bhattacharya, S., Banerjee, M. Mukherjee, A. K., *Spectrochim. Acta Part A,* **2001**, *57*, 2409.

[20]Datta, K., Mukherjee, A. K., Banerjee, M., Seal, B. K., *Spectrochim. Acta Part A,* **1997**, *53*, 2587.

Received: 20.07.2015.
Accepted: 14.08.2015.

CHANGES IN THE CONTENT OF SUGARS AND ORGANIC ACIDS DURING RIPENING OF *COFFEA ARABICA* AND *COFFEA CANEPHORA* FRUITS

Yukiko Koshiro[a], Mel C. Jackson[b], Chifumi Nagai[b] and Hiroshi Ashihara[a]*

Keywords: sucrose, citric acid, malic acid, quinic acid, seed, pericarp, *Coffea arabica*, *Coffea canephora*.

Changes in concentration (% of dry weight) and content (mg/organ) of sucrose, glucose, fructose and some organic acids in pericarps and seeds of *Coffea arabica* cv. Mokka, *C. arabica* cv. Catimor and *C. canephora* were monitored during the development and ripening of fruits. The coffee fruits were categorized into five stages 1 to 5 which corresponded to small, medium and large sizes of green fruits, ripening (pink) fruits and fully-ripened (red) fruits, respectively. In all samples, the major sugars in young fruits (stage 1) were fructose (~5 % dry weight) and glucose (~3 % dry weight). Significant amounts of sucrose were also found in the later stages of development. The concentration of sucrose in ripened pericarp and seeds (stage 5) in two cultivars of *C. arabica* (19–25 % of dry weight in pericarp and 8–18% in seeds) was higher than those in *C. canephora* (8 % in pericarp and 5 % in seeds). Sucrose was accumulated exclusively in seeds of two cultivars of *C. arabica*. In contrast, both sucrose and the reducing sugars, fructose and glucose, accumulated in pericarps of all coffee samples and in seeds of *C. canephora*. The concentration of malic acid, citric acid, lactic acid, oxalic acid and quinic acid changed during development and ripening of fruits. The values of most organic acid fluctuated between 0–1%, except for a transient, high content of quinic acid (>2%) in young fruits. Characteristic accumulation patterns of organic acids were found in different organs; citric acid concentration was high in seeds, but malic acid or oxalic acid was high in pericarps. Possible metabolic routes of metabolites are discussed.

*Corresponding Authors
Fax: +81-3-5700-4225
E-Mail: ashihara.hiroshi@ocha.ac.jp
[a] Department of Biology, Ochanomizu University, Tokyo, 112-8610, Japan
[b] Hawaii Agriculture Research Center, Kunia, Hawaii, 96759 USA

Introduction

Coffea arabica and *C. canephora*, belonging to the Rubiaceae family, are woody, perennial, evergreen dicotyledonous species that are cultivated to produce, respectively, Arabica and Robusta coffee beans. Coffee seeds accumulate sizable amounts of caffeine, trigonelline, chlorogenic acids and sucrose.[1,2] Therefore, the biochemistry and metabolism of coffee plants are interesting from the viewpoint of the diversity of nitrogen and carbohydrate metabolism. In addition, these coffee seed constituents seem to be closely related to the quality of commercial coffee beans.[1] Caffeine and chlorogenic acids increase bitterness, while sucrose and trigonelline are converted to aroma compounds.[3] It has been generally believed that the higher cup quality of *C. arabica* coffee compared to *C. canephora* may be depended on the higher content of trigonelline and sucrose and low levels of caffeine and chlorogenic acids.[4] As a result, concentration of these compounds in seeds before and after roasting were often surveyed by food chemists.[5-8]

As part of a series of our research to elucidate the metabolism in coffee plants, we have reported the fluctuation of the levels of caffeine, trigonelline and chlorogenic acids in pericarps and seeds during growing and ripening fruits of *C. arabica* and *C. canephora*.[9,10] In the present study, we determined the levels of sugars and organic acids in fruits of *C. arabica*, cv. Mokka and cv. Catimor and *C. canephora*. Rogers et al.[11] reported the changes in the levels of various metabolites including sugars and organic acids in developing coffee seeds, but the comparison of metabolites in seeds and pericarps have not been carried out. From the results obtained, we discuss the accumulation profile of sugars and organic acids and possible metabolic pathways related to the biosynthesis of these metabolites.

Experimental

Plant mMaterial

Fruits of *Coffee arabica* cv. Mokka (MA2-7) and cv. Catimor (T5175-7-1), and *Coffea canephora* (#6621), were harvested at the Experimental Station of Hawaii Agriculture Center, Kunia Station, Oahu Island, Hawaii in 2003. These coffee trees were cultivated at the same site at an altitude of ~150 m above sea level. Initially, we collected coffee fruits at the defined dates after flowering using the same branches of the same trees. However, growth of individual fruits varies widely. We therefore defined the growth stages from the sizes and colour of the fruits. In the present study, fruits were divided into five stages according to the growth and maturity of coffee fruits. The final sizes of fruits differed between three plant materials; *C. arabica* cv. Catimor fruits (~1900 mg dry weight) were larger than *C. arabica* cv. Mokka (~500 mg dry weight); *C. canephora* fruits (~480 mg dry weight) were similar but slightly smaller than Mokka.

Analysis of endogenous sugars and organic acids

After harvesting, whole fruits (stage 1) or pericarps and seeds of fruits (stages 2-5) were immediately frozen and lyophilized, and ground to a fine powder using an IKA

Universalmühle M20 blade grinder (IKA-Labortechnik, Staufen, Germany). A powdered sample (~1 g) was mixed with 10 ml of 50 % (v/v) methanol containing 8 mM sulphuric acid. The sample was sonicated for 15 min and then filtered through a glass microfiber filter (Whatman, Grade GF/A), and a 5 ml aliquot of filtrate was evaporated to a volume of less than 2.5 ml using a rotary evaporator. Distilled water was added to make a final volume of 5 ml. The extract (2 ml) was passed through a 1.0 ml bed volume Sep-Pak C18 SPE cartridge (Waters), preconditioned with 1 ml of methanol. Residual unbound extract was eluted by addition of 1 ml of distilled water. The eluent was then filtered through a 0.45 µm nylon filter (Millipore), prior to HPLC.

For HPLC analysis, a Shimadzu SCL-10A controller and LC-10AS pump (Shimadzu Corporation, Japan) were used. Chromatographic separations were achieved using a Rezex ROA organic acid ion exchange column (300 x 7.5 mm) with a Carbo-H^+ guard column (4 mm x 3 mm), (Phenomenex USA, Torrance, CA). The mobile phase consisted of 6.5 mM sulphuric acid in distilled water at a flow rate of 0.4 ml/min. The 24 min run time was followed by a column wash step using a mobile phase of distilled water at a flow rate of 0.52 ml/min for 10 min. The column was re-equilibrated using the original mobile phase at a flow rate of 0.52 ml/min for further 27 min. Sugars and organic acid was detected using a Waters 410 differential refractometer (Waters Associates) and a Shimadzu SPD-10A UV-VIS detector.

Results and discussion

Growth stages of coffee fruits

As mentioned in a previous paper,[12] we have defined the five growth stages of coffee fruits from the sizes and maturation. In the initial stage of coffee fruit development, the fruits consist of pericarp and perisperm. In the later stage, the locular space of seeds is progressively filled with endosperm, up to full seed maturity.[13,14] Whole fruits were therefore used in the stage 1, whereas in the later stages, pericarp and seeds were separated and used in the estimation of caffeine and the content of metabolites.

Fruits of stages 1 to 3 are green-coloured small, medium and large sizes. They corresponded approximately to the rapid expansion and pericarp growth stage, the endosperm formation stage and the dry matter accumulation stage as described by Cannell.[15] Fruits of stage 4, contained pre-ripened seeds, and the fruit skin colour had changed from green to pink. Fruits at stage 5 were fully ripened and red coloured.

Changes in sugar contents

In *Coffea* fruits, sucrose, glucose and fructose are major free sugars. Changes in the concentration of these sugars are expressed as a percent of dry weight and shown in Table 1. Small amounts of glucose and fructose were found in whole fruits at stage 1 and pericarps and seeds at stage 2, but little or no amount of sucrose was detected in any of the samples. In green-coloured large size fruits (stage 3), accumulation of sucrose began in seeds (Figure 1). The concentration in *C. arabica* (6.8% and 4.3% for cv. Mokka and cv. Catimor, respectively) were higher than in *C. canephora* (1.3%). During ripening of fruits, the sugar contents increased both in pericarp and seeds (Figure 1). In pericarps of all the *Coffea* fruit examined, fructose and glucose had accumulated accompanied by an increase in sucrose. In contrast, the major sugar in seeds of *C. arabica* cv. Mokka and cv. Catimor was sucrose (9.9 % and 8.4 % of dry weight, respectively) which, respectively comprised 73 % and 67 % of the total sugars of stage 5 seeds. In contrast, sucrose concentration in *C. canephora* (4.6 % of dry weight) in stage 5 seeds was lower at 27 % of total sugar content (Table 1). In ripened pericarp, total sugar contents in two varieties of *C. arabica* comprised more than 50 % of the dry weight, while the level in *C. canephora* was 26 % of dry weight.

Table 1. Concentration of sucrose (Suc), glucose (Glu) and fructose (Fru) in pericarps and seeds of coffee fruits.

	Stage	Pericarp			Seed		
		Suc	Glu	Fruct	Suc	Glu	Fru
C. arabica cv. Mokka	1*	0.00	3.11	4.98			
	2	0.00	0.57	1.22	0.00	1.62	1.89
	3	1.10	1.47	2.57	6.80	0.00	0.44
	4	12.03	10.42	13.53	10.35	0.88	1.56
	5	19.33	13.47	17.35	9.89	1.54	2.18
C. arabica cv. Catimor	1*	0.00	2.87	4.55			
	2	0.36	0	0.03	0.20	0.00	0.76
	3	1.20	3.98	3.91	4.30	0.78	1.73
	4	10.50	6.51	9.22	4.99	0.62	1.08
	5	24.48	11.94	16.36	8.44	1.62	2.46
C. canephora	1*	0.00	3.06	4.93			
	2	0.00	0.08	0.56	0	0.28	0.84
	3	0.00	0.48	2.03	1.31	0.39	1.23
	4	2.65	2.46	6.61	2.18	0.00	0.80
	5	8.08	5.34	12.63	4.56	5.08	7.18

Values are shown as % of dry weight. *Whole seeds were used in stage 1 and shown in the pericarp column.

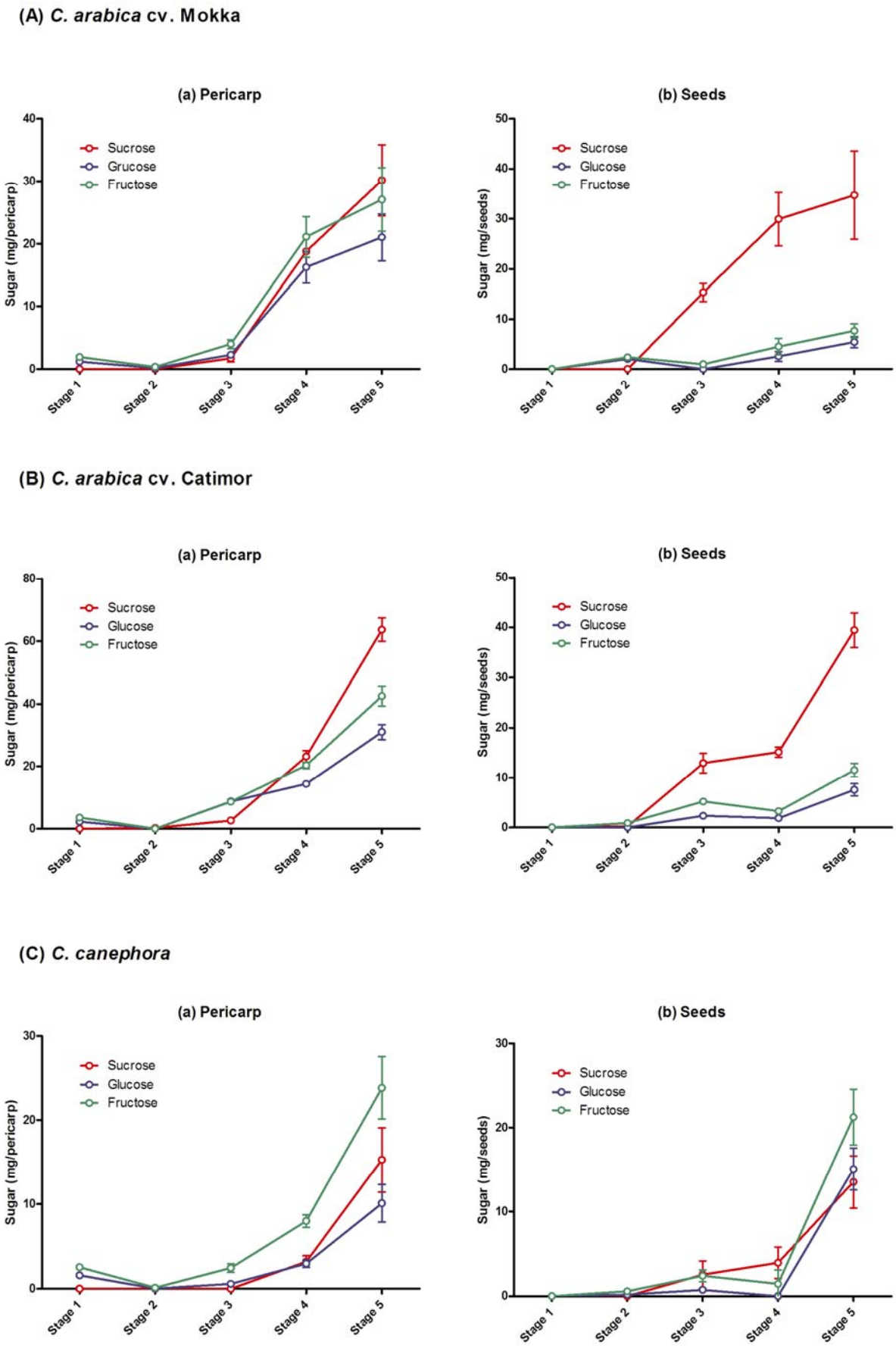

Figure 1. Accumulation of sucrose, glucose and fructose in a pericarp (a) and seeds (b) of *Coffea arabica* cv. Mokka (A), *C. arabica* cv. Catimor (B) and *C. canephora* (C) fruits. A fruit contained two seeds; therefore, the values are expressed as mg per a pericarp (a) or mg per two seeds (b) and SD whole fruits were used in stage 1 and shown the pericarp figures.

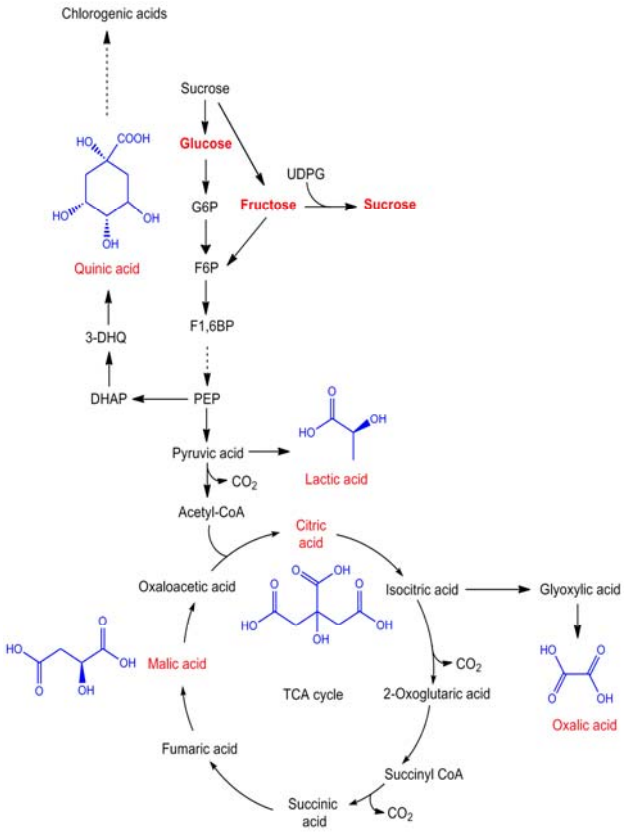

Figure 2. Structures and possible biosynthetic pathways of major organic acids in coffee fruits. DHAP, 3-deoxy-D-arabino-heptulosonic acid 7-phosphate; 3-DHQ, 3-dehydroquinic acid; F1,6-BP, fructose-1,6-bisphosphate; F6P, fructose-6-phosphate; G6P, glucose-6-phosphate; PEP, phosphoenolpyruvate; UDPG, UDP-glucose.

Rogers et al.[11] also reported that the levels of glucose and fructose were higher than sucrose in young coffee seeds, but at the end of seed development, sucrose became the major free sugar as a consequence of decrease in the two reducing sugars.

Although the varieties of coffee plants in their research were different from our studies, the sucrose content in *C. arabica* (5–12% of dry weight) was higher than that of *C. canephora* (4–5% of dry weight). Therefore, a higher concentration of sucrose in *C. arabica* compared in *C. canephora* seems to be an inherent character.

Changes in organic acid contents

The present study revealed that the major organic acids in coffee fruits are quinic acid, malic acid, citric acid, lactic acid and oxalic acid. Structures of these organic acids and possible biosynthetic routes in coffee fruits are illustrated in Figure 2. Quinic acid is synthesized from 3-dehydroquinic acid, an intermediate of the shikimic acid pathway.[16] Malic acid and citric acid are members of the tricarboxylic acid cycle (TCA) cycle and lactic acid is formed from pyruvic acid, the end product of glycolysis.[17]

Three pathways for oxalic acid biosynthesis have been proposed in plants, oxidation of glyoxylic acid, catabolism of ascorbic acid and oxaloacetic acid breakdown. Although no research has been published on oxalic acid biosynthesis in coffee plants, a recent study using transgenic rice plants revealed that glyoxylic acid rather than ascorbic acid or oxaloacetic acid is the principal precursor for oxalate biosynthesis.[18]

Quinic acid accumulated in pericarps during the first three stages of development of *C. arabica* and *C. canephora* fruit and then decreased during maturation (Figure 3). The maximum concentrations of quinic acid in pericarps were found in stage 2 of *C. arabica*, cv. Catimor (2.5% of dry weight) and C. canephora (1.6%) and in stage 3 of *C. arabica* cv. Mokka (0.9%), while the concentrations declined in stage 5 of all samples to 0.4–0.5% of dry weight (Table 2). In seeds of all coffee samples, the highest quinic acid concentration occurred at stage 2 (0.5–2.0% of dry weight) and lower values (0.2–0.3 %) were found in stage 5.

Table 2. Concentration of organic acids in pericarps and seeds of coffee fruits.

	Stage	Pericarp					Seed				
		Qui	Mal	Cit	Lac	Oxa	Qui	Mal	Cit	Lac	Oxa
C. arabica cv. Mokka	1*	1.076	0.166	0.234	0.210	0.520					
	2	0.464	0.182	0.164	0.389	0.220	0.500	0.190	0.253	0.412	0.501
	3	0.930	0.605	0.270	0.558	0.809	0.240	0.334	0.689	0.191	0.096
	4	0.679	1.102	0.170	0.601	0.970	0.331	0.528	0.822	0.205	0.156
	5	0.437	0.932	0.276	0.456	1.070	0.270	0.419	0.618	0.171	0.198
C. arabica cv. Catimor	1*	0.550	0.076	0.032	0.186	0.270					
	2	2.460	0.909	0.984	1.665	1.414	0.704	0.425	0.287	0.896	0.502
	3	1.331	0.799	0.336	0.927	0.391	0.344	0.391	0.414	0.37	0.192
	4	0.810	0.829	0.184	0.625	0.355	0.196	0.326	0.489	0.247	0.168
	5	0.383	0.765	0.239	0.375	0.266	0.190	0.332	0.412	0.194	0.141
C. canephora	1*	0.633	0.000	0.071	0.358	0.343					
	2	1.577	0.223	0.229	1.012	0.570	2.045	0.000	0.034	0.151	0.187
	3	1.483	0.253	0.776	1.483	0.967	0.428	0.168	0.244	0.289	0.216
	4	1.006	0.586	0.000	1.566	0.716	0.174	0.331	0.321	0.274	0.165
	5	0.493	0.742	0.323	0.907	0.633	0.183	0.314	0.511	0.306	0.223

Values are shown as % of dry weight. *Whole seeds were used in stage 1 and shown in the pericarp column. Qui, quinic acid; Mal, malic acid; Cit, citric acid; Lac, lactic acid; Oxa, oxalic acid.

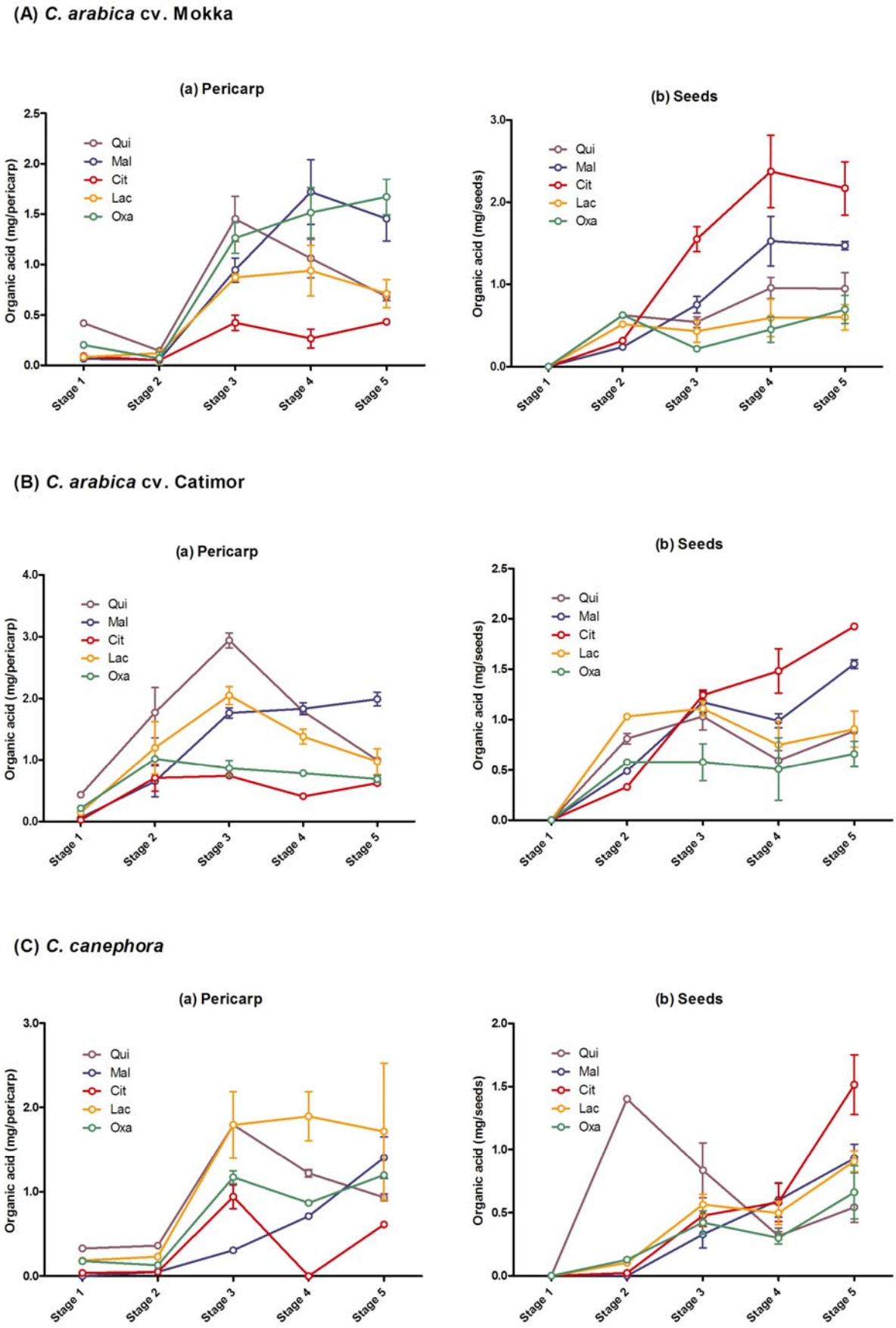

Figure 3. Fluctuation of levels of quinic acid (Qui), malic acid (Mal), citric acid (Cit), lactic acid (Lac) and oxalic acid (Oxa) in a pericarp (a) and seeds (b) during development and ripening of *Coffea arabica* cv. Mokka (A), *C. arabica* cv. Catimor (B) and *C. canephora* (C) fruits. The values are expressed as mg per a pericarp (a) or mg per two seeds (b) and SD whole fruits were used in stage 1 and shown the pericarp figures.

Rogers et al.[11] also reported that high concentration of quinic acid in young coffee seeds and the levels decreased to much lower levels in the end of seed development. Since quinic acid is a polyol moiety of chlorogenic acids, its transient accumulation may be related to its utilization for the synthesis of chlorogenic acids.[10]

The pattern of accumulation of carboxylic acids in pericarp and seeds was different; the most significant difference was found in the accumulation of citric acid which is a major carboxylic acid in seeds (Fig. 3). Concentrations of citric acid in the stage 5 seeds were 0.6 %, 0.4 % and 0.5 % of dry weight of *C. arabica*, cv. Mokka, *C. arabica*, cv. Catimor and *C. canephora*, respectively. In contrast, concentrations of malic acid (0.7–0.9% of dry weight) were higher than those of citric acid (0.2–0.3% of dry weight) in pericarps of all coffee fruit samples (Table 2). Substantial quantities of lactic acid were found in pericarps (0.2–1.7% of dry weight) and seeds (0.2–0.9% of dry weight) in all coffee samples examined (Table 2). Oxalic acid content in pericarp (0.2–1.4% dry weight) is usually higher than in seeds (0.1–0.5% dry weight). Accumulation of oxalic acid was found in pericarps of *C. arabica* cv. Mokka (Figure. 3).

Conclusion

In fruits of coffee plants, sugars and organic acids are synthesized from photosynthates, mainly sucrose, transported from leaves or the epidermal tissues of fruits. Although the detailed metabolic and enzymatic studies have not been investigated in coffee, sucrose transported to sink tissues seems to be degraded to glucose and fructose by invertase and/or UDP-glucose and fructose by sucrose synthase.[19] In *C. arabica*, it has been shown that activity of invertase is higher than that of sucrose synthase in early stages of fruits development.[20] In the growing and developing stages of coffee fruits, hexoses are actively metabolized and organic acids appeared to be synthesized as shown in the routes illustrated in Figure 2.[12] During maturation and ripening stage of coffee fruits, storage of sucrose was initially accompanied by the reduction of metabolic activity,[12] Geromel et al.[20] reported the contribution of sucrose synthase, but not sucrose phosphate synthetase, is important for sucrose accumulation in *C. arabica* seeds at this stage of development. Turnover of carboxylic acids appears to be rapid during fruit development stages where active respiration occurs.[12] In the later stages of fruit ripening, metabolic activity declines and these organic acids may be accumulated as storage compounds. Seed specific accumulation of sucrose and citric acid was observed in both *C. arabica* and *C. anephora*. Arguably, this may be caused by special metabolism in seeds and/or the specific transport of sucrose and citric acid from pericarp to seeds.

The data obtained in this study are important to understand the primary and secondary metabolism of coffee plants. In addition these data are of value when considering metabolic engineering to produce higher quality coffee beans. Since the pericarp of coffee, especially *C. arabica*, contains high concentrations of sugars and organic acids, this tissue also has commercial value which may be used for beverage production.

References

[1]Clarke, R. J. and Vitzthum, O. G., *Coffee Recent Development*, Blackwell Science, **2001**, 1-257.

[2]Crozier, A., Ashihara, H. and Tomas-Barberan, F., *Teas, Cocoa and Coffee: Plant Secondary Metabolites and Health*, Wiley-Blackwell, **2012**, 1-252.

[3]Ky, C., Louarn, L.J., Dussert, S., Guyot, B., Hamon, S. and Noirot, M., *Food Chem.*, **2001**, *75*, 223-230.

[4]Bertrand, B., Guyot, B., Anthony, F. and Lashermes, P., *Theor. Appl. Genet.*, **2003**, *107*, 387-394.

[5]Clarke, R. J., *Quality Control in the Food Industry, Vol. 4, Second Ed.* Academic Press, **1987**, 161-191.

[6]Franca, A.S., Mendonca, J.C.F. and Oliveira, S. D., *LWT-Food Sci. Technol.*, **2005**, *38*, 709-715.

[7]Farah, A., Monteiro, M.C., Calado, V., Franca, A.S. and Trugo, L.C., *Food Chem.*, **2006**, *98*, 373-380.

[8]Mazzafera, P. *Food Chem.*, **1999**, *64*, 547-554.

[9]Koshiro,Y., Zheng, X., Wang, M., Nagai, C. and Ashihara, H., *Plant Sci.*, **2006**, *171*, 242-250.

[10]Koshiro,Y., Jackson, M.C., Katahira, R., Wang, M., Nagai, C. and Ashihara, H., *Z. Naturforsch.* **2008**, *62c*, 731-742.

[11]Rogers, W. J., Michaux, S., Bastin, M. and Bucheli, P., *Plant Sci.*, **1999**, *149*, 115-123.

[12]Koshiro, Y., Nagai, C. and Ashihara, H., *Eur. Chem. Bull.*, **2015**, *4*, 296-302.

[13]Mendes, A. J. T., *Amer. J. Bot.*, **1941**, *28*, 784-789.

[14]Rogers, W. J., Bezard, G., Deshayes, A., Meyer, I., Petiard, V. and Marraccini, P. *Plant Physiol. Biochem.*, **1999**, *37*, 261-272.

[15]Cannell, M. G. R., *Coffee: Botany, Biochemistry and Production of Beans and Beverage*, Croom Helm, **1985**, 108-134.

[16]Herrmann, K. M. and Weaver, L. M., *Annu. Rev. Plant Physiol. Plant Mol. Biol.*, **1999**, *50*, 473-503.

[17]Dennis, D.T. and Blakeley, S.D., *Biochemistry and Molecular Biology of Plants*, Amer. Soc. Plant Physiol., **2000**, 630-675.

[18]Yu, L., Jiang, J., Zhang, C., Jiang, L., Ye, N., Lu, Y., Yang, G., Liu, E., Peng, C., He, Z. and Peng, X., *J. Exp. Bot.*, **2010**, *61*, 1625-1634.

[19]Bowsher, C., Steer, M. and Tobin, A., *Plant Biochemistry*, Garland Science, **2012**, 195-236

[20]Geromel, C., Ferreira, L.P., Guerreiro, S.M.C., Cavalari, A.A., Pot, D., Pereira, L.F.P., Leroy, T., Vieira, L.G.E., Mazzafera, P. and Marraccini, P. *J. Exp. Bot.*, **2006**, *57*, 3243-3258.

Received: 26.07.2015.
Accepted: 20.08.2015.

SPECTROPHOTOMETRIC DETERMINATION OF MESALAMINE USING SODIUM NITROPRUSSIDE AS CHROMOGENIC REAGENT

Theia'a N. Al-Sabha[a]* and Nagham N. Habeeb[a]

Keywords: spectrophotmetry, sodium nitroprusside, mesalamine.

A simple, sensitive and accurate spectrophotometric method has been developed for the determination of mesalamine in pure and commercial dosage forms. The method is based on the reaction of mesalamine with sodium nitroprusside in the presence of hydroxylamine hydrochloride in alkaline medium to give a highly green colored species which absorb maximally at 703 nm. Beer's law is obeyed in the concentration range of 0.0-30 µg mL^{-1} with molar absorptivity = 2.0367×10^4 L mol^{-1} cm^{-1}. The average recovery is 103.0 % and relative standard deviation is less than 1.5 % (n = 6). The proposed method has been applied successfully for determination of mesalamine in commercial pharmaceutical products such as tablet and suppositories. There is no interference from the excipients.

* Corresponding Author
E-Mail: dr_theiaa@yahoo.co.uk
[a] Chemistry Department, College of Education, Mosul University, Mosul, Iraq.

Introduction

Mesalamine or 5-aminosalicylic acid, is an anti-inflammatory drug used to treat inflammation of the digestive tract (Crohn's disease) and mild to moderate ulcerative colitis. Mesalamine is a bowel-specific aminosalicylate drug that is metabolized in the gut and has its predominant actions there, thereby having fewer systemic side effects. Sulfasalazine is believed to be metabolized to mesalamine, which is considered as the active compound .[1]

Several techniques such as fluorimetry,[2] voltammetry,[3] coulometry,[4] chromatography[5-8] have been reported for the determination of mesalamine. These techniques require sophisticated instruments, expensive reagents, involve several manipulation steps and derivatization reactions. Literature survey revealed many spectrophotometric methods including different reactions have been reported for determination of mesalamine. These reactions are charge transfer complex formation,[9,10] diazotization and coupling,[11,12] oxidative coupling,[13,14] Schiff's base[15,16] and oxidation-reduction[17] reactions. Derivative formation[18] and UV spectrophotometric[19] methods have also been reported. Most of these methods are either insufficiently sensitive or tedious and required an extraction step or suffered from interferences.

The present work is a development of a simple, sensitive and selective spectrophotometric method for determination of mesalamine based on its reaction with sodium nitroprusside (SNP) in the presence of hydroxylamine hydrochloride (HAH) in alkaline medium.

Experimental

Apparatus

Shimadzu UV-1650 PC UV-Visible spectrophotometer equipped with a 1.0-cm path length silica cell and Philips PW (9421) pH-meter with a combined glass electrode were used. All calculations in the computing process were done in Microsoft Excel for Windows.

Reagents

Mesalamine was procured from State Company for Drug Industries and Medical Appliances, Sammara-Iraq, SDI. SNP solution of 0.2 % (w/v) strength was prepared by dissolving 0.2 g of SNP in 100 mL of distilled water. HAH solution (0.02 M) was prepared by dissolving 0.139 g of HAH in 100 mL of distilled water. Stock solution of mesalamine (100 µg mL^{-1}) was prepared by dissolving 0.01 g of pure mesalamine in a 5 mL of ethanol and diluted to the mark with distilled water in a 100 mL-volumetric flask. This solution was further diluted with water as per requirement. A 1.0 M solution of potassium hydroxide was prepared by dissolving 5.6098 g of the base in 100 mL in water and a 0.1 M solution was prepared by its dilution with distilled water.

Recommended procedure

Aliquots of mesalamine solution containing 0.2-25 µg mL^{-1} of the drug were pipetted into a series of 10 mL standard volumetric flasks. A 0.5 m1 of 0.02 M HAH followed by 1.0 mL of 1% SNP and 2.5 mL of 0.1 M KOH solutions were added to each flask and the contents were diluted to the mark with distilled water. The mixture was allowed to stand for 20 min and the absorbance of coloured product formed was measured at room temperature at 703 nm against a reagent blank prepared in a similar manner without mesalamine.

Determination form tablets of commercial preparations

The contents of 10 tablets (each tablet contains 400 or 500 mg mesalamine as Mesacol or Pentasa formulations) were powdered, mixed thoroughly and weighed accurately to an amount equivalent to 100 mg of mesalamine. The mixture was dissolved with 10 mL absolute ethanol and 40 mL distilled water, stirred well and filtered through a Whatmann No.42 filter paper. The residue was washed with distilled water for complete recovery of the drug. The filtrate and washings were diluted to 100 mL with water. It was further diluted according to the need and then analyzed by following the recommended procedure.

Pentasa suppository

The content of Pentasa suppository (containing 1 g of mesalamine) was transfer to a 1 L volumetric flask containing 500 mL of absolute ethanol and 250 mL of distilled water, sonicated for 5 min and diluted to the mark with distilled water. The resulting solution was filtered through a Whatmann No.42 filter paper. From this solution suitable dilutions were made to obtain the working solutions and then analyzed by following the recommended procedure.

Results and discussion

The method is based on the reaction of mesalamine with SNP in the presence of HAH and potassium hydroxide to form a faint brown colour which after 20 min became a deep green coloured complex, having maximum absorption at 703 nm where as blank reagent show no absorbance at this wavelength (Figure 1).

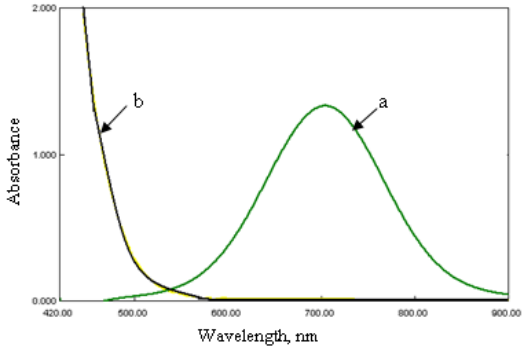

Figure 1. Absorption spectra of (a) (12 μg mL^{-1}) mesalamine with SNP and HAH against reagent blank (b) reagent blank against water (Conditions as mentioned in the recommended procedure).

The effect of various parameters on the absorption intensity of the complex formed was studied and the reaction conditions are optimized.

Effect of pH and Buffer Solutions

The reaction takes place in alkaline solution, therefore, to test the efficacy of different bases, 1.0 mL of 0.1 M solution of different bases were used in the recommended procedure. The results (Figure 2) indicated that KOH gave the maximum absorbance. The effect of pH was examined by addition of different volumes of 0. 1.0 M solution of KOH in the range of 0.0-3.0 mL. It was found that 2.5 mL KOH gave maximum absorbance and the optimum pH was found to be 11.93 (Figure 3). The effect of different buffer solutions, such as carbonate and phosphate of pH 11.93, were also studied and found to have no effect. Therefore 2.5 mL of 0.1 M KOH was used in other experiments.

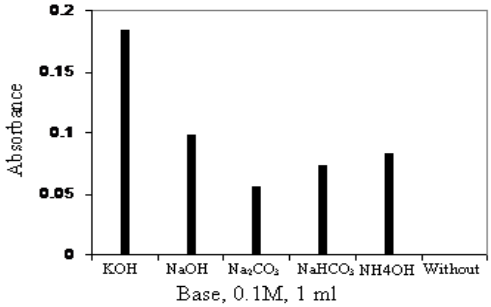

Figure 2. Effect of bases on the absorption of 2 μg ml^{-1} mesalazine with SNP.

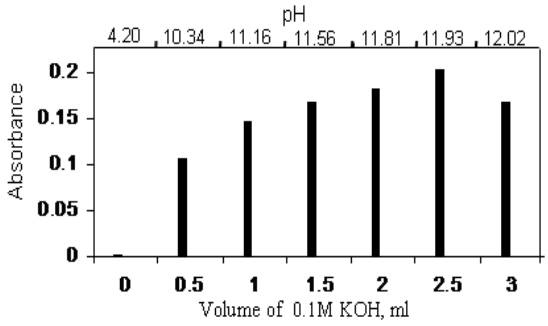

Figure 3. Effect of KOH and pH on the absorbance of 2 μg mL^{-1} mesalamine with SNP.

Variation of SNP concentration

The effect of changing the SNP concentration on the absorbance of solution containing a fixed amount of the drug, KOH and HAH was studied, It was found, that absorbance increases with increasing SNP concentration and reached the maximum value on using 1.0-2.0 mL of 1 % solution and further increase causes a gradual decrease in absorbance. Therefore 1.0 mL of 1 % solution was used in subsequent experiments.

Variation of HAH concentration

The effect of various volumes of a 0.02 M solution of HAH in the range of 0.0 to 3.0 mL on the intensity of absorption was investigated. It was observed that a volume of 0.5 mL of 0.02 M solution of HAH gave the highest absorbance and this concentration was chosen for further work.

Effect of surfactants

Addition of various surfactants viz., tween-80, triton x-100, cetyltrimethylammonium bromide and sodium dodecyl sulphate decreases the absorbance.

Effect of temperature and developing time

The reaction time was determined by following the color development at room temperature and in thermostatically controlled water-bath at 40 °C. The absorbance was measured against reagent blank treated similarly. It was observed that the sensitivity reached maximum after 20 min at room temperature (25 °C) and was stable for more than 100 min. Room temperature was therefore, chosen for the subsequent experiments.

Effect of order of addition

It was observed that the best results are obtained when the reagents are mixed in the order described in the recommended procedure. Changes in the order result in loss of color intensity.

Analytical parameters

Under the optimum experimental conditions described in the recommended procedure, a calibration graph of the coloured product was constructed by plotting absorbance versus concentration. The correlation is good (r = 0.9918). Beer's law is obeyed in the range of 0.05-30 µg mL^{-1}, and the molar absorptivity (ε) value indicated a high sensitivity of the method. The optical characteristics and statistics for the proposed method are summarized in Table 1.

Table 1. Summary of optical characteristics and statistics for the proposed method.

Parameter	Value
λ_{max}	703 nm
Linear range (µg mL^{-1})	0-30
Limit of detection (µg mL^{-1})	0.0248
Limit of quantification (µg mL^{-1})	0.0826
Slope	0.113
Intercept	0.053
Correlation coefficient (r)	0.9918
Sandell's sensitivity (µg cm^{-2})	0.0084
ε (L mol^{-1} cm^{-1})	2.0367×10^4

Precision and accuracy

The accuracy and precision of the proposed method were estimated by measuring the content of mesalamine in pure form at three different concentration levels within the Beer's law limit in six replicates. The relative standard deviation (representing precision) in the range of 0.23 to 1.4 and mean percent recovery (representing accuracy) of 98.74 obtained by the proposed method can be considered to be satisfactory.

Interference

The extent of interference by some excipients, viz., sucrose, glucose, fructose, sodium chloride and starch, which are often found in pharmaceutical preparations, was studied by measuring the absorbance of solutions containing 2 µg mL^{-1} of mesalamine and 100, 500 and 1000 µg mL^{-1} of excipients in the final volume of 10 mL. It was found that these excipients do not interfere in the present method. The range of recovery is between 96.2 and 102.1 %. We consider that this variation is acceptable.

Applications

Application of the proposed method to the assay of pharmaceutical sample of mesalamine as tablet and pentasa suppository gave reproducible and accurate results as shown in Table 2. The obtained results were compared statistically by a Student's *t*-test for accuracy and a variance ratio *F*-test for precision by the standard method[20] at the 95% confidence level with six degrees of freedom, as mentioned in Table 2. The results showed that the experimental *t*-test and *F*-test were less than the theoretical value (t= 2.57, F= 4.284, n=6), indicating that there was no significant difference between the proposed method and official method.

Stoichiometry, stability constant and reaction mechanism

The mole ratio of the reaction product formed between the mesalamine and SNP was investigated by applying the Job's method of continuous variation[21] using equimolar solutions (5×10^{-3} M) of the drug and SNP. The results shown in Figure 4 indicated that the product was formed in the ratio of 1:2 for mesalamine : SNP. The stability constant (K_c) of the product was determined by applying Eqn. (1).

$$K_c = 1 - \alpha / 4\alpha^3 C^2 \qquad (1)$$

where

K_c is the stability constant,

α is the degree of dissociation and

C is the concentration of the product which is equal to the concentration of drug.

The value of K_c (average of measurements at three concentrations) was found to be 2.79×10^5 L^2 mol^{-2}. This indicated that the product is highly stable.

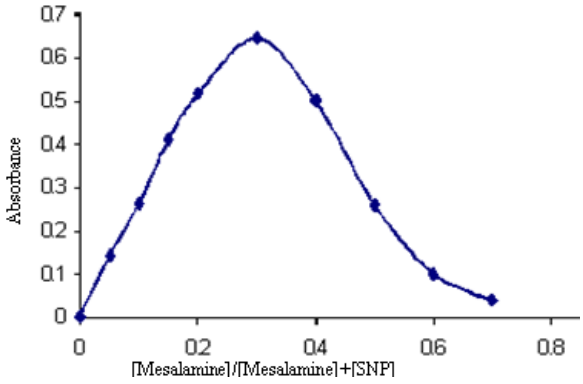

Figure 4. Continuous variation plot of mesalamine-SNP complexation.

Table 2: Assay of mesalamine in pharmaceutical preparations using the proposed method and its comparison with the official method.

Procedure applied	Pharmaceutical preparation	Drug amount present ($\mu g\ mL^{-1}$)	Recovery[a] (%)	Drug content found (mg)	Average recovery	Certified value
Proposed method	Mesacol tablet[b]	2 5 10 15	99.9 101.2 98.9 101.5	399.6 404.8 395.6 406.0	401.5 mg (2.04, 2.15)[e]	400 mg
	Pentesa tablet[c]	2 5 10 15	99.5 97.8 103.3 97.7	397.5 489.0 516.5 488.5	497.9	500 mg
	Pentesa suppository[d]	2 5 10 15	99.5 96.2 102.3 99.8	0.995 0.962 1.023 0.992	0.993 g (2.32, 1.96)	1.0 g
British Pharmacopoeia	Pure mesalamine	50	101.06	50.532	-	50 mg

[a]Average of six determinations. [b]Manufactured by Universal Pharmaceutical Industries unipharama–Damascus – Syria; [c]Manufactured by Ferring AS, INHOUSE PHARMACY.BIZ., [d]Manufactured by Ferring Leciva, Czech Republic. [e]Figures in parenthesis are the calculated values for *t*, and *F* respectively.

The formation of the complex between SNP and mesalamine is an aromatic electrophilic reaction, which is represented by Scheme 1. In a strongly alkaline medium, phenol is converted to phenolate ion. Hence the electrophilic reaction can take place more easily because the benzene ring is activated due to the presence of anionic oxygen. It is suggested, the nitroso group of the SNP attacks the phenolate moiety in mesalamine at ortho-position. The electronic properties of the substituents in the benzene ring affect the extent of reaction, and consequently the sensitivity of the method.[22]

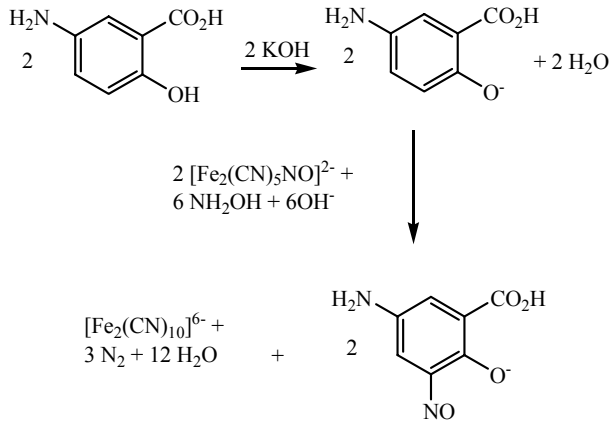

Scheme 1. The mechanism of reaction between mesalamine, sodium nitroprusside and hydroxylamine hydrochloride in a basic medium.

Comparison with other spectrophotometric methods

The proposed method compares favorably with other reported methods. As shown in Table 3, the proposed method is more sensitive than other methods, needs no heating and the product is stable for a longer time.

Table 3. Comparison of the proposed method with other spectrophotometric methods

Analytical parameter	SNP	Ref. 9	Ref. 16	Ref. 17
λ_{max} (nm)	703	571.6	320	520
pH	11.9	9.8	Acidic	-
Temp. (°C)	R.T.	25	R.T.	100
Development Time (min)	20	5	-	15
Stability Period (min)	>100	45	120	-
Beer's law ($\mu g\ mL^{-1}$)	0.05 – 30	1.25-30	2.0-30	4.0-24
ε ($L\ mol^{-1}\ cm^{-1}$)	2.03 x 10^4	3.4 x 10^3	1.283 x 10^4	0.38 x 10^3
Recovery (%)	98.74	100.44	100.34	99.93
RSD (%)	≤1.44	1.67	0.409	0.684
Application	Tablet, Enema	Tablet, Capsule	Tablet	Tablet

Conclusion

The proposed spectrophotometric method is simple, accurate and more sensitive than the other methods. No significant difference in the recovery between the proposed and official method was obtained. The method does not require any pre-treatment or extraction steps and was applied successfully for the assay of the pharmaceutical preparations for tablets and pentasa suppositories of mesalamine.

References

[1]http://en.wikipedia.org/wiki/Mesalazine, Safety Information about Lialda". Lialda Side Effects, 2007.

2Abdolmohammad-Zadeh, H. and Kohansal, S., *J. Braz. Chem. Soc.,* **2012***, 23,* 473.

[3]Nigovic, B. and Lmunic, B., *J. Pharm. Biomed. Anal.*, **2003**, *31*, 169.

[4]Ahdullin, I. F., Chernysheva, N. N. and Budnikov, G. K., *J. Anal. Chem.*, **2002,** *57*, 721.

[5]Gandini, C., Caccialanza, G., Kitsos, M. and Massolini, G., *J. Chromatogr. A*, **1991,** *540*, 416.

[6]Pumala, K. and Edelbroek, P., *Ramathibodi Med. J.,* **1992**, *15*, 338.

[7]Hussain, F. N., Ajjan, R. A., Moustafa, M., Anderson, J. C. and Riley, S. A., *J. Chromatogr. B. Biomed. Sci. Appl.*, **1998**, *25*, 257.

[8]Bystrowska, B., Nowak, J. and Brandys, J., *J. Pharm.Biomed. Analysis*, **2000**, *22*, 341.

[9]Al-Enizzi, M. S., Al-Sabha, T. N., Al-Ghabsha, T. S., *Jordan J. Chem.* **2012**, *7,* 87.

[10]Al-Sabha, T. N., Al-Enizzi, M. S. and Al-Taee, O. A., *Eur. Chem. Bull.*, **2014**, *3*, 377.

[11]Reddy, M. P., Prabhavahi, K., Reddy, N. R. and Reddy, P. R., *Global J. Pharm.*, **2011**, *5*, 101.

[12]Patel, K. M., Patel, C. N., Panigrahi, B., Parikh, A. S. and Patel, H. N., *J. Young Pharm.*, **2010,** *2*, 284.

[13]Darak, V. R., Karadi, A. B., Arshad, M. D. and Patil, D., *Curr. Pharm. Res*., **2011,** *1*, 232.

[14]Shakeela, S., Ram, B. S. and Sekaran, C. B., *Chiang Mai J. Sci.*, **2011**, *38*, 551.

[15]Sama, N. S., Gurupadayya, B. M. and Kumar, A., *J. Pharm. Res.*, **2011**, *4*, 39.

[16]Chandra, B. S., Bhogela, S. S., Shaik, M., Vadlamudi, C. S., Chappa, M. and Maddirala, N. S., *Quim. Nova*, **2011**, *34*, 1068

[17]Narala, S. and Saraswathi, K., *Int. J. Res. Pharm. Biomed. Sci.,* **2010**, *1*, 10.

[18]Ali D. S., *Tik. J. Pure Sci.*, **2009**, *14*, 42.

[19]Gatkal S. H., Mhatre, P. R., Chopade, V. V. and Chaudhari, P. D., *Int. J. Pharm. Sci. Res*., **2013**, *4*, 401.

[20]*British Pharmacopoeia*, **1993**, H. M. Stationary Office, UK: London.

[21]Job, P, "*Spectrochemical Methods of Analysis*", Wiley Intersience: New York, **1971**, p 346.

[22]Kang, C., Wang, Y., Li, R., Du, Y., Li, J., Zhang, B., Zhou, L., Du, Y., *Microchem J*., **2000**, *64*, 161.

Received: 23.07.2015.
Accepted: 22.08.2015.

SYNTHESIS, SPECTROSCOPIC CHARACTERIZATION, X-RAY ANALYSIS OF DMSO SOLVATED 5'-CHLORO-1H,1"H-[3,3':3',3"-TERINDOL]-2'(1'H)-ONE

Sakshi Sharma[a], Goutam Brahmachari[b], Bubun Banerjee[b], Rajni Kant[a] and Vivek K. Gupta[a]*

Keywords: crystal structure, direct methods, hydrogen bond, 5'-chloro-1H,1"H-[3,3':3',3"-terindol]-2'(1'H)-one.

The title compound 5'-chloro-1H,1"H-[3,3':3',3"-terindol]-2'(1'H)-one is synthesized via one-pot multicomponent reaction (MCR) at room temperature using commercially available sulfamic acid as inexpensive and environmentally benign organo-catalyst. It crystallizes in the monoclinic space group $P2_1/n$ with the unit-cell parameters: a = 15.3117(15), b = 10.9302(8), c = 16.591(2) Å, α = 90.00° β = 98.224(10)°, γ = 90.00° and Z = 4. The crystal structure was solved by direct methods using single-crystal X-ray diffraction data collected at room temperature and refined by full-matrix least-squares procedures to a final R-value of 0.0735 for 2539 observed reflections. Both the DMSO solvent molecules take part in the inter- and intramolecular interactions that are responsible for the formation of hydrogen bonded network. Two C-H···π inter-molecular hydrogen bonds are also present in the crystal structure.

*Corresponding Authors
Mob: +91 9419102467
E-Mail: vivek_gupta2k2@hotmail.com
[a] X-ray Crystallography Laboratory, Post-Graduate Department of Physics & Electronics, University of Jammu, Jammu Tawi - 180 006, India
[b] Laboratory of Natural Products & Organic Synthesis, Department of Chemistry, Visva-Bharati (a Central University), Santiniketan – 731235, West Bengal, India.

Introduction

Bis(indolyl)indolin-2-ones represent a "privileged" structural motif well distributed in naturally occurring compounds[1] possessing a broad spectrum of biological activities, such as anti-inflammatory,[2] anti-HIV,[3] antitumor[4] activities etc. Investigation of the structural features of biologically relevant bis(indol-3-yl)indolinone derivatives is, thus, of considerable interest to the researchers. In this communication, we wish to report on the green synthesis of one such derivative, namely 5'-chloro-1H,1"H-[3,3':3',3"-terindol]-2'(1'H)-one via one-pot multicomponent reaction at room temperature using commercially available sulfamic acid as inexpensive and environmentally benign organo-catalyst, and its crystal structure. The structure of the title compound was elucidated by detailed spectral methods and XRD studies.

Experimental

Synthesis

The synthesis of the title compound, 5'-chloro-1*H*,1"*H*-[3,3':3',3"-terindol]-2'(1'*H*)-one (**1**), was carried out via one-pot multi-component reaction in aqueous ethanol using low-cost and environmentally benign sulfamic acid as catalyst at room temperature. An oven-dried screw cap test tube was charged with a magnetic stir bar, indole (0.117 g, 1 mmol), 5-chloroisatin (0.090 g, 0.5 mmol), sulfamic acid (0.009 g, 20 mol % as organo-catalyst), and EtOH-H_2O (1:1 v/v; 4 ml) in a sequential manner; the reaction mixture was then stirred vigorously at room temperature for 3 h.[5] The progress of the reaction was monitored by TLC. On completion of the reaction, a solid mass precipitated out that was filtered-off followed by washing with aqueous ethanol. The white solid mass was then subjected to recrystallization from aqueous ethanol to obtain pure title compound (0.170 g, yield 86 %) with the m.p. 567-569 K. The structure of (**1**) was confirmed by analytical as well as spectral studies including FT-IR, ^{1}H NMR, ^{13}C NMR, and TOF-MS. Unit crystal was obtained from DMSO as a solvent. For crystallization, 50 mg of the compound dissolved in 5 ml DMSO and left for several days at ambient temperature which yielded white block shaped crystals. The chemical structure of the title compound is given in Figure 1.

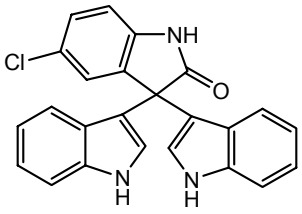

Figure 1. Chemical structure of the title compound.

5'-Chloro-1*H*,1"*H*-[3,3':3',3"-terindol]-2'(1'*H*)-one

This compound was obtained as white solid (0.170 g, 86 %). m.p. 567-569 K. IR (KBr): 3356, 3119, 3053, 2969, 1701, 1614, 1534, 1474, 1425, 1335, 1236, 1171, 1113, 1005, 876, 824, 750 cm^{-1}. ^{1}H NMR (400 MHz, DMSO-d_6) δ = 11.04 (1H, s, -N*H*), 11.03 (s, 1H, -N*H*), 10.78 (s, 1H, -N*H*), 7.38 (2H, d, J = 8.4 Hz, aromatic H), 7.30 (1H, dd, J = 8.0, 2.4 & 2.0 Hz, aromatic H), 7.23 (1H, br s, aromatic H), 7.21-7.17 (2H, m, aromatic H), 7.05 (2H, d, J = 7.2 Hz, aromatic H), 7.02 (1H, t, J = 4.4 & 4.0 Hz, aromatic H),

6.90 (2H, d, J = 2.4 Hz, aromatic H), 6.83 (2H, t, J = 7.6 & 7.2 Hz, aromatic H). ^{13}C NMR (100 MHz, DMSO-d_6) δ = 178.80, 140.69, 137.35 (2C), 137.02, 128.27, 125.91 (2C), 125.85 (2C), 125.09, 124.84 (2C), 121.49 (2C), 120.93 (2C), 118.84 (2C), 113.91, 112.16 (2C), 111.54, 53.26. TOF-MS 420.0881 $[M + Na]^+$. Anal. Calcd. for $C_{24}H_{16}ClN_3O$: C, 72.45, H, 4.05, N, 10.56. **F**ound: C, 72.47, H, 4.03, N, 10.54.

X-Ray Structure determination

X-ray intensity data of 9775 reflections (of which 4821 were unique) were collected on *X'calibur* CCD area-detector diffractometer equipped with graphite monochromated MoK_α radiation (λ = 0.71073 Å). The crystal used for data collection was of dimensions 0.30 x 0.20 x 0.20 mm. The cell dimensions were determined by least-squares fit of angular settings of 1851 reflections in the θ range 3.61° to 24.31°**.** The intensities were measured by ω scan mode for θ ranges 3.52° to 25.00°. 2539 reflections were treated as observed ($I > 2\sigma(I)$). Data were corrected for Lorentz, polarization and absorption factors. The structure was solved by direct methods using SHELXS97.[5] All non-hydrogen atoms of the molecule were located in the best E-map. Full-matrix least-squares refinement was carried out using SHELXL97.[6] The final refinement cycles converged to an R = 0.0735 and w$R(F^2)$ = 0.1818 for the observed data. Residual electron densities ranged from -0.431 < Δρ < 0.385 eÅ^{-3}. Atomic scattering factors were taken from International Tables for X-ray Crystallography (1992, Vol. C, Tables 4.2.6.8 and 6.1.1.4). The crystallographic data are summarized in Table 1.

Table 1. Crystal data and other experimental details.

CCDC Number	**1413889**
Crystal description	Block
Crystal size	0.30 x 0.20 x 0.20 mm
Empirical formula	$C_{28}H_{28}ClN_3O_3S_2$
Formula weight	554.10
Radiation, Wavelength	Mo *K*α, 0.71073 Å
Unit cell dimensions	*a*= 15.3117(15) Å
	b = 10.9302(8) Å
	c= 16.591(2) Å
	α= 90.00°
	β = 98.224(10) °
	γ= 90.00°
Crystal system, space group	monoclinic , P 21/n
Unit cell volume	742.79(9)Å^3
No. of molecules per unit cell, Z	4
Absorption coefficient	0.326 mm^{-1}
F(000)	1160
θ range for entire data collection	3.52 <θ< 25.00
Reflections collected / unique	9775/ 4821
Reflections observed $I > 2\sigma(I)$)	2539
Range of indices	*h*= -18 to 9
	k=--9 to 12
	l= -19 to 19
No. of parameters refined	354
Final *R*-factor	0.0735
w$R(F2)$	0.1818
R_{int}	0.0443
R_σ	0.0901
Goodness-of-fit	1.031
Final residual electron density	-0.431<Δρ<0.385 eÅ^{-3}

Result and Discussions

An ORTEP[7] view of the compound with atomic labeling is shown in Figure 2. The geometry of the molecule was calculated using the WinGX[8], PARST[9] and PLATON[10] software.

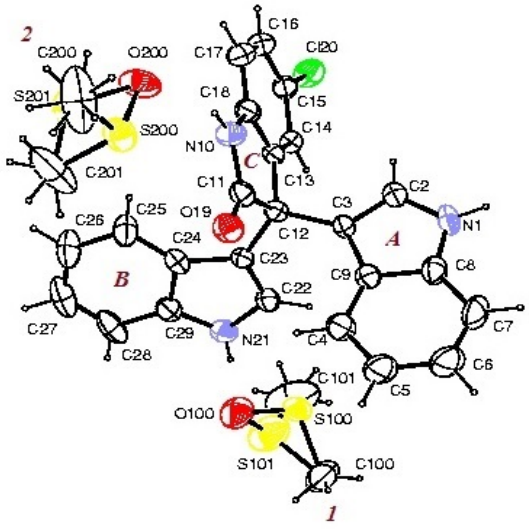

Figure 2. ORTEP view of the molecule with displacement ellipsoids drawn at 40 %. H atoms are shown as small spheres of arbitrary radii.

The asymmetric unit cell consists of the molecule of title compound. The best packing view has been obtained down b-axis (Figure 3). The asymmetric unit of title compound, '$C_{28}H_{28}ClN_3O_3S_2$, 2(C_2H_6OS)', comprises of two indole rings (*A*) and (*B*), an oxindole ring (*C*), connected through a carbon atom C12 and two DMSO solvent molecules (*1*) and (*2*). The oxindole ring is substituted by a chlorine atom at position C15.

In the molecule, the expected geometric parameters are observed. The geometry of both the indole rings, (*A*) and (*B*), indicates a high degree of similarity in terms of their bond lengths and bond angles and are in good agreement with the standard values.[11] The bond lengths and bond angles of the title molecule are quite close to the corresponding values in a related structure 3,3-bis(1H-indol-3-yl)indolin-2-one, ($C_{24}H_{17}N_3O$).[12]

The indole moieties are individually planar where as the five-membered ring in an oxindole system (N10/C11/C12/C13/C18) in the title compound deviates slightly from planarity and adopts a conformation halfway between that of half-chair and envelope with asymmetry parameters [Δ$C2$(C11-C12) = 1.756] and [ΔC_s(C11) = 0.930].[13]

The dihedral angle between the planes defined by the constituent pyrrolidine and benzene rings in a chloro substituted oxindole ring is 1.42(14)°. By comparison, this angle is 4.22 (13)° in indole-3-carbaldehyde[14] and 0.29(11)° in indole-3-carboxylic acid[15]. The indole ring systems A and B make dihedral angle of 67.97(11)° with each other; the oxindole ring C is twisted with respect to these indole rings at angles 71.58(9)° and 82.38(9)°, respectively (Table 2).

Table 2. Selected bond lengths (Å), bond angles (º) and torsion angles(º) for non hydrogen atoms (e.s.d.'s are given in parentheses).

Bond distances(Å)		Bond angles(°)		Torsion angles(°)	
N1-C2	1.357(5)	N1-C8-C7	130.2(5)	C3-C12-C13-C14	69.9(5)
N1-C8	1.365(6)	C3-C9-C4	135.5(4)	O19-C11-C12-C13	-69.5(5)
N10-C11	1.356(5)	C3-C12-C13	110.3(3)	C11-C12-C23-C22	-143.5(4)
N10-C18	1.404(5)	N10-C18-C17	127.9(4)	C18-N10-C11-O19	174.9(4)
C11-O19	1.213(5)	C12-C13-C14	130.3(4)	C17-C16-C15-Cl20	-178.2(4)
C15-Cl20	1.741(5)	C11-C12-C23	111.5(3)	C23-C12-C13-C14	-57.2(5)
N21-C29	1.363(6)	C23-C24-C25	136.4(4)		
N21-C22	1.373(5)	N21-C29-C28	130.1(5)		

Table 3. Geometry of intermolecular hydrogen bonds.

D-H…A	D-H (Å)	H…A (Å)	D…A (Å)	θ[D-H…A (º)]
N1-H1..O200i	0.86	2.11	2.848(6)	143
N10-H10-O200ii	0.86	2.03	2.826(5)	154
N21-H21..S100ii	0.86	2.80	3.572(6)	150
N21-H21..O100ii	0.86	1.97	2.821(7)	170
C201-H20C...O19iii	0.96	2.46	3.378(9)	161
C200-H20G-Cl20i	0.96	2.82	3.574(9)	136
C17-H17...Cg1iv	0.93	2.74	3.662(5)	169
C25-H25...Cg2i	0.93	2.83	3.328(6)	114

Symmetry codes: (i) -x+1/2+1, -y-1/2, -z+1/2; (ii) x, y, z; (iii) -x+2, -y, -z; (iv) - x+3/2, y+1/2, -z+1/2

The C-Cl distance [C15-Cl20 = 1.741(5) Å] in an oxindole ring is comparable with the molecules of its type.[16,17] The N10—C18 and N10—C11 bond lengths [1.404(5) Å and 1.356(5) Å, respectively] differ from the corresponding mean values of 1.419 and 1.331 Å reported for γ –lactams[11]. The C11-O19 bond length [1.213(5) Å] is comparable with the mean value of 1.232 Å reported for γ – lactams.[18] The bond lengths N10-C11 and C11=O19 in the oxindole ring indicates hetero π- electron delocalization over atoms N10, C11 and O19. In particular, the contribution of the lone pair of electrons on the N atom to the N—C bond in the N—C=O group is revealed.

The average value of endocyclic angles in all three phenyl rings are close to 120º as expected for fully delocalized systems. The angles around atom C12 [C3–C12–C11=108.2(3)°, C3–C12–C13=110.3(3)°, C3–C12–C23=113.5(3)°, C11–C12–C13=101.0(3)°, C11–C12–C23=111.5(3)° and C13–C12–C23=111.6(3)°] deviate significantly from the ideal tetrahedral value of 109.4°. In the benzene rings of the the ring systems A, B and C, the endocyclic angles at C4-C9-C8=117.9(4)°, C25-C24-C29=118.7(4)°, C14-C13-C18=120.8(4)° are narrowed while those at C7-C8-C9=122.1(5)°, C24-C29-C28=121.6(5) and C13-C18-C17=122.0(4)° are widened from 120.0° respectively. This would appear to be a real effect caused by the fusion of the smaller pyrrole ring to the six-membered benzene ring, a feature commonly observed in indole derivatives. In both the solvent molecules 1 and 2, the S atoms are disordered over two sites with occupancy ratio of 0.636 : 0.363.

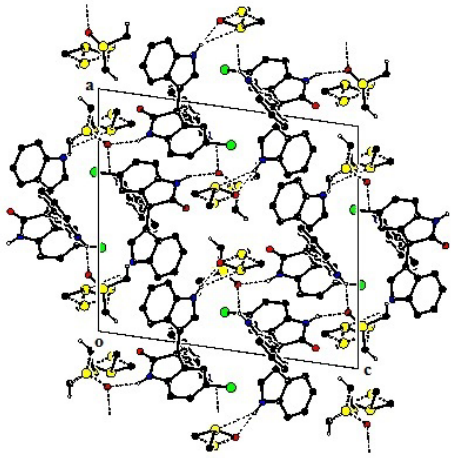

Figure 3. The packing arrangement of the molecules viewed down the b-axis.

The inter- and intramolecular hydrogen bonds are responsible for the formation of hydrogen bonded network thus, providing stability to the molecules in the unit cell. Both the DMSO solvents take part in the inter- and intramolecular interactions. In addition, two C–H···π inter-molecular hydrogen bonds are also observed in the crystal structure. The geometry of intra- and inter-molecular hydrogen bonds as well as C–H···π inter-molecular hydrogen bonds is given in (Table 3).

Acknowledgments

GB is thankful to the CSIR, New Delhi for financial support [Grant No. 02(0110)/12/EMR-II]. BB is grateful to the UGC, New Delhi for awarding him a Senior Research Fellowship.

References

[1]Kobayashi, M., Aoki, S., Gato, K., Matsunami, K., Kurosu, M., Kitagawa, I., *Chem. Pharm. Bull.*, **1994***, 42,* 2449-2451.

[2]Natarajan, A., Fan, Y. H., Chen, H., Guo, Y., Iyasere, J., Harbinski, F., Christ, W. J., Aktas, H., Halperin, J. A., *J. Med. Chem.*, **2004**, *47*, 1882.

[3]Bal, R. T., Anand, B., Yogeeswari, P., Sriram, D., *Bioorg. Med. Chem. Lett.*, **2005**, *15*, 4451.

[4]Tripathy, R., Reiboldt, A., Messina, P. A., Iqbal, M., Singh, J., Bacon, E. R., Angeles, Th. S., Yang, Sh. X., Albom, M. S., Robinson, C., *Bioorg. Med. Chem. Lett.*, **2006**, *16,* 2158.

[5]Brahmachari, G., Banerjee, B., *ACS Sustainable Chem. Eng.*, **2014**, 2, 2802.

[6]Sheldrick, G.M., *Acta Cryst.,* **2008**, *A64*, 112.

[7]Farrugia, L.J. *J Appl Cryst.,* **1997**, *30*, 565.

[8]Farrugia, L.J., *J Appl Cryst.,***1999**, *32*, 837.

[9]Nardelli, M., *J Appl Cryst*., **1995**, *28*, 659.

[10]Spek, A.L., *Acta Cryst*., **2009**, *D65*, 148.

[11]Allen, F. H., Kennard,O., Watson,D.G., Brammer, L., Orpen,A.G., Taylor, R. *J. Chem.Soc., Perkin Trans-II.*, **1987**, S1.

[12]Selvanayagam, S., Mahesh Chandak, S., Velmurugan, D., Ravikumarc, K., Raghunathand, R., *Acta Cryst*., **2005**, *E61*, o3122.

[13]Duax, W. L., Norton, D. A., *Atlas of Steroid Structures, Plenum*, New York, **1975**, Vol. 1.

[14]Ng, S. W., *Acta Cryst*., **2007,** *E63*, o2732.

[15]Smith, G., Wermuth, U. D., Healy, P. C., *Acta Cryst.*, **2003,** *E59*, o1766.

[16]Hachula, B., Zerzucha, P., Zubko, M., Kusz, J., *Acta Cryst*., **2011**, *C67*, o413.

[17]Xing, X.-N., Li, L., Zhu, X.-Y., Chen, J.-R., *Acta Cryst*. **2007**, *E63*, o2969.

[18]Nerskov-Lauritsen, L., Burgi, H.-B., Hofmann, P., Schmidt, H. R., *Helv. Chim. Acta.*, **1985**, *68*, 76.

Received: 17.07.2015.
Accepted: 25.08.2015.

ROLE OF INTERMOLECULAR INTERACTIONS IN LINEAR FURANOCOUMARIN DERIVATIVES

Ahsan Elahi[a] and Rajni Kant[a]*

Keywords: furanocoumarin, lattice energy, intermolecular interactions, PIXEL.

Energy calculations have been performed on a series of ten molecules of linear furanocoumarin derivatives to obtain the total stabilization energy i.e. lattice energy of the crystal and also the energy of neighbouring molecular pairs participating in the stabilization of the crystal. The total stabilization energy (lattice energy) lies in the range -16 to -40 kcal mol^{-1}. Analysis of the energetics of the neighbouring molecular pairs in these structures shows the presence of different intermolecular interactions participating in the crystal packing. In addition to the significance of coulombic nature of bifurcated C-H…O hydrogen bonds, the stabilizing role of π…π stacking interactions has been realized in these structures. A careful observation of energetics of different molecular pairs involving C-H…O hydrogen bond reveals that motifs involving C(sp^2)-H…O hydrogen bonds are more stabilized than those of C(sp^3)-H…O.

Corresponding Authors
Fax: +91 191 243 2051
E-Mail: rkant.ju@gmail.com
[a] Department of Physics & Electronics, University of Jammu, Jammu Tawi -180 006, India.

Introduction

Furanocoumarins are an important class of heterocyclic compounds consisting of a furan ring fused with the coumarin nucleus. They can be grouped into the linear and angular type depending on symmetric or asymmetric loading of the furan ring with the coumarin nucleus. The most abundant linear furanocoumarins are psolaren, xanthotoxin, bergapten and isopimpinellin. Pharmacological studies have indicated that linear furanocoumarins such as isoimperatorin, notopterol and bergapten possess anti-inflammatory, analgesic, anti-cancer and anti-coagulant activities.[1] Furanocoumarins have received much attention on account of their ability to perform cycloaddition reactions with DNA during irradiation with UV light,[2-6] a property that has given rise to wide-ranging photo chemotherapeutic applications.[7]

The different activities (chemical and biological) may be due to the presence of different types of interactions prevailing in the crystal structure. The role of strong intermolecular interactions such as N-H...O/N and O-H…O/N is well understood[8,9] in addition to weak C–H…π[10-12] and π … π interactions.

The recent focus is to investigate the role of weak intermolecular interactions and its influence on crystal packing. In addition to the description of the crystal packing in terms of the presence of different intermolecular interactions, based purely on the concept of geometry (distance–angle criteria), it is also very important to analyze the intermolecular interaction energies of different non-covalent interactions in the solid state in order to obtain more detailed insight into the crystal packing.[13-16] In this regard, a series of ten structures belonging to linear furanocoumarin derivatives have been taken into account and their lattice energies have been calculated theoretically. All the molecular pairs involved in the crystal packing were extracted, the nature and energies associated with the intermolecular interactions associated with these molecular pairs were analyzed to explore the role of these interactions in the stabilization of the crystal lattice. A representative illustration of the linear furanocoumarin moiety indicating the atomic numbering scheme used in the present work is shown in Figure1. The chemical name, molecular code and chemical structure of linear furanocoumarin derivatives are presented in Table 1 and their precise crystallographic details in Table 2a and 2b.

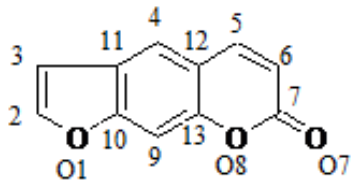

Figure 1. Linear furanocoumarin moiety indicating the numbering scheme.

Computation of interaction energies

The lattice energies of all the compounds have been calculated by PIXEL using the Coulomb-London-Pauli (CLP) model of intermolecular Coulombic, polarization, dispersion, and repulsion energies.[27-29]. For this purpose H atoms were moved to their neutron value. The total lattice energies partitioned into their Coulombic, polarization, dispersion and repulsion contributions for all the molecules are presented in Table 3. The interaction energies of the molecular pairs (partitioned into different components) extracted from the .mlc file, generated after the completion of calculation, along with the involved intermolecular interactions are listed in Table 4. The molecular pairs are arranged in decreasing order of their stabilizing energies. The geometrical restrictions placed on the intermolecular H-bonds present in the selected molecular pairs are the sum of the van der Waals radii + 0.4Å and the directionality is greater than 110°. Molecular motifs and packing diagrams were generated using Mercury software.[30]

Table 1. Chemical name, coding scheme and chemical structure of linear furanocoumarin derivatives.

Chemical name	Code	Structure
Furo[3,2-g]benzopyran-7-one[17]	**M-1**	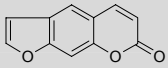
8-Methoxyfuro[3,2-g]benzopyran-7-one[18]	**M-2**	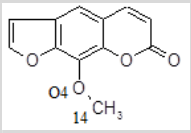
9-(1,1-Dimethyl-2-propenyl) 4-hydroxy-7H-furo[3,2-g]benzo-pyran-7-one[19]	**M-3**	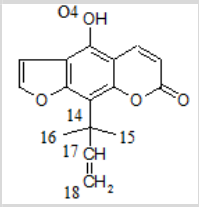
4-((3,3-Dimethyl oxiranyl) methoxy)-7H-furo[3,2-g]benzopyran-7-one[20]	**M-4**	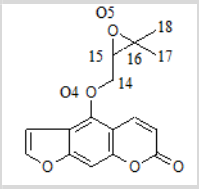
4-((2,4,4-Trimethyl-1-cyclohexen-1-yl)methoxy)-7H-furo[3,2-g]benzopyran-7-one[21]	**M-5**	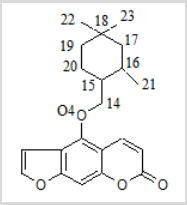
5,8-Dimethoxyfuro[3,2-g]benzopyran-7- one[22]	**M-6**	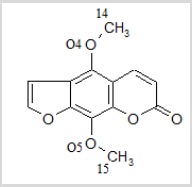
2,3-Dihydro-2-(1-hydroxy-1-methyl ethyl)-7H-furo[3,2-g][1]benzo pyran-7-one[23]	**M-7**	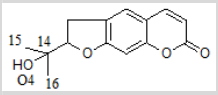
9-(3-Methylbut-2-enyloxyfurano)[3,2-g]benzopyran-7-one[24]	**M-8**	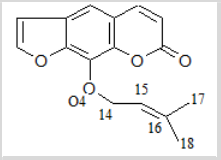
2,3-Dihydro-2-(1-hydroxy-1-methyl ethyl)-9-methoxy-7H-furo[3,2-g][1]benzo pyran-7-one[25]	**M-9**	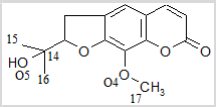
4-{[(2E)-5-Hydroxy-3,7-dimethylocta-2,6-dien-1-yl]oxy}-7H-furo[3,2-g][1]benzo pyran-7-one)[26]	**M-10**	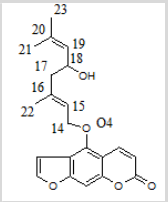

Results and discussion

Furo[3,2-g]benzopyran-7-one (M-1)

The principal stabilizing molecular pairs extracted from crystal packing along with their interaction energies are presented in Figure 2. The molecules are packed with the involvement of C(sp^2)-H4…O8 hydrogen bonds along with C-H…H-C (motif 1) generating molecular chains along a-axis. This interacting pair has a contribution of - 4.44 kcal mol^{-1} towards the stabilization of the crystal packing. The chains thus formed are then interconnected via weak C(sp^2-)H2…O7 (motif 4, *I.E.* = -3.2 kcal mol^{-1}) and C(sp^2)-H6…O1 (motif 5, *I.E.* = -0.95 kcal mol^{-1}) hydrogen bonds generating a molecular sheet in the ab plane (Figure 3a). The packing in the crystal also displays the formation of molecular chains via motif 5 along b-axis. These chains are then stacked via π…π stacking (motif 2, *I.E.* = -4.23 kcal mol^{-1}, 90% contribution to stabilization from dispersion component) forming layers down the bc plane (Figure 3b). Furthermore, additional stabilization of -4.21 kcal mol^{-1} was found to be imparted by motif 3 showing the presence of weak C-H…O (involving H5, H4 and H3 with O7, O8 and O1 respectively) along with C-H…π (involving H3 with C9 and C10) hydrogen bonds.

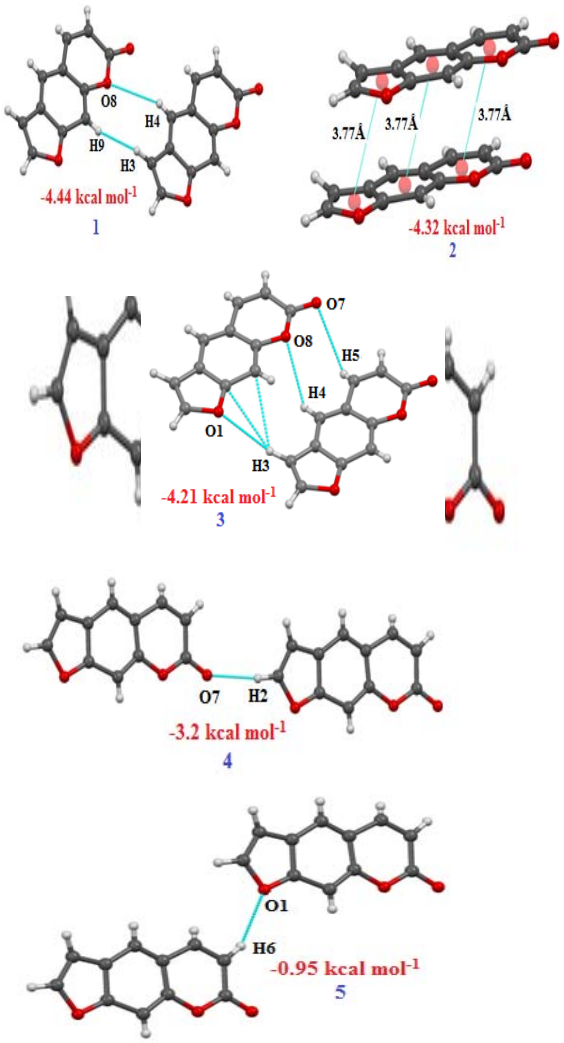

Figure 2. Molecular pairs (**1-5**) along with their interaction energies in **M-1**.

Table 2a. Precise crystal data for linear furanocoumarin derivatives

Data	M-1	M-2	M-3	M-4	M-5	M-6	M-7
Formula	$C_{11}H_6O_3$	$C_{12}H_8O_4$	$C_{16}H_{14}O_4$	$C_{16}H_{14}O_5$	$C_{21}H_{22}O_4$	$C_{13}H_{10}O_5$	$C_{14}H_{14}O_4$
Formula weight, g mol^{-1}	186.16	216.19	270.29	286.29	338.4	246.21	246.25
Crystal system	Triclinic	Orthorhombic	Monoclinic	Triclinic	Monoclinic	Monoclinic	Monoclinic
Space group	P1	$Pna2_1$	C2/c	P1	$P2_1/n$	$P2_1/c$	$P2_1$
a(Å)	5.926(8)	12.911(6)	8.976(3)	8.485(1)		16.9357(5)	5.7210(10)
b(Å)	9.56(2)	15.804(8)	16.621(2)	11.054(2)	6.732(2)	4.3669(10)	13.8100(10)
c(Å)	3.777(6)	4.882(5)	17.818(2)	7.868(1)	24.375(4)	16.2558(4)	7.8640(10)
α(°)	86.1(2)	90	90	103.31(1)	12.027(3) 90	90	90
β(°)	91.6(2)	90	95.79(2) 90	94.97(1)	115.10(2) 90	117.218(10)	100.390(10)
γ(°)	100.8(2)	90		105.88(1)		90	90
Z	1	4	8	2	4	4	2
R	0.095	0.083	0.050	0.048	0.051	0.044	0.0523

Table 2b. Precise crystal data for linear furanocoumarin derivatives

Data	M-8	M-9	M-10
Formula	$C_{16}H_{14}O_4$	$C_{15}H_{16}O_5$	$C_{21}H_{22}O_5$
Formula Weight	270.27	276.28	354.39
Crystal System	Triclinic	Orthorhombic	Triclinic
Space group	$P\bar{1}$	$P2_12_12_1$	$P\bar{1}$
a(Å)	11.1150(10)	7.9166(9)	6.4317(10)
b(Å)	11.8240(10)	9.7410(10)	8.0912(16)
c(Å)	11.9290(10)	17.435(3)	17.206(3)
α(°)	64.90	90	91.802(15)
β(°)	83.53	90	94.240(13)
γ(°)	89.25	90	97.473(15)
Z	4	4	2
R	0.043	0.031	0.043

Table 3. Lattice energy (in kcal mol^{-1}) of compounds **(M1 –M10)**

Molecule	E_{Cou}	E_{Pol}	E_{Disp}	E_{Rep}	E_{Tot}
M-1	-4.25	-3.13	-23.94	14.98	-16.34
M-2	-8.60	-3.80	-24.90	14.31	-22.96
M-3	-12.71	-7.22	-32.50	23.68	-28.72
M-4	-15.12	-6.12	-36.01	26.72	-30.54
M-5	-11.70	-4.42	-39.81	26.05	-29.94
M-6	-14.24	-4.68	-33.58	23.97	-28.53
M-7	-18.92	-7.93	-30.31	26.69	-30.49
M-8	-13.02	-4.66	-30.06	18.97	-28.80
M-9	-19.95	-7.64	-32.31	23.82	-36.08
M-10	-18.70	-7.60	-49.68	35.30	-40.70

8-Methoxyfuro[3,2-g]benzo pyran-7-one (M-2)

The key structural motifs providing maximum contribution towards stabilization are shown in Figure 4. The most stabilized molecular pair in the crystal structure formed via π…π molecular stacking, has a contribution of -5.81 kcal mol^{-1} (motif 1) to the stabilization of the crystal packing.

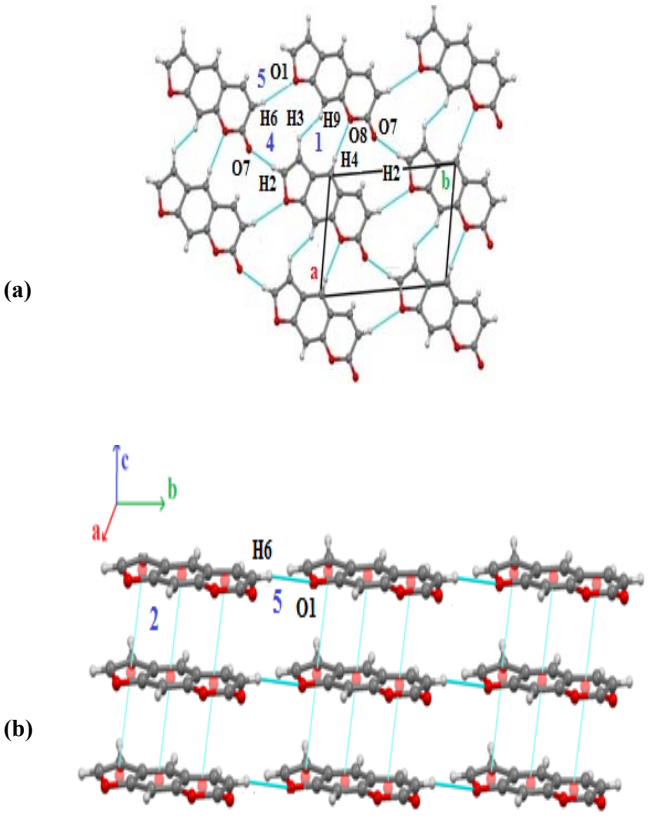

Figure 3. Packing of the molecules in **M-1** depicting **(a)** formation of molecular sheet in the *ab* plane **(b)** molecular chains stacked via π…π interaction down the *bc* plane.

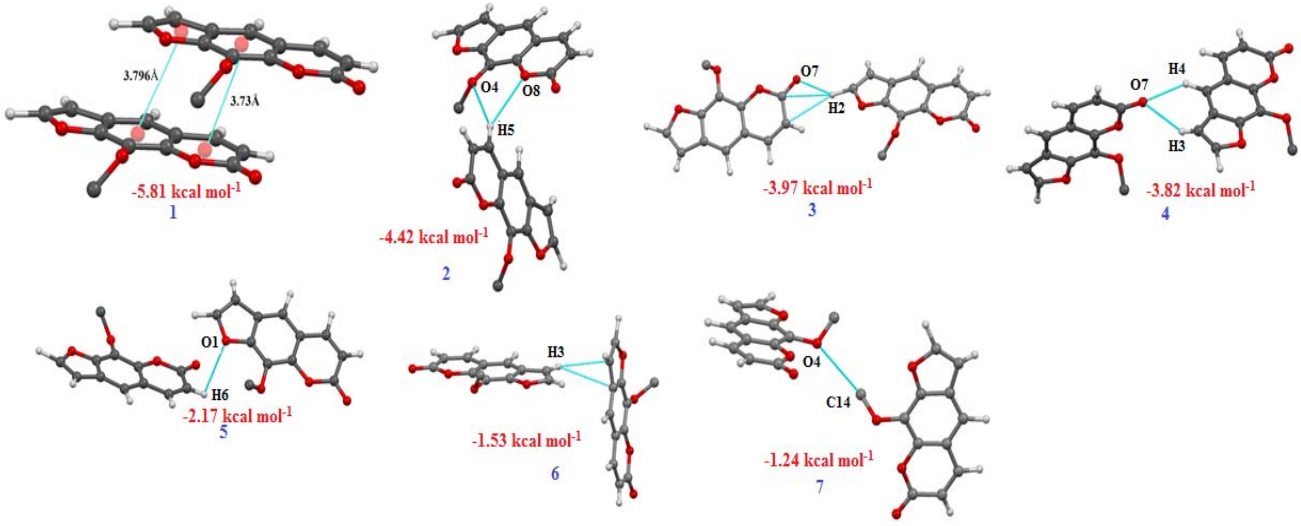

Figure 4. Molecular pairs (**1-7**) along with their interaction energies in **M-2**.

Table 4. Interaction energies (*I.E.*) (kcal mol^{-1}) between molecular pairs related by a symmetry operation and the associated intermolecular interactions in the crystal

Motif	Centroid distance, Å	E_{Coul}	E_{Pol}	E_{Disp}	E_{Rep}	E_{Tot}	Symmetry	Important interactions
M-1								
1	6.938	-2.13	-1.03	-3.32	2.03	-4.44	-1+x,y,-1+z	C4-H4…O8, C3-H3…H9-C9
2	3.777	-0.07	-0.93	-10.37	7.07	-4.32	x,y,-1+z	π…π
3	5.926	-1.07	-0.72	-4.64	2.25	-4.21	-1+x,y,z	C5-H5…O7, C4-H4…O8, C3-H3…O1, C3-H3…π
4	11.100	-3.51	-1.07	-1.50	2.89	-3.20	1+x,1+y,1+z	C2-H2…O7
5	9.560	-0.24	-0.24	-1.53	0.59	-0.95	x,-1+y,z	C6-H6…O1
M-2								
1	4.882	-0.50	-0.72	-8.22	3.63	-5.81	x,y,-1+z	π…π
2	7.077	-1.53	-0.72	-3.18	1.00	-4.42	1/2+x,1/2-y,z	C5-H5…O4, C5-H5…O8
3	10.773	-3.77	-1.05	-1.72	2.56	-3.97	1/2-x,-1/2-y, -3/2+z	C2-H2…O7, C2-H2…π (C6,C7)
4	8.597	-2.94	-1.03	-1.88	2.05	-3.82	-1/2+x,1/2-y,-1+z	C3-H3…O7 C4-H4…O7
5	8.270	-0.31	-0.24	-2.19	0.57	-2.17	1/2-x,1/2+ y, 1/2+z	C6-H6…O1
6	8.516	-0.09	-0.45	-2.75	1.57	-1.53	-x,-y, 1/2+z	C3-H3…π(C3, C11)
7	8.533	-0.22	-0.26	-1.96	1.29	-1.24	1-x,-y,-1/2+z	C14…O4

M-3								
1	4.191	0.02	-2.17	-14.43	8.79	-7.81	-x,y,1.5-z	C17-17…O7, C17-H17…π, stacking
2	8.978	-5.99	-3.94	-5.80	9.67	-6.09	1/2-x,1/2 +y, 1.5-z	C3-H3…O7, O4-H4O…O7, O4-H4O…O8, C18-18b…O4
3	6.362	-1.72	-0.45	-7.02	4.15	-5.02	1/2-x,1/2-y,1-z	C16-H16c…π
4	9.569	-2.67	-0.78	-3.82	2.89	-4.39	1/2+x,1/2-y,1/2+z	C6-H6…O1, C2-H2…O7,H…H
5	9.445	-1.65	-0.47	-2.65	1.38	-3.39	-1/2+x, 1/2+ y, z	$C(sp^2)$-H3… H16b-$C(sp^3)$
6	8.756	-0.86	-0.24	-2.98	0.86	-3.25	-1/2-x,1/2-y,1-z	$C(sp^3)$-H15b…$C2(sp^2)$
7	10.085	-0.81	-0.33	-3.34	2.03	-2.46	-x,-y,1-z	$C(sp^3)$- H15a …C18
8	6.768	-2.48	-0.764	-5.28	1.64	-1.91	1-x,y,1.5-z	C=O…O=C, C16-16b…O7, stacking
9	10.643	-0.52	-0.335	-2.17	1.17	-1.88	-x,1-y,1-z	H…H
10	9.445	-0.41	-.170	-1.50	0.41	-1.67		C18-H18a…O4
M-4								
1	4.783	-6.91	-1.53	-14.82	10.97	-12.31	-x,-y,2-z	π…π, C14-14b…O8
2	7.386	-5.68	-1.98	-12.04	8.48	-11.23	1-x,1-y, 2 -z	C17-H17c…π, C18-H18a…π, C18-H18c…O5, C14-H14a…O5
3	7.385	-3.39	-1.82	-7.36	5.30	-7.29	-x,-y,1-z	C15-H15…O7, C17-H17a…O7, C5-H5…π
4	8.485	-1.82	-0.86	-5.83	3.20	-5.30	-1+x,y,z	C17-H17b…π, C18-H18b…π, C14-14b…O8, C15-H15… π (C1)
5	10.818	-4.21	-1.96	-3.01	4.42	-4.78	-1-x,-y,2-z	C9-H9…O7
6	7.868	-2.55	-1.12	-5.06	4.16	-4.59	x,y,-1+z	C5-H5…O1, C2-H2…O5
7	11.710	-1.07	-0.86	-1.88	1.50	-2.32	-1-x,-y,1-z	C6-H6…O7
8	9.751	-0.50	-0.24	-1.91	0.28	-1.36	1-x,1-y,3-z	C2-H2…H18c -C18
9	12.061	0.12	-0.09	-1.29	0.41	-0.84	-1+x,y, 1+ z	C17-H17b…O1
M-5								
1	5.685	-7.82	-2.84	-18.07	14.79	-13.95	1-x,1-y, 1-z	π…π, C14-14b…O8, C21-21a…O7

2	5.717	-13.95	-1.79	-17.47	13.47	-12.31	-x,1-y,1-z	π…π, C14-14a…O8
3	9.500	-1.41	-1.36	-10.37	7.07	-6.09	1/2+x,1/2-y, 1/2+z	C-H… π, H…H
4	11.013	-1.94	-0.76	-1.55	1.72	-2.53	-1+x,y,-1+z	C2-H2…O7
5	13.155	-0.33	-0.07	-1.65	0.31	-1.74	1/2-x,1/2+ y, 1/2-z	C22-H22c…O1
6	14.112	-1.004	-0.41	-0.91	0.57	-1.74	1/2-x,1/2+ y, 1.5-z	C22-H22a…O7
7	6.732	0.91	-0.29	-2.91	1.15	-1.15	-1+x,y,z	H…H
M-6								
1	4.367	-2.68	-1.93	-14.77	11.47	-7.91	x,1+y,z	π…π, C15-H15c…O8, C15-H15c…O5, C14-H14c…O4
2	8.156	-3.96	-1.22	-4.71	3.82	-6.07	x,-1.5-y,-1/2+z	C3-H3…O7, C14-14c…O7, C14-14a…C7
3	9.004	-2.48	-0.69	-2.24	2.17	-3.25	-x,-1-y,-z	C15-H15b…O5
4	8.898	-0.78	-0.62	-4.21	2.61	-3.01	1-x,-2-y,1-z	C14-H14b…O4, H…H
5	8.926	-2.10	-0.79	-1.41	1.48	-2.79	x,-1/2-y,-1/2+z	C14-H14a…O7
6	9.327	-1.46	-0.24	-2.19	1.15	-2.75	-x,-2-y,-z	CH_3…CH_3
7	8.779	-1.27	-0.43	-2.05	1.17	-2.58	1-x,1/2+y, 1/2-z	C6-H6… π
8	8.72	-1.50	-0.52	-1.98	1.46	-2.56	-x,1/2+y, 1/2-z	C2-H2…O1
M-7								
1	8.030	-9.63	-3.75	-5.11	9.77	-8.72	1-x,-0.5+y, -z	C6-H6…O1, O4-H4O...O7
2	5.721	-0.91	-1.46	-9.42	6.14	-5.64	-1+x,y,z	C2-H2...π
3	7.864	-1.46	-0.96	-3.37	1.84	-3.94	x,y,-1+z	C4-H4…O7, H...H
4	10.526	-2.25	-0.74	-8.46	1.15	-3.77	1+x,y,-1+z	C3-H3a…O7
5	8.601	-2.74	-0.96	-3.01	3.39	-3.35	1-x,-0.5+y, -1-z	C4-H4…O4 C5-H5…O4
6	7.964	-1.43	-0.36	-2.89	2.01	-2.68	2-x,-0.5+y, -z	C16-H6b...π, C16-H6c...O7, C16-H6c...π
7	9.442	0.14	-0.59	-3.56	2.41	-1.63	2-x, 0.5+y, -1-z	H4…H16b H4…H15c

M-8								
1 A…B	7.415	-5.9	-1.88	-7.76	5.95	-9.58	x,1+y,z	C4′-H4′…O7 C5′-H5′…O7 C5′-H5′…O8 C6-H6′…O4 C17-H17b… O7′
2 A…A	5.697	-4.34	-1.09	-11.78	8.65	-8.60	1-x,2-y,-z	π…π
3 B…B	5.228	-2.48	-1.41	-10.39	5.81	-8.48	-x,1-y,-z	π…π
4 A…B	8.625	-4.54	-1.43	-4.75	4.04	-6.69	x,y,z	C5-H5…O7′ C5-H5…O8′ C6-H6…O4′
5 A…B	8.119	-1.74	-0.64	-4.78	2.13	-5.04	-1+x,-1+y,z	C3′-H3′…O1 C3′-H3′…O4 C15-H15…π
6 A…A	7.858	-0.88	-0.35	-6.214	2.72	-4.76	1-x,2-y,1-z	C17-H17C… C2 C14-H4a… C15
7 A…B	6.425	-0.76	-0.50	-6.72	3.25	-4.73	-x,1-y,1-z	C17′-H17a′…π C18′-H18a′…π
8 A…B	8.707	-2.13	-0.74	-4.32	2.61	-4.58	-1+x,y,z	C3-H3…O4′
9 A…B	9.103	-1.15	-0.67	-4.32	2.72	-3.42	-x,1-y,-z	C5-H5… π
10 B…B	8.027	-0.76	-0.41	-3.06	1.34	-2.92	-x,1-y,1-z	H…H
11 A…A	11.115	-3.29	-1.17	-1.74	3.32	-2.91	1+x,y,z	C2-H2...O7
12 B…B	11.115	-2.53	-0.97	-1.69	2.63	-2.58	1+x,y,z	C2-H2′...O7′
M-9								
1	9.502	-8.60	-3.01	-5.02	7.24	-9.37	1/2-x,1-y, -1/2+z	O5-H5o…O7, C15-H15a…O8, C15-H15a…O4
2	6.391	-2.96	-1.05	-6.12	3.56	-6.57	-1/2+x,1/2-y, 1-z	Molecular stacking, C2-H2…O7
3	7.917	-4.21	-1.74	-5.99	5.83	-6.14	-1+x,y,z	C6-H6…O4, C5-H5…O1, C4-H4…O5
4	6.721	-0.81	-0.64	-7.07	3.77	-4.78	-x,-1/2+y, 1/2-z	C16-H16a…π, C4-H4… C15, H15b…H3b
5	10.135	-1.69	-0.69	-2.01	0.84	-3.58	-1/2-x,1-y, -1/2+z	C3-H3b…O7, H6…H15b
6	8.994	-2.01	-0.48	-1.98	1.05	-3.42	-1/2+x,3/2-y, 1-z	C-17-H17b…O7
7	9.769	-0.88	-0.50	-3.12	1.55	-2.94	1-x,-1/2+y, 1/2-z	CH_3...CH_3- moeity

M-10								
1	5.617	-12.76	-4.2	-17.85	16.08	-18.73	1-x,2-y,1-z	O5-H5O…O8, O5-H5O…O7, C22-H22a…O7, C22-H22b…O7, stacking
2	7.079	-4.25	-2.72	-8.84	6.83	-8.98	2-x,2-y,1-z	C19-H19…O7, C17-H17a…O7, H…H
3	9.537	-4.11	-1.24	-11.59	9.08	-7.86	1-x,3-y,1-z	π…π
4	10.971	-3.65	-1.81	-5.78	6.02	-5.21	-1+x,1+y,z	C2-H2…O5, C2-H2…C20
5	6.432	-0.26	-0.78	-9.7	5.04	-5.18	-1+x,y,z	Stacking, H…H
6	8.091	-1.48	-1.05	-5.87	3.60	-4.78	x,-1+y,z	C14-H14a…O5, C-H…C
7	15.871	-1.31	-0.59	-7.19	4.56	-4.54	2-x,1-y,-z	C-H…C
8	12.987	-2.5	-0.62	-3.34	2.65	-3.82	-x,3-y,1-z	C9-H9…O1

Adjacent stacks are then interconnected via weak C2-H2…O7 and C2-H2…π (motif 3, *I.E.* = -3.97 kcal mol^{-1}, the major contribution being the coulombic energy) and C6-H6…O1 (motif 5, *I.E.*= -2.17 kcal mol^{-1}) forming layers in the *bc* plane (Figure 5). The second most stabilized pair involves the interaction of bifurcated donor atom H5 with O4 and O8, contributing -4.42 kcal mol^{-1} towards the stabilization. Additional stabilization to the structure comes from motif 4 which shows the presence of bifurcated acceptor C-H…O interaction (involving O7 with H4 and H3) having stabilizing energy of -3.82 kcal mol^{-1}. Motif 6 (-1.53 kcal mol^{-1}) and 7(-1.24 kcal mol^{-1}) also provide small but significant contribution towards crystal stability.

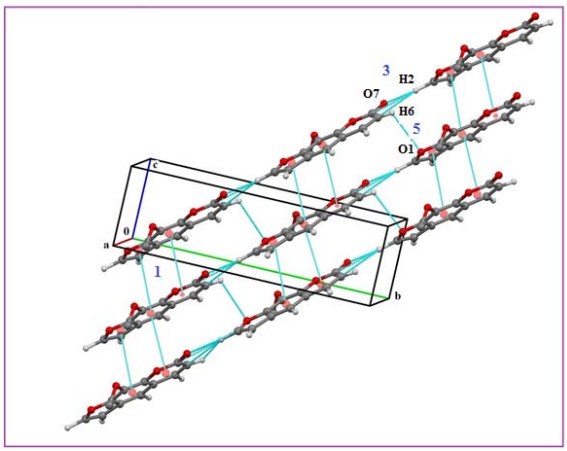

Figure 5. Packing of the molecules in **M-2** showing the stacking of parallel molecular chains down the *bc* plane.

9-(1,1-Dimethyl-2-propenyl)4-hydroxy-7H-furo[3,2-g]benzo-pyran-7-one (M-3)

The important molecular motifs (1-10) along with their interaction energies are shown in Figure 6. The most stabilized molecular pair consists of C-H…π interaction along with C-C stacking (involving C4 of benzene ring of both the molecules) with C…C distance being 3.384Å and hence resulting in a total interaction energy of -7.81 kcal mol^{-1}.

The combined nature of the interaction is mainly dispersive in nature (85% contribution to total stabilization from dispersion component).

This motif along with motif 3 (C16-H16c…π, -5.02 kcal mol^{-1}) results in the stacking of the molecules along the crystallographic *a* axis. These stacks are then interconnected via motif 2 (bifurcated O-H…O and C-H…O hydrogen bonds, -6.09 kcal mol^{-1}, with almost equal contributions from dispersion and coulombic components, Table 4), 5 (H3…H16b, -3.99 kcal mol^{-1}), 7(C15-H15a…C18, -2.46 kcal mol^{-1}), 9 (H2…H3, -1.88 kcal mol^{-1}) and 10 (C18-H18a…O4, -1.67 kcal mol^{-1}) forming layers down the ab plane (Figure 7a). However down the *ac* plane, similar stacks are interconnected to form layers via motif 4 (C-H…O and H…H interaction, -4.39 kcal mol^{-1}), 6 (dimeric C15-H15b…C2, -3.25 kcal mol^{-1}) and 8 (dimeric C=O…O=C along with C16-H16b…O7, -1.91 kcal mol^{-1}) (Figure 7b.)

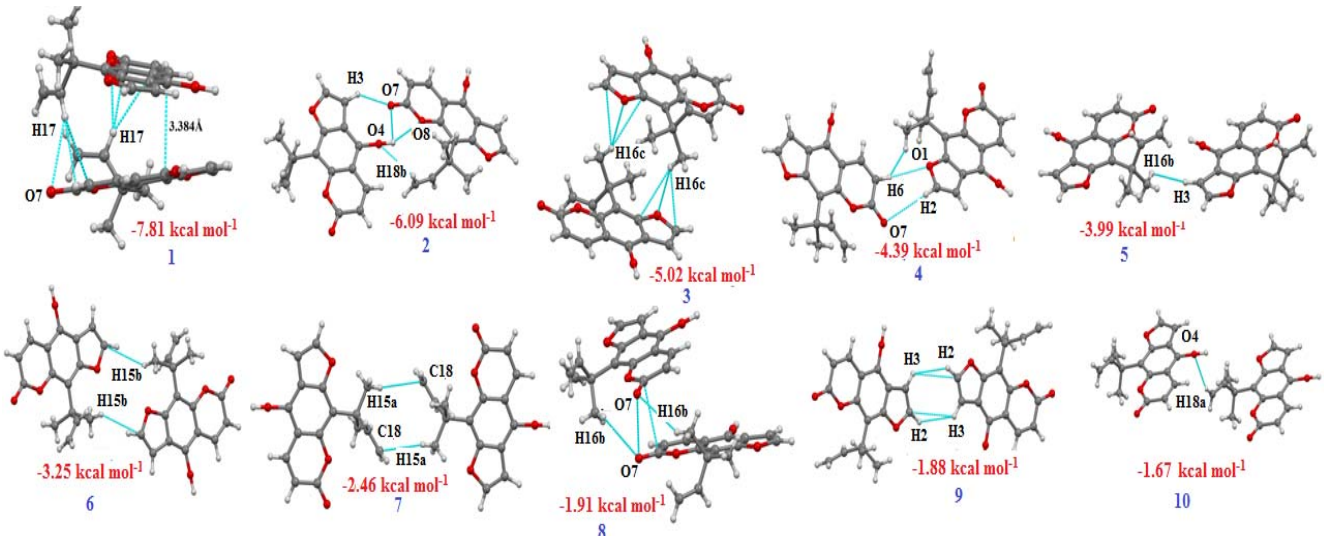

Figure 6. Molecular pairs (1-10) along with their interaction energies in **M-3.**

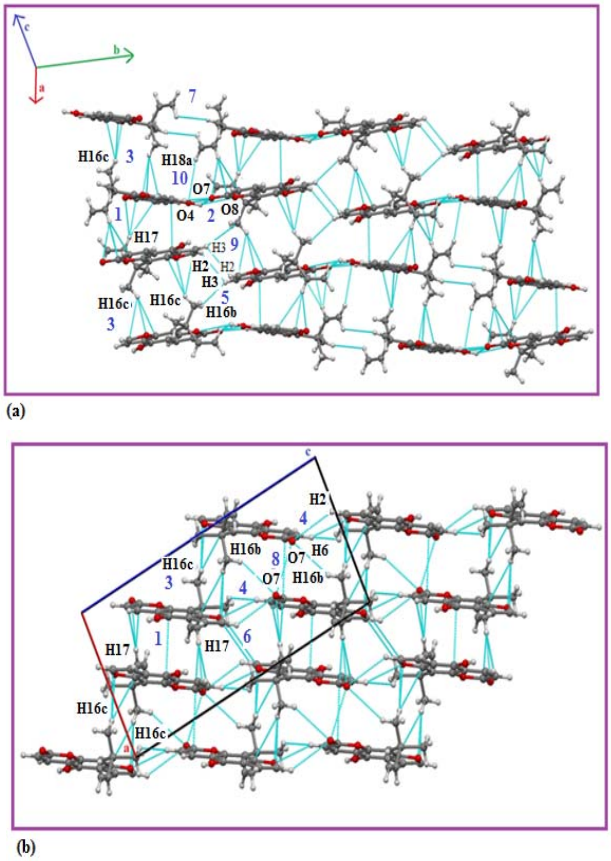

Figure 7. Packing of the molecules in **M-3 (a)** *ab* plane **(b)** *ac* plane

4-((3,3-Dimethyloxiranyl)methoxy)-7H-furo[3,2-g]benzopyran-7-one (M-4)

The molecular pairs (1-9) extracted from the crystal packing are shown in Figure 8 along with their respective interaction energies. The most stabilized molecular pair in the crystal structure, formed via π…π stacking along with C-H…O (involving H14b with O8) has a contribution of -12.31 kcal mol^{-1} (with major dispersion contribution) to the stabilization of the crystal packing. These molecular stacks are then interconnected via dimeric C-H…O involving H6 with O7 (motif 7, -2.32 kcal mol^{-1}) and H…H interaction (motif 8, -1.36 kcal mol^{-1}) (Figure 9a).

The second stabilized pair involves the presence of dimeric bifurcated C-H...O (involving H14a and H18c with O5) along with dimeric C-H...π interaction forming dimers contributing -11.23 kcal mol^{-1} towards stabilization. The third most stabilized motif shows the presence of another bifurcated acceptor C-H…O (involving H15 and H17a with O7) and C-H…π, forming dimers related by centre of symmetry with an interaction energy of -7.29 kcal mol^{-1} and the combined nature of the interaction is mainly dispersive in nature. These molecular dimers are then interconnected via motif 5, 8 and 9 forming sheets in the ac plane (Figure 9b). Motif 5 (-4.78 kcal mol^{-1}) shows the presence of dimeric C(sp^2)-H9...O7 whereas motif 9 (-0.84 kcal mol^{-1}) shows the presence of C17-H17b...O1 interaction. Moreover motif 4 showing the presence of C14-H14b...O8 along with C-H...π hydrogen bonds, provide additional stabilization of -5.30 kcal mol^{-1}.

4-((2,4,4-Trimethyl-1-cyclohexen-1-yl) methoxy)-7H-furo[3,2-g]benzopyran-7-one (M-5)

The important molecular pairs (1-7) providing maximum stabilization to the crystal are shown in Figure 10. The packing of the molecules in the crystal displays the stacking of the molecules via the alternate arrangement of motif 1 and 2 along the crystallographic a-axis.

Both the motifs (1 and 2) shows the presence of π...π stacking along with weak C(sp^3)-H...O hydrogen bonds, contribute -13.95 and -12.31 kcal mol^{-1} respectively towards stabilization of the crystal structure. The nature of the interaction in both the motifs is predominantly dispersive with almost 65% contribution to net stabilization.

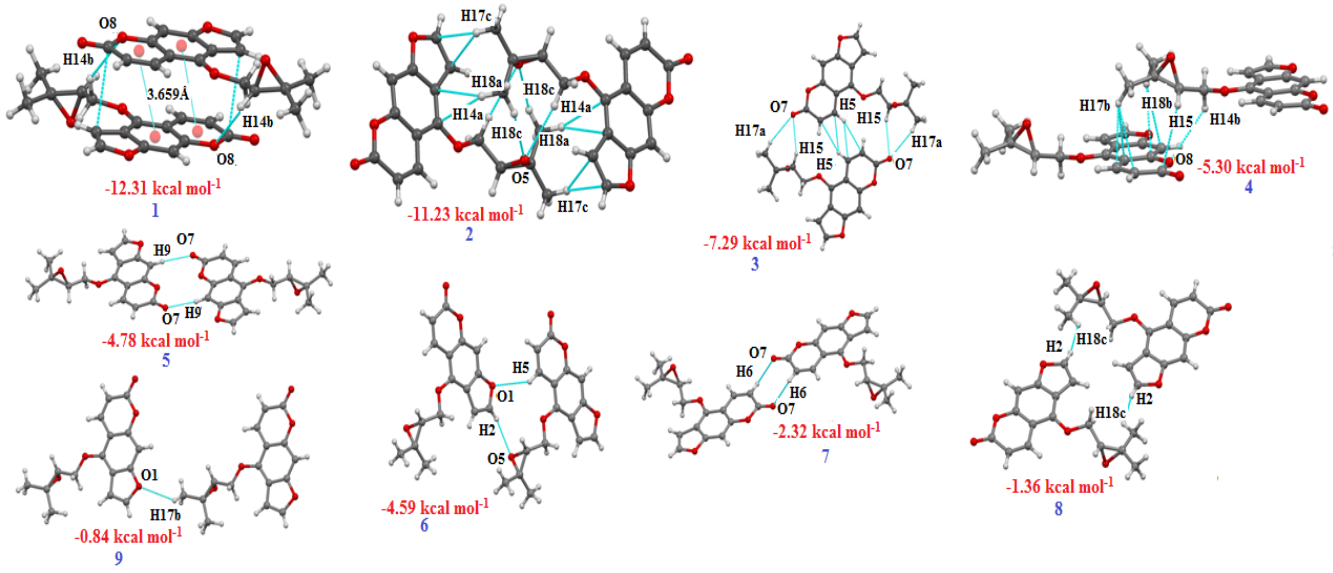

Figure 8. Molecular pairs (1-9) along with their interaction energies in **M-4.**

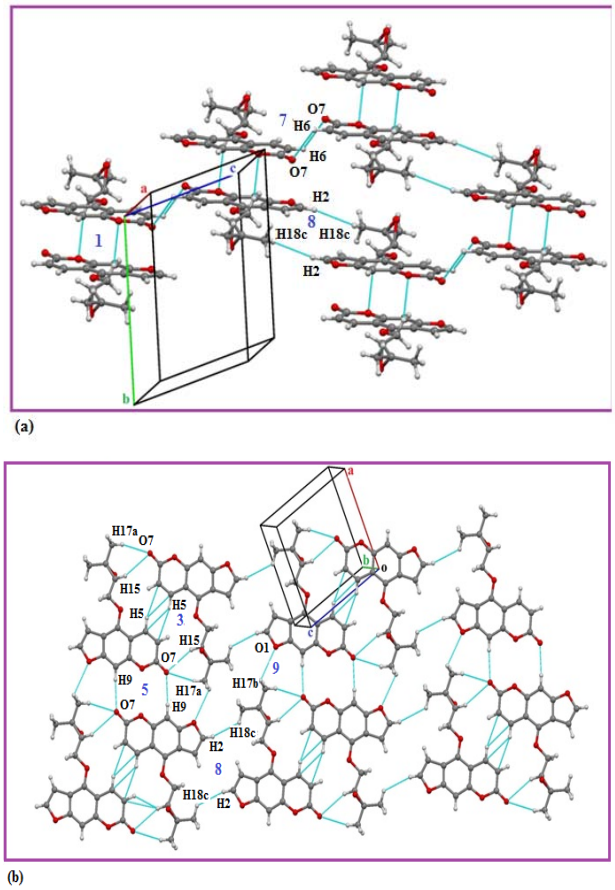

Figure 9. Packing of the molecules in **M-4** depicting **(a)** aromatic stacking interaction down the bc plane **(b)** molecular sheets in the ac plane

These stacks are then interlinked via C(sp^2)-H2…O7 (motif 4, -2.53 kcalmol^{-1}) hydrogen bonds along the *c* axis forming layers down the *ac* plane (Figure 11a). The packing in the crystal also involves the formation of molecular chains along the *b* axis via C(sp^3)-H22c…O1 hydrogen bond, contributing -1.74 kcal mol^{-1} (motif 5). These molecular chains are then interconnected via another C(sp^3)-H22a…O7 hydrogen bonds of same stabilization energy (motif 6, -1.74 kcal mol^{-1}) (Figure 11b)

5,8-Dimethoxyfuro[3,2-g]benzopyran-7- one (M-6)

The key structural motifs (1-8) providing maximum stabilization to the crystal are shown in Figure 12. The molecules in the crystal stack together via π…π along with weak C(sp^3)-H..O hydrogen bonds (motif 1, -7.91 kcal mol^{-1}, 75% contribution to total stabilization from dispersion component) resulting in the formation of a molecular ladder. The weak bifurcated C-H…O involving H3 and H14c with O7 along with weak C(sp^3)-H14a…C7 (motif 2, -6.07 kcal mol^{-1}) and another C-H…O hydrogen bond involving H14a with O7 (motif 5, -2.79 kcal mol^{-1}) connect the molecular ladder in a zig-zag manner along the *c* axis (Figure 13a.). The third most stabilized molecular motif in the crystal are the molecular pairs formed via dimeric weak C-H…O hydrogen bonds (involving H15b with O5, motif 3, -3.25 kcal mol^{-1}) with comparable contribution from coulombic (-2.48 kcal mol^{-1}) and dispersion energy (-2.24 kcal mol^{-1}). These dimeric units are then connected by weak C-H…O (involving H14b with O4) hydrogen bonds along with C-H…H-C interaction (motif 4, -3.01 kcal mol^{-1}) forming chains. These chains are then stacked via motif 1 forming layers (Figure 13b). Moreover, the presence of motif 7 which involves C-H...π interactions and motif 8 showing C-H...O interaction, both having almost similar stabilization energies (-2.58 and -2.56 kcal mol^{-1}) were also observed to stabilize the crystal packing.

2,3-Dihydro-2-(1-hydroxy-1-methylethyl)-7H-furo[3,2-g][1] benzopyran-7-one (M-7)

The principal stabilizing motifs (1-7) imparting maximum energy contribution to the crystal packing are presented in Figure 14.

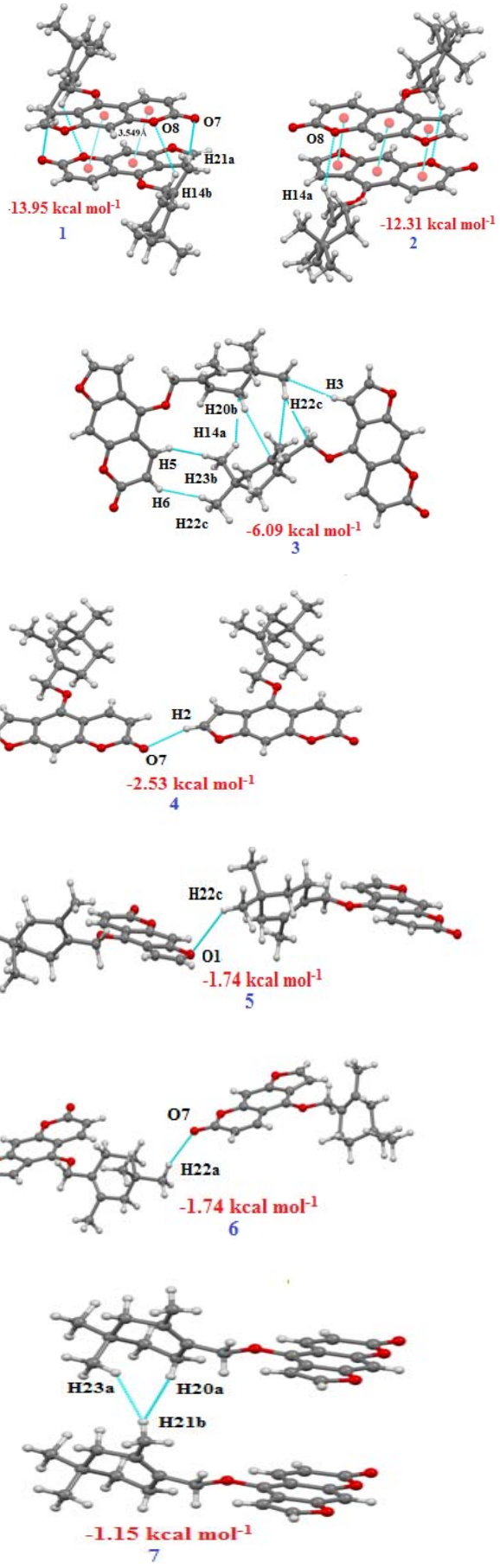

Figure 10. Molecular pairs (1-7) along with their interaction energies in **M-5**

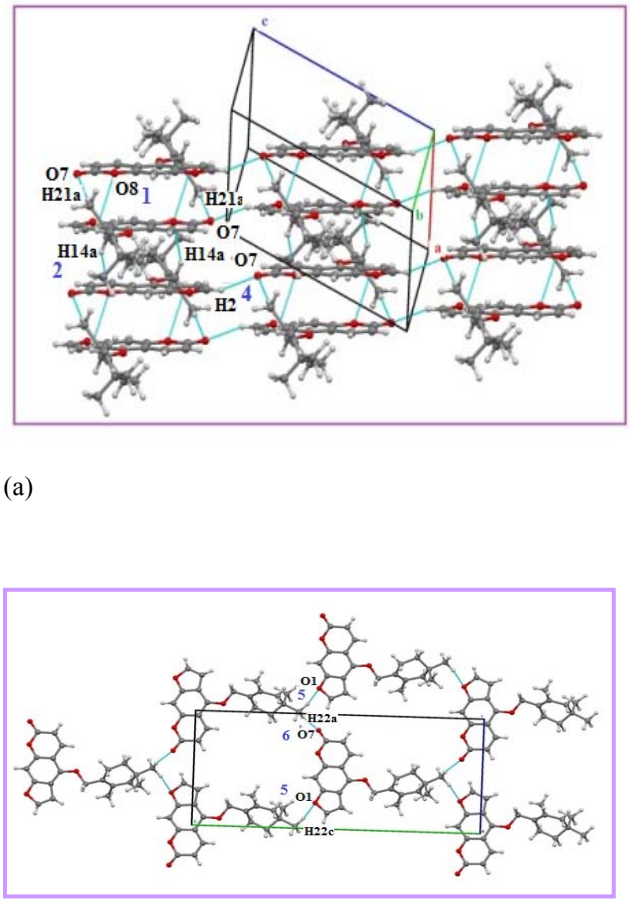

(a)

(b)

Figure 11 Packing of the molecules in **M-5** depicting **(a)** stacking of molecules down the ac plane **(b)** molecular chains formed via C-H…O hydrogen bonds

The most stabilized molecular pair in M-7 consist of short O4-H4O…O7 interaction along with weak C-H…O (involving H6 with O1) and hence resulting in an interaction energy of -8.72 kcal mol^{-1}(motif 1, Figure 14).

It is to be noted that the coulombic contribution towards the net interaction energy for motif 1 is −9.63 kcal mol^{-1} which is 50% of the total stabilization energy. Motif 1 along with bifurcated C-H…O involving H4, H5 with O4 (motif 5, *I.E.*= -3.35 kcal mol^{-1}) is involved in the formation of zig-zag chains along the crystallographic *b* axis. Another weak C-H…O involving H3a with O7 (motif 4, *I.E.*= -3.77 kcal mol^{-1} with major contribution from dispersion) along with C-H…C and C-H…H-C (motif 7, *I.E.*= -1.63 kcal mol^{-1}) interconnect the zig-zag chains (Figure 15).

The second most stabilized motif involves the presence of weak C-H...π interaction contributing -5.64 kcal mol^{-1} (90% contribution to net stabilization from dispersion component) towards stabilization of crystal. It has been observed that motif 3 (-3.94 kcal mol^{-1}) and 6 (-2.68 kcal mol^{-1}) also make significant contributions towards the stabilization of the crystal structure.

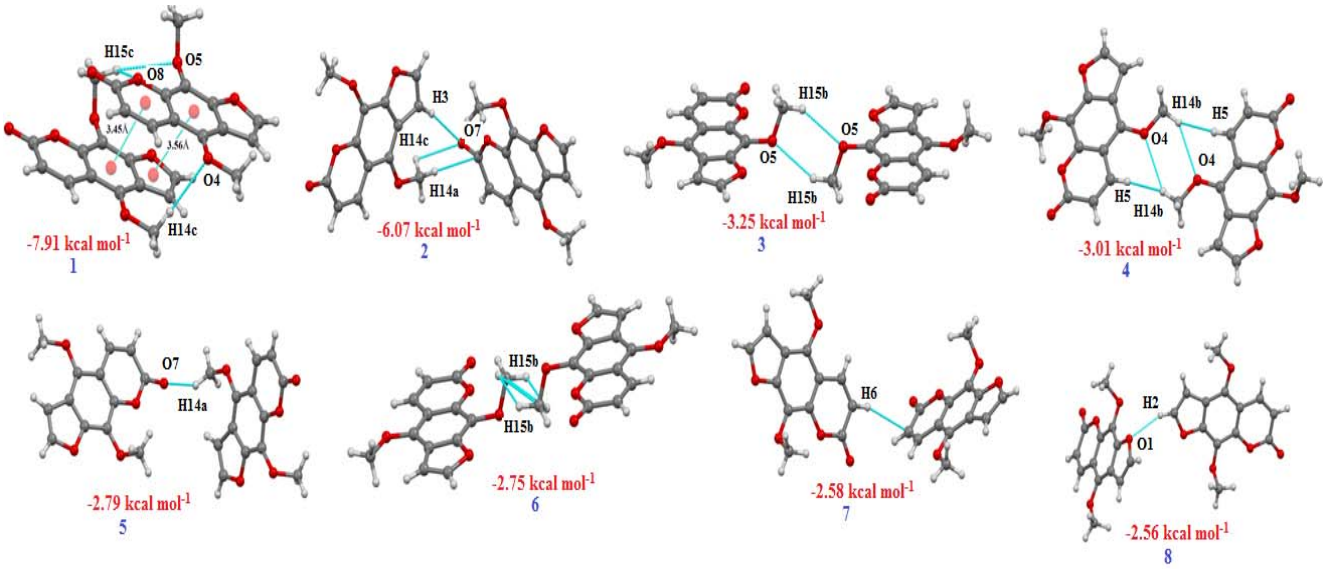

Figure 12. Molecular pairs (1-8) along with their interaction energies in **M-6**

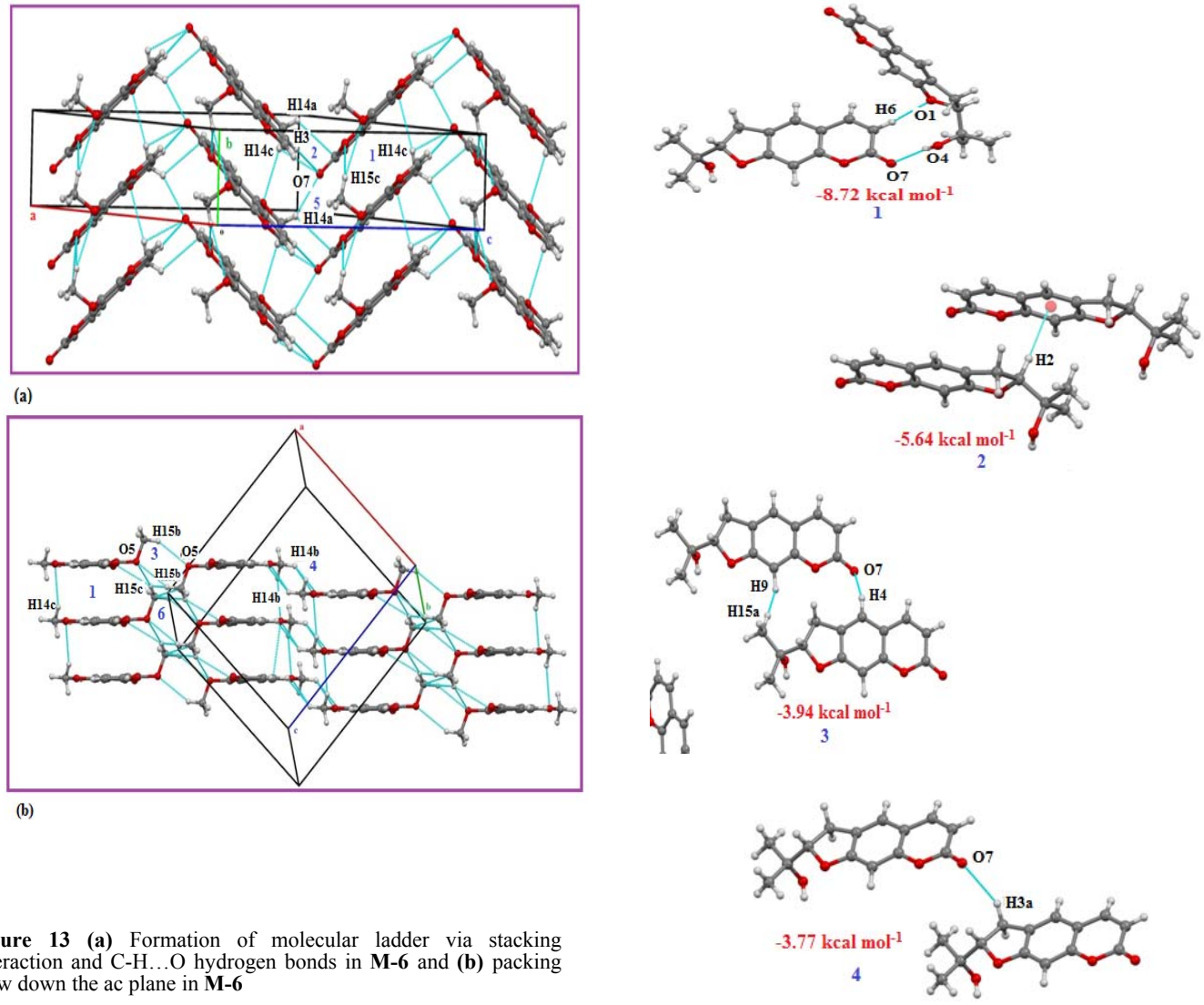

Figure 13 (a) Formation of molecular ladder via stacking interaction and C-H…O hydrogen bonds in **M-6** and **(b)** packing view down the ac plane in **M-6**

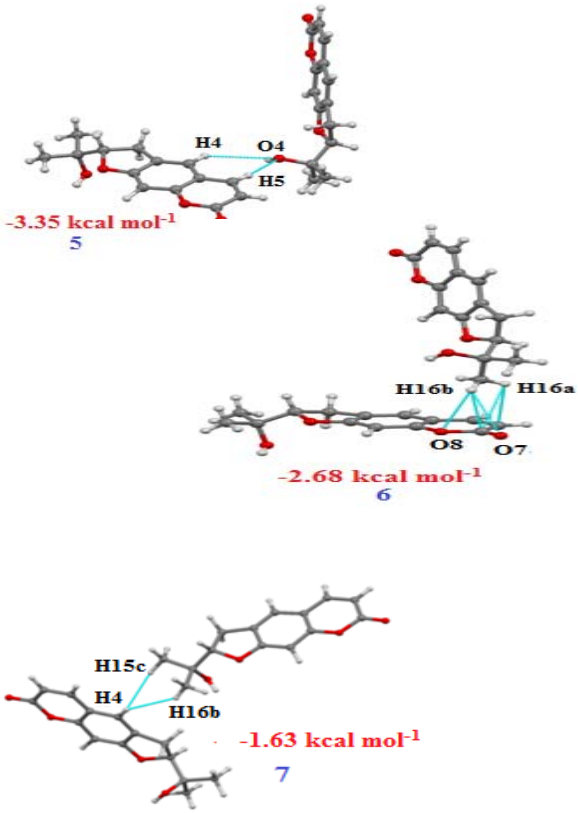

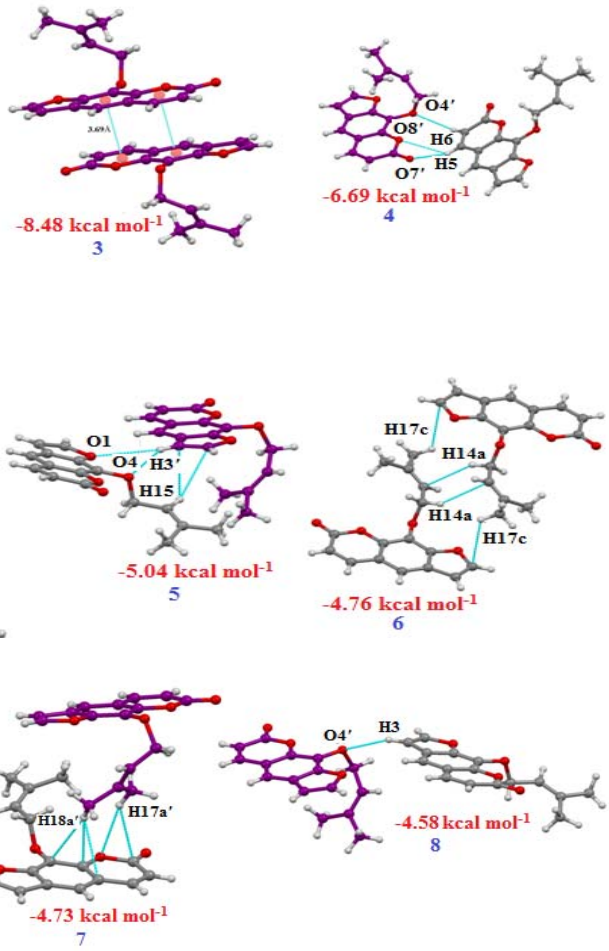

Figure 14. Molecular pairs (1-7) along with their interaction energies in **M-7**

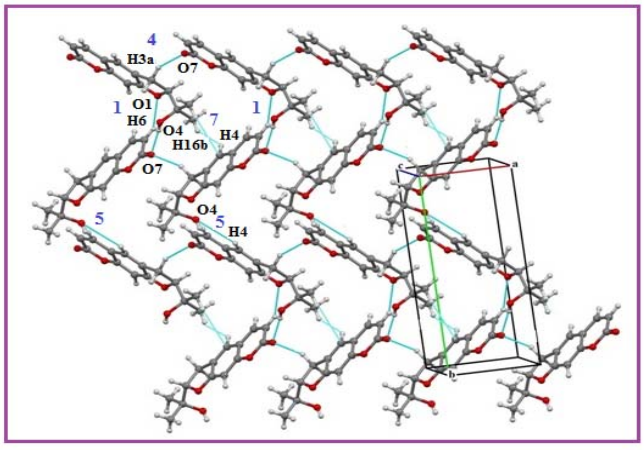

Figure 15. Formation of zig-zag chains via O-H…O and C-H…O hydrogen bonds in **M-7.**

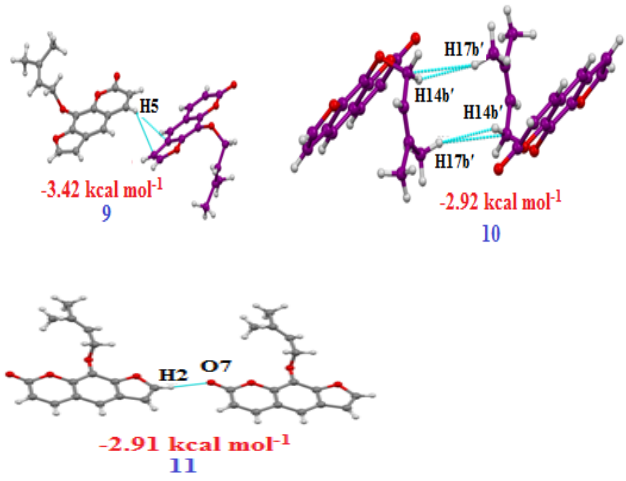

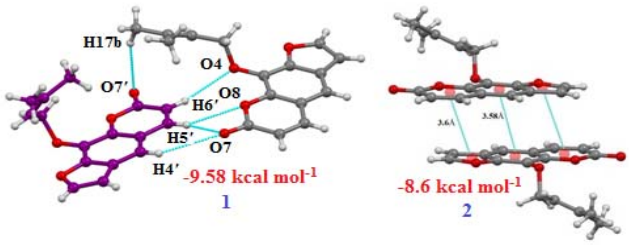

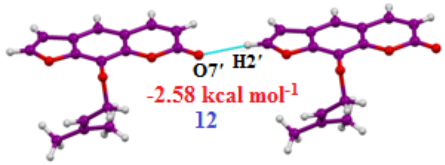

Figure 16. Molecular pairs (1-12) along with their interaction energies in **M-8**

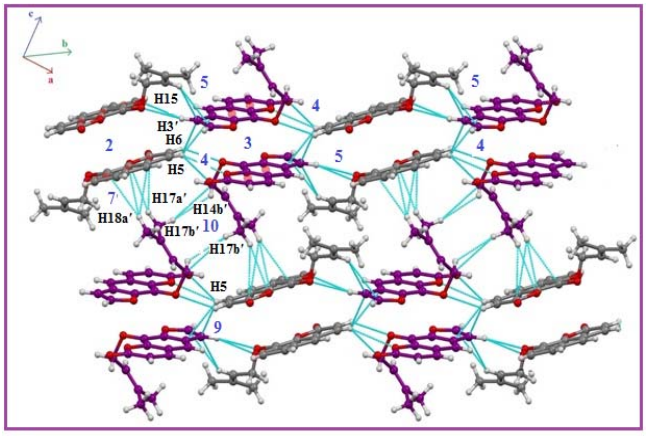

(a)

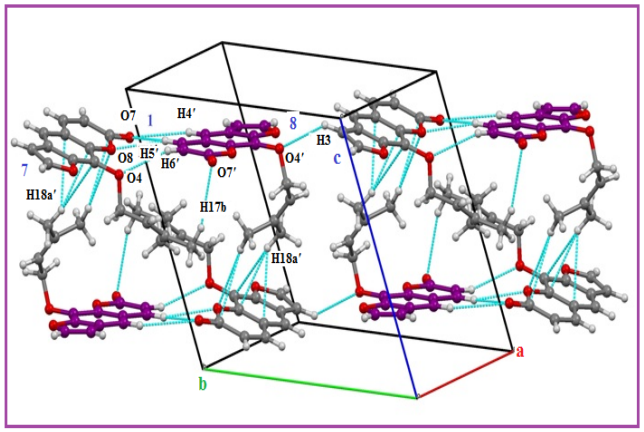

(b)

Figure 17. Packing of the molecules in **M-8 (a)** down the bc plane **(b)** showing stacking of molecular chains formed via C-H…O hydrogen bonds

9-(3-Methylbut-2-enyloxyfurano)[3,2-g]benzopyran-2-one(M-8)

The important stabilizing molecular pairs (1-12) extracted from the crystal packing are presented in Figure 16. The molecule crystallizes with two molecules in the asymmetric unit [molecule A (carbon atom = grey colour) and B (carbon atom = purple colour)]. The two molecules in the asymmetric unit are interacting via weak C-H…O hydrogen bonds (involving bifurcated donor atom H5 with O7′ and O8′, H6 with O4′) and this pair is fourth most stabilized pair in the crystal, energy being -6.69 kcal mol^{-1}. This pair (motif 4) along with motif 5 (showing the presence of bifurcated donor C-H…O interaction along with C-H…π, -5.04 kcal mol^{-1}) propagates along the b-axis forming chains. The chains so formed are then stacked along c axis utilizing motifs 2,3 7,9 and 10 as shown in Figure 17a.

Both the motifs 2 and 3 involves π…π stacking and provide almost equal contributions (-8.6 and -8.48 kcal mol^{-1}) towards stabilization, with maximum contribution from dispersion component. The packing in the crystal also displays the formation of molecular chains via motif 1 (the most stabilized motif showing the presence of C-H…O hydrogen bonds having stabilization energy -9.58 kcal mol^{-1}) and 8 (involving C(sp^2)-H3…O4′, *I.E.* = -4.58 kcal mol^{-1}). The chains so formed are then interconnected via motif 7 (-4.73 kcal mol^{-1}) showing the presence of C-H…π interaction (Figure 17b).

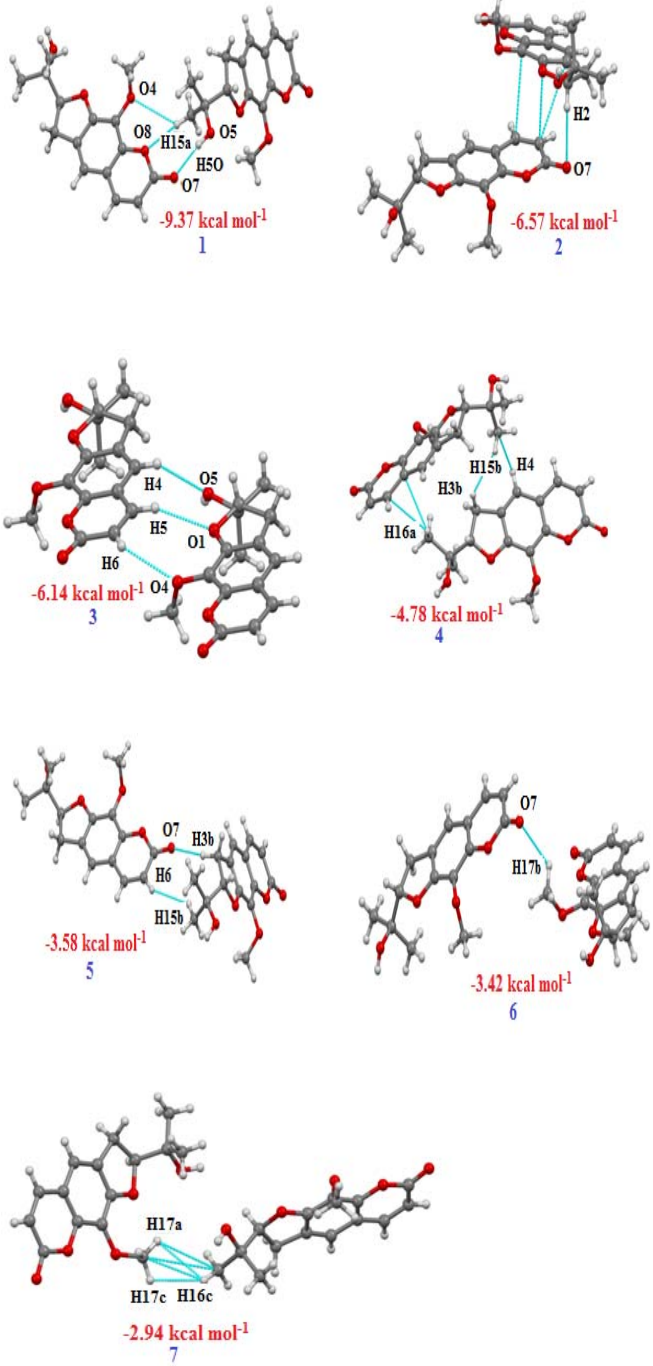

Figure 18. Molecular pairs (1-7) along with their interaction energies in **M-9**

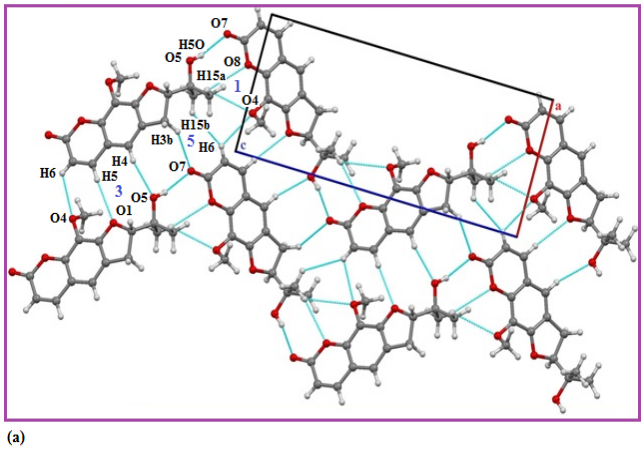

(a)

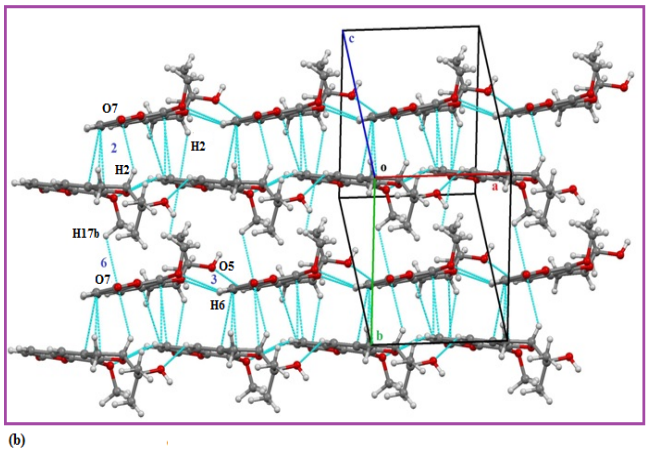

Figure 19a. Zig-zag chains formed via O-H…O and C-H…O hydrogen bonds in ac plane in **M-9 (b)** packing view of the molecules down the ab plane in **M-9**

2,3-Dihydro-2-(1-hydroxy-1-methylethyl)-9-ethoxy-H-furo[3,2-g][1]benzopyran-7-one (M-9)

The important molecular motifs (1-7) extracted from the crystal packing are shown in Figure 18. The strong O5-H5O…O7 and bifurcated donor C-H…O involving H15a with O8 and O4 (motif 1, -9.37 kcal mol^{-1}, the major contribution being the coulombic energy) participate in the formation of zig-zag chains along the crystallographic c axis. The zig-zag chains are then interconnected with the presence of motif 3 (C-H…O hydrogen bonds, -6.14 kcal mol^{-1}) and motif 5 (C3-H3b…O7 hydrogen bond along with H6…H15b, -3.58 kcal mol^{-1}) (Figure 19a). The second most stabilized pair shows the presence of molecular stacking along with C2-H2…O7 and hence contributing -6.57 kcal mol^{-1} (with major dispersion component, Table 4) towards the stabilization. These stacks are then connected via motif 3 forming layers. Two such layers are then interconnected via C17-H17b …O7 hydrogen bonds (motif 6, -3.42 kcal mol^{-1}) (Figure 19b).

4-{[(2E)-5-Hydroxy-3,7-dimethylocta-2,6-dien-1-yl]oxy}-7H-furo[3,2-g][1]benzopyran-7-one) (M-10)

The molecular pairs providing maximum stabilization to the structure extracted from the molecular packing are shown in Figure 20.

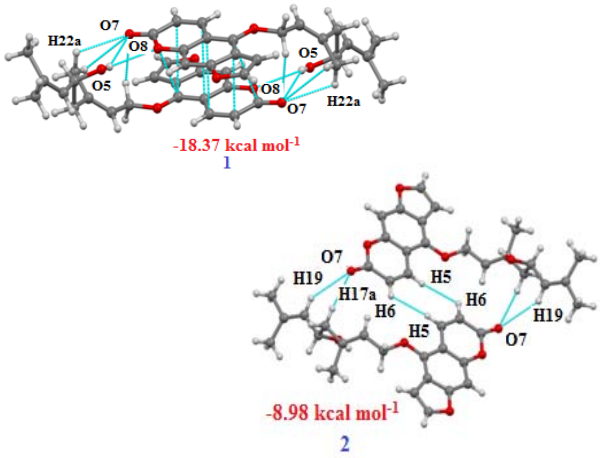

Figure 20 Molecular pairs (1-8) along with their interaction energies in **M-10**

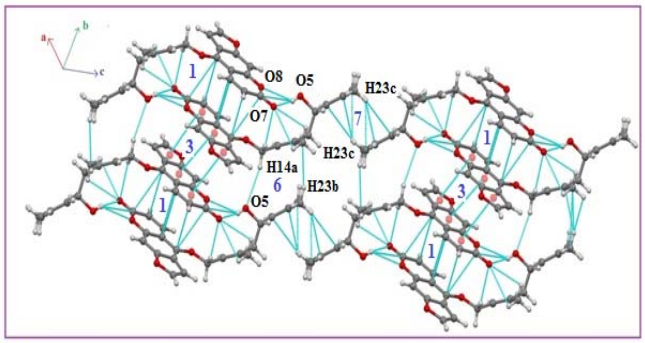

(a)

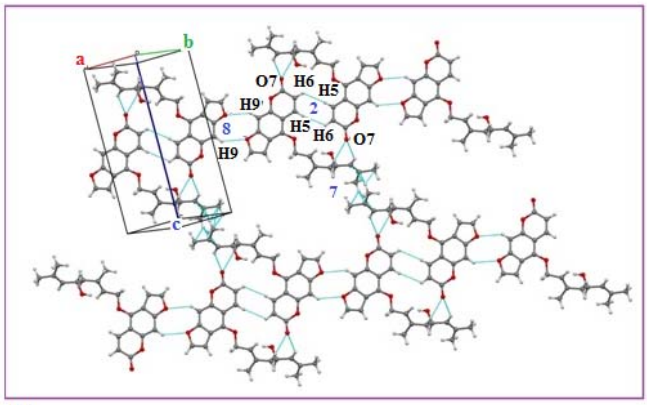

(b)

Figure 21 Packing of the molecules in **M-10 (a)** stacking of molecules down the *bc* plane **(b)** formation of molecular chains via C-H…O hydrogen bond

The most stabilized molecular pair 1 shows the presence of O-H…O and weak C-H…O resulting in the formation of dimer related by centre of symmetry. Along with these interactions, it also involves stacking interaction (C-C stacking) and hence resulting in a total interaction energy of -18.73 kcal mol^{-1} with significant contribution from coulombic (-12.76 kcal mol^{-1}) and dispersion (-17.85 kcal mol^{-1}) energies. These dimeric units are then staked along b-axis via motif 3 (*I.E.* = -7.86 kcal mol^{-1}) involving π…π interaction. Adjacent stacks are then interconnected via motif 6 and 7 as shown in Figure 21a. Motif 6 (-4.72 kcal mol^{-1}) shows the presence of weak C-H…O along with C-H…C interaction whereas C(sp^3)-H23c…C(sp^3) interactions binds the molecules in motif 7 (-4.54 kcal mol^{-1}). The second stabilized pair showing the presence of dimeric bifurcated C-H…O hydrogen bond along with H…H interaction (motif 2, *I.E.* = -8.98 kcal mol^{-1}) and dimeric C9-H9…O1 hydrogen bonds (motif 8, *I.E.* = -3.82 kcal mol^{-1}) are involved in the formation of molecular chains. The chains so formed are then interconnected via motif 7 (Figure 21b).

A careful analysis of some key supramolecular motifs obtained in these compounds leads to the following relevant observations:

1. The maximum stabilization to the crystal structure comes from molecular pairs showing the presence of π…π stacking along with weak C-H…O hydrogen bonds with energy ranging between -7 to -13.95 kcal mol^{-1}.
2. The energy of the molecular pairs interacting via C(sp^2)-H…O lies in the range -0.95 to -3.77 kcal mol^{-1} with average value being -2.53 kcal mol^{-1} while that of molecules interacting via C(sp^3)-H…O lies in the range –0.84 to -3.42 kcal mol^{-1} with average value of -2.07 kcal mol^{-1}.
3. The energy of the molecular pairs interacting via bifurcated C-H…O interaction ranges between -4 to -6 kcal mol^{-1} with 45-50% contribution from coulombic component.
4. The lattice energy of the structures lies in the range -16 to -40 kcal mol^{-1}.

Conclusions

Crystallographic analysis of crystal packing in the identified structures of linear furanocoumarin derivatives with inputs from PIXEL energy calculations suggest the presence of molecular pairs which are the key structural motifs beneficial for the packing of molecules. It has been observed that structural motifs involving π–π stacking and bifurcated C-H…O are the most significant contributors towards stabilization of structures. Dispersion energy is the major stabilization component in case of stacking interactions. Analysis of C-H…O hydrogen bonds shows that molecular pairs involving C(sp^2)-H…O hydrogen bonds are more stabilized than those involving C(sp^3)-H…O. The knowledge gained about the role of weak non bonded interactions can be utilized in various scientific disciplines including biochemistry and rational drug design, crystal engineering and molecular devices to materials science and the mechanical properties of solids.

References

[1]Qian, G. S., Wang, Q., Leung, K. S. Y., Qin, Y., Zhao, Z., Jiang, Z. H., *J. Pharm. Biomed. Anal.,* **2007**, *44*, 812 – 817.

[2]Zarbska, Z., *J. Photochem. Photobiol. B*, **1994**, *23*, 101-109.

[3]Moor, A. C. E., Gasparro, F. P., *Clin. Dermatol*., **1996**, *14*, 353-365.

[4]Brown, D. A., *J. Photochem. Photobiol.* B, **2001**, *63*, 148 - 161.

[5]Zolek, T., Paradowska, K., Wawer, I., *Solid State Nucl. Magn. Reson*., **2003**, *23*, 77- 87.

[6]Dewick, P. M., M*edicinal Natural Products. A Biosynthetic Approach,* 3rd Ed., John Willey and Sons, Ltd. United Kingdom, **2009,** 163.

[7]Miolo, G., Stefanids, M., Santella, R. M., Dall Acqua, F., Gasparro, F. P., *J. Photochem. Photobiol.* B, **1989**, *3*, 101 - 112.

[8]Desiraju, G. R., *Angew. Chem., Int. Ed.,* **2011**, *50*, 52- 59.

[9]Arunan, E., Desiraju, G.R., Klein, R. A., Sadlej, J., Scheiner, S., Alkorta, I., Clary, D. C., Crabtree, R. H., Dannenberg, J. J., Hobza, P., Kjaergaard, H. G., Legon, A. C., Mennucci, B., Nesbitt, D., *J. Pure Appl. Chem.,* **2011**, *83*, 1637-1641.

[10]Nishio, M., Umezawa, Y., Honda, K., Tsuboyama, S.,Suezawa, H., *Cryst. Eng. Comm.*, **2009**, *11*, 1757- 1788.

[11]Takahashi,O., Kohno, Y., Nishio, M., *Chem. Rev*., **2010**, *110*, 6049 - 6076.

[12]Nishio, M., *Phys. Chem. Chem. Phys*., **2011**, *13*, 13873- 13900.

[13]Dunitz, J. D., Gavezzotti, A., *Chem. Soc. Rev*., **2009**, *38,* 2622-2633.

[14]Maschio, L., Civalleri, B., Ugliengo, P., Gavezzotti, A., *J. Phys. Chem.,* **2011***, 115*, 11179- 11186.

[15]Kaur, G., Panini, P., Chopra, D., Choudhury, A. R., *Cryst. Growth Des.,* **2012**, *12*, 5096- 5110.

[16]Vasylyrva, V., Shishkin, O. V., Maleev, A. V., Merz, K.,*Cryst. Growth Des*., **2012**, *12,* 1032 - 1039.

[17]Bideau, J.P., Bravic, G., Desvergne, J. P., *Cryst. Struct. Commun*., **1979**, *8*, 695.

[18]Stemple, N. R., Watson, W. H., *Acta Cryst. B,* **1972**, *28*, 2485 - 2489.

[19]Padha, N., Subramanian, E., Das, A. K., Mazumdar, S. K., Goswami, K. N., *Cryst. Res. Technol.,* **1995**, *30*, 205- 209.

[20]Singh, A., Gupta, V. K., Rajnikant, Goswami, K. N., *Cryst. Res. Technol.,* **1995**, *30*, 991- 996.

[21]Magotra, D. K., Gupta, V. K., Kant, R., Goswami, K. N., Thappa, R. K., *Acta Cryst. C,* **1995**, *51*, 2196 - 2198.

[22] Napolitano, H. B., Silva, M., Ellena, J., Rocha, W. C., Vieira, P. C., Thiemann, O. H., Oliva, G., *Acta Cryst. E,* **2003**, *59,* o1506 – o1508.

[23]Goswami, S., Gupta, V. K., Sharma, A., Gupta, B. D., *Bull. Mater. Sci*., **2005**, *28(7)*, 725 - 729.

[24]Kant, R., Dinesh., Shawl, A. S., Singh, T. P., Goel, V., Sharma, B., *J. Chem. Cryst.,* **2005**, *35*, 913- 916.

[25]Bauri, A.K., Sabine, F., Lindner, H.J., Nayak, S.K., *Acta Cryst E,* **2006***, 62*, o2900 – o2901.

[26]Schinkovitz, A., Belaj, F., Kunert, O., Bauer, R., *Acta Cryst E,* **2009**, *65,* o545.

[27]Gavezzotti, A. *J. Phys. Chem. B,* **2002**, *106*, 4145 - 4154.

[28]Gavezzotti, A. *J. Phys. Chem. B,* **2003**, *107*, 2344 - 2353.

[29]Gavezzotti, A. *New J. Chem*., **2011**, *35*, 1360 - 1368.

[30] Macrae, C. F., Bruno, I. J., Chisholm, J. A., Edgington, P. R., McCabe, P., Pidcock, E., Rodriguez-Monge, L., Taylor, R., Streek J., Wood, P. A., *J. Appl. Crystallogr.,* **2008**, *41*, 466–470.

Received: 22.08.2015.
Accepted: 11.09.2015.